University of Alberta

Evaluation of Digital Photogrammetry for Measuring Cast Blast Efficiency

by

Jovan Radmanovic 

A thesis submitted to the Faculty of Graduate Studies and Research

in partial fulfillment of the requirements for the degree of

Master of Science

in

Mining Engineering

Department of Civil and Environmental Engineering

Edmonton, Alberta

Fall 2006

Your file Votre référence
ISBN: 978-0-494-22351-2
Our file Notre référence
ISBN: 978-0-494-22351-2

Abstract

Use of digital photogrammetry instead of GPS/laser survey techniques for cast blast monitoring in an operating coal mine was assessed. Photographs were taken before and after six cast blasts at the Highvale coal mine. Conventional surveying methods are typically limited to measuring coordinates of less than 100 points. The photogrammetric approach, under optimal field conditions, can measure hundreds of thousands of points resulting in higher spatial resolution and more accurate volumes. The fieldwork effort, area coverage of each digital terrain model, and the model accuracy are documented. Recommendations for optimal camera position and image acquisition mode to minimize fieldwork and to maximize areal coverage are given. Practical limitations and operational challenges involved with using the photogrammetry are discussed. Cast blast efficiency is calculated from the percentage of the blasted overburden volume thrown into its final position. The results were verified and compared with traditional surveying using cross section analysis.

Acknowledgments

I would like to thank my advisor Dwayne Tannant for helping me throughout my research project. I thank Tony Smith and Al Brown for their authorization and support on this project. I am especially grateful to Julie Christensen, Klaus Oldach and Dave Rosgen for valuable fieldwork and data compiling assistance.

Finally, I would like to thank my wife Svetlana and my children Ana, Vanja and Irina for their patience and constant support.

Table of Contents

List of Tables

List of Figures

1 Introduction

1.1 Problem statement

The cast blast technique is often used in open pit coal mines. It is designed to use explosive energy to effectively and economically displace overburden horizontally into the adjacent mined-out pit. The more overburden removed by the explosive, the less blasted material there is left to be handled with mechanical equipment such as draglines and bulldozers.

The efficiency of a cast blast is measured from the overburden volume thrown by the blast into its final position as a percentage of the total volume of blasted overburden. Cast blast efficiency, like overburden volumes and muck pile location are usually determined using conventional surveying methods. Conventional survey techniques require a field surveying crew to establish a horizontal and vertical control network and then make numerous measurements of the pre- and post-cast pit topography. A conventional survey takes hours of fieldwork to gather less than 100 coordinates. The bench face is usually not well surveyed and this can lead to erroneous interpretation of the volumes moved and the cast blast efficiency. A better technique may be the use of three-dimensional digital photogrammetry. A goal of this research is to evaluate the suitability of digital photogrammetry for overburden volume measurements and hence cast blast efficiency determination.

1.2 Research objectives

This research was focused on application of the 3D photogrammetry measuring technique as a replacement of conventional survey techniques in an operating coal mine. The ultimate objective was to use 3D digital terrain models obtained from the photogrammetry measuring technique to evaluate cast blast efficiency. The two main research objectives were to:

- Develop an optimal field imaging photogrammetry technique, addressing ground area coverage, digital terrain model accuracy, and analysis of the time and effort involved.

- Calculate the volume and location of the cast-blasted overburden in order to quantify cast blast efficiency using the blasted volumes and cross-section analysis.

1.3 Methodology

The use of ground-based digital photogrammetry as a tool for measuring and mapping rock mass structures is now well established although not yet routinely used in mining industry (Tannant et al., 2006). Numerous studies and research projects are exploring photogrammetric techniques for monitoring of landslides and slope displacements. Information gathered using 3D imaging are used in verifying geotechnical design of slopes and understanding the slope behaviour (Stylianidis et al., 2003, and Bitelli et al., 2004). Also, several case studies conducted at coal mines in Australia and United States point toward application of digital photogrammetry in geotechnical data collection and pit wall mapping (Birch, 2005).

To compute overburden volumes needed to assess cast blast efficiency, a major requirement is to build a fully representative 3D digital terrain model (DTM) of the pit before and after each cast blast. Three dimensional models are generated from photographs of the bench face and the spoil pile acquired from several camera stations. The digital terrain models are dimensionally accurate and related to the mine coordinate system. The DTM obtained after the cast blast is compared with the DTM obtained before the blast to calculate the volume and the location of blasted overburden.

The photographs are processed using Adam Technology's photogrammetric software package, 3DM CalibCam (Adam Technology, 2004a) and 3DM Analyst (Adam Technology, 2004b). 3DM CalibCam is camera calibration and block adjustment software designed to be used in conjunction with 3DM Analyst. 3DM Analyst is a three-dimensional measurement system capable of extracting 3D data from digital images. It operates on photogrammetric principles of determining the 3D locations of objects from pairs of 2D images. The software is able to automatically generate a high-accuracy 3D surface model of an object that can be seen in at least two images. The generated digital terrain models are suitable for many mine design applications like pit wall mapping,

geotechnical data collection, cross-section and contour generation, and distance and volume measurements. The general step-by-step procedure is given in Figure 1.

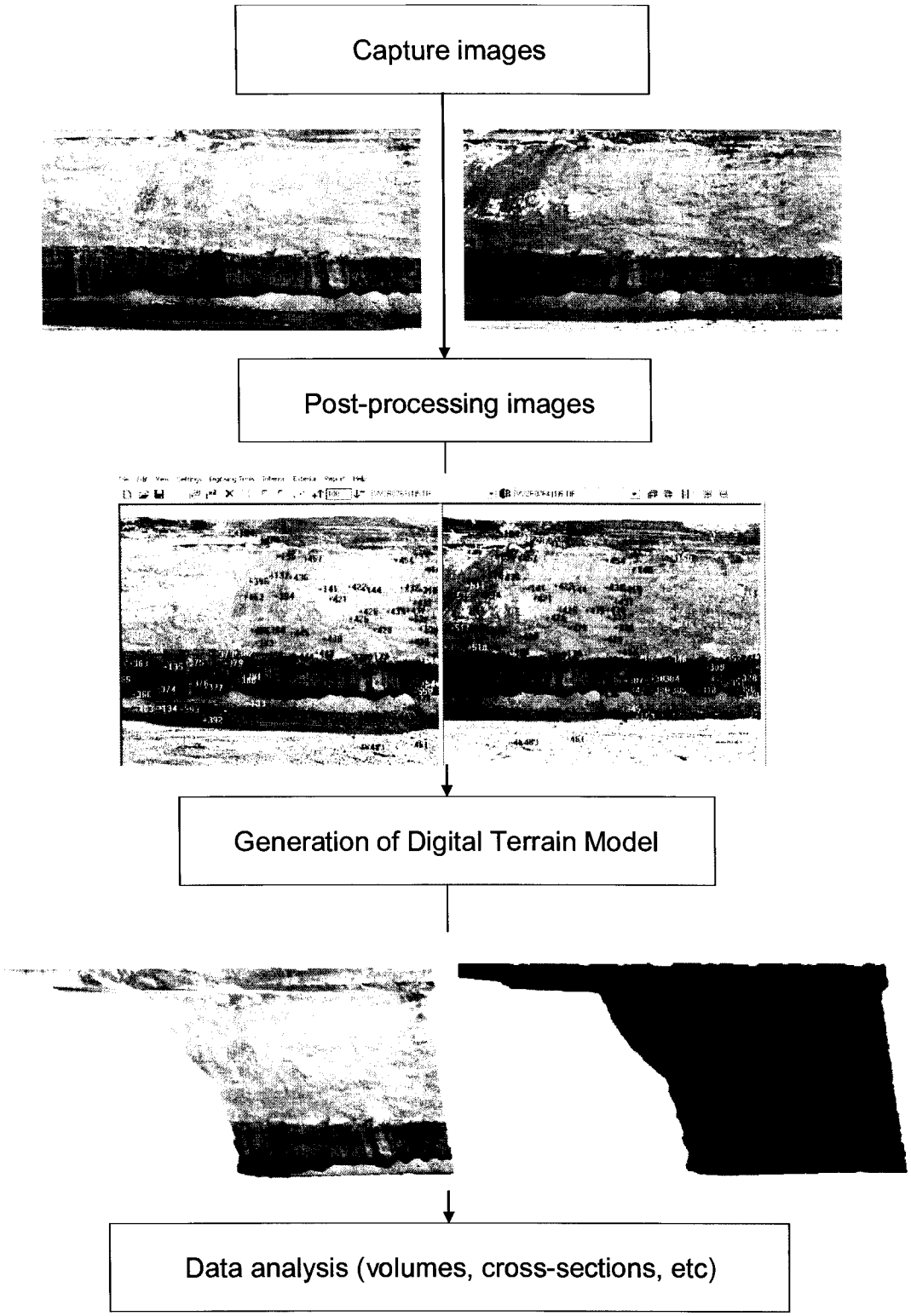

Figure 1 General photogrammetric procedure

2 Highvale Coal Mine

2.1 Introduction

The Highvale Coal Mine is located about 70 km west of the city of Edmonton, near the south shore of Lake Wabamun (Figure 2). Access is westward from Edmonton on Highway 16, and southward via a provincial road just east of Lake Wabamun. It is the largest surface strip coal mine in Canada, and one of three surface coal mines in Alberta owned by Transalta corporation. The owner contracts Luscar Ltd. to operate the mine.

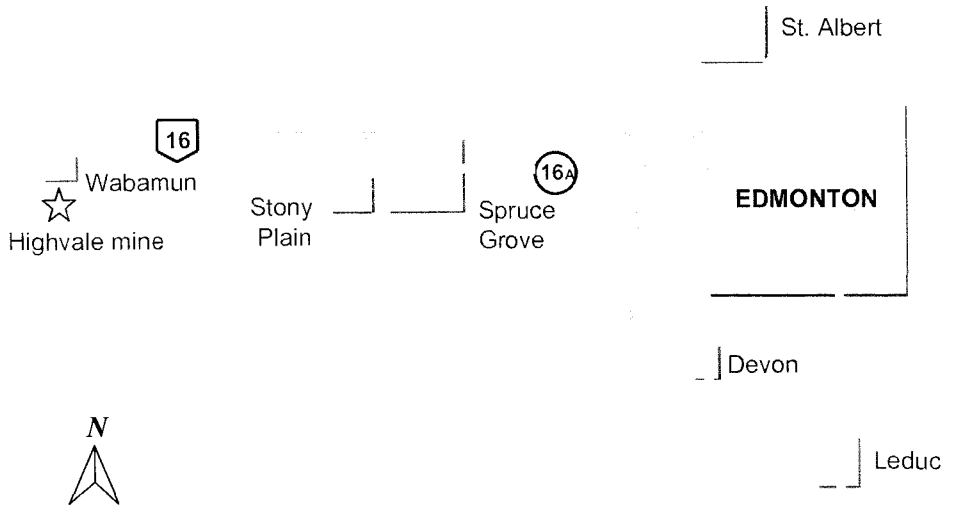

Figure 2 Location map

The Highvale Coal Mine has been in operation since 1970 and was opened to supply thermal coal to the Sundance Generating Station, which is the largest thermal generating plant in Western Canada (>2000 MW output). The Sundance Generating Station consumes 9.3 million tonnes of coal a year; all produced by the Highvale Mine. The mine ships an additional 3.5 million tonnes of coal to the 760 MW Keephills Generating Station (Transalta, 2003).

The Highvale Mine exploits Late Cretaceceous to Early Tertiary coal bearing deposits. This coal deposit is known as the Ardley Coal Zone and is one of the Alberta's most important sources of the thermal coal. Coal analyses and petrographic descriptions of the

seams indicate that the coal belongs to sub bituminous B classification, and is bright and banded in nature (Alberta Geological Survey, 2005).

The coal seams of the Ardley Zone are found at a shallow depth. The total thickness of the coal-bearing interval is about 12 to 15 m, and its depth rarely exceeds 70 m. The coal zone, as shown in Figure 3, consists of six major seams, with the thickest coals occurring near the top of the deposit. The coal zone is divided into Upper Seam (seams 1 and 2) and Lower seam (seams 3 to 6) (Lyatsky and Lawton, 1988).

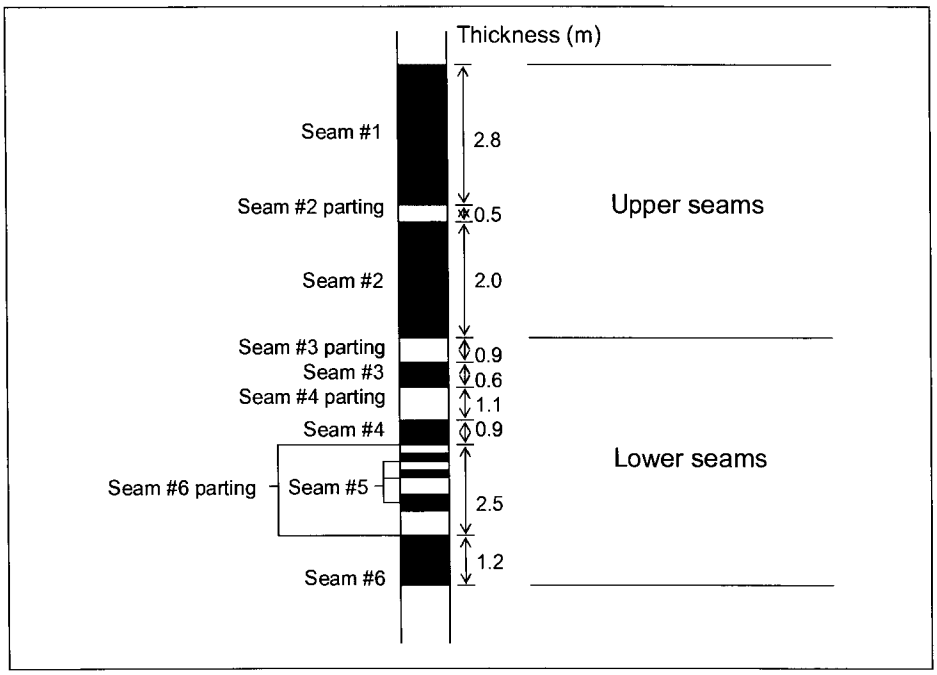

Figure 3 Coal zone at the Highvale Mine

2.2 Mining method

Highvale Mine operates 24 hours a day, seven days a week, using a conventional strip mining technique. The first step in the mining process is removal and storage of the top soil from the proposed mining area. Under the top soil is an overburden layer of shale and sandstone. A typical pit section is given in Figure 4 and Figure 5. In order to expose the coal seam, the overburden is drilled and blasted. Stripping of the overburden is done using large draglines which pile the overburden along the pit edge (Figure 6).

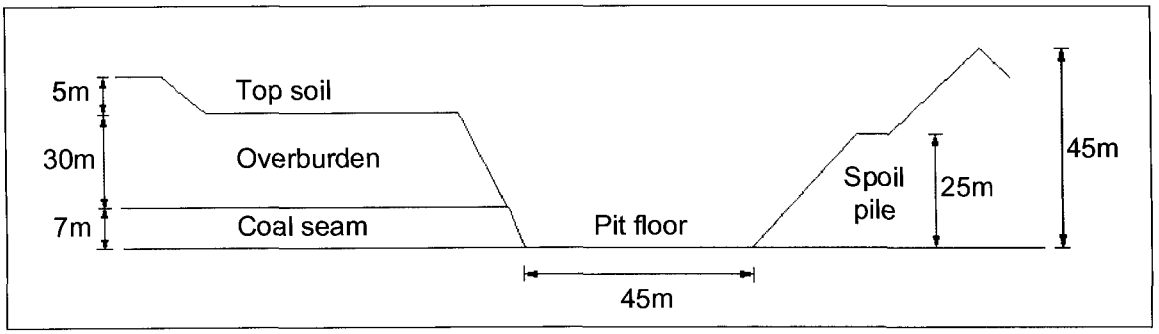

Figure 4 Typical Pit 2 cross-section at the Highvale Mine

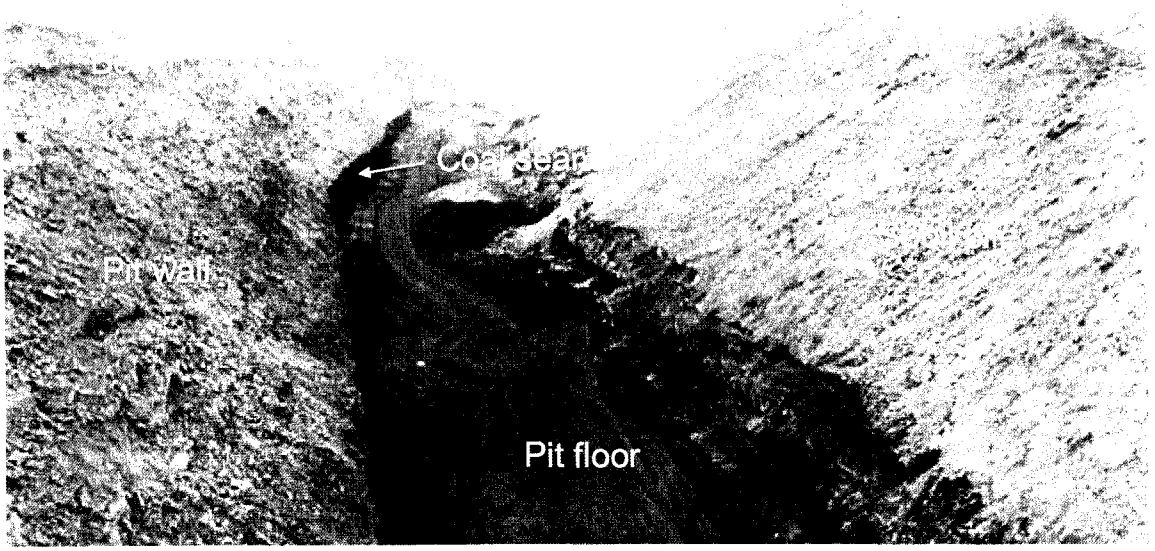

Figure 5 Photo of a typical pit section

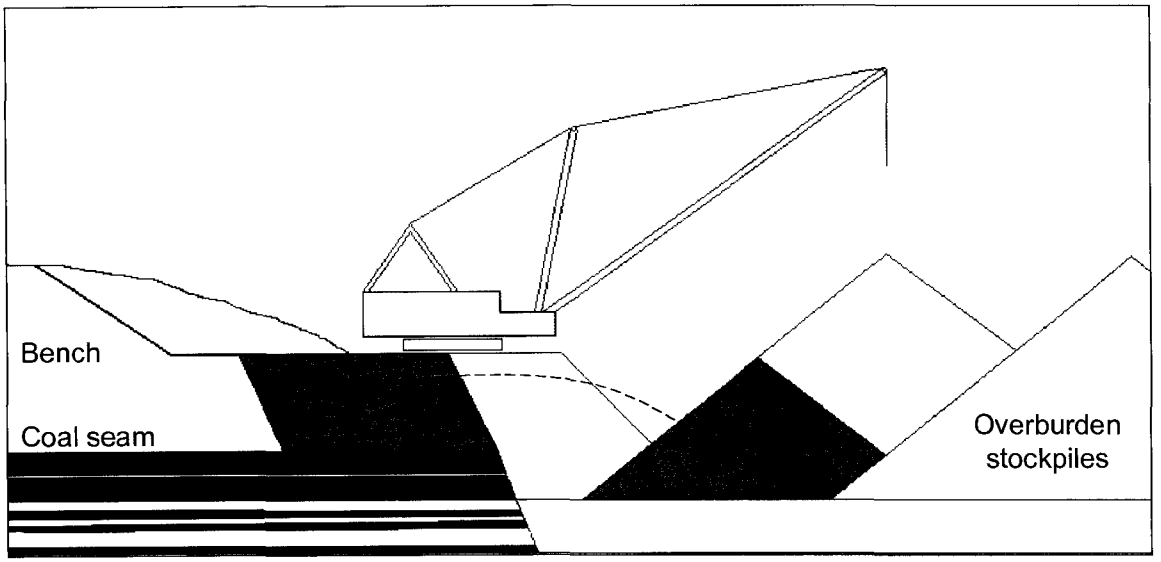

Figure 6 Strip mining sequence at the Highvale Mine

The mine operates four electric-powered walking draglines:

- Marion 8750, 76 cubic metre bucket
- Marion 8050, 48 cubic metre bucket
- Bucyrus-Erie 1360, 41 cubic metre bucket
- Marion 7800, 27 cubic metre bucket.

In addition to draglines, the major mining equipment fleet consists of shovels, drills, front-end loaders and trucks. Transalta owns all plant facilities as well as the draglines, electric shovels and coal haul trucks, while Luscar runs their own supporting fleet of dozers, graders, and scrapers, primarily used for reclamation work.

The exposed coal seam is drilled and blasted, and then loaded and transported to the nearby power plants. When excavation is over, mine support equipment levels the overburden piles and puts back previously stored top soil. After the land is landscaped and replanted, local farmers lease the land for hay and crop production.

The pits that are currently in production at Highvale Mine are Pit 2, Pit 4 and Pit 7 (Figure 7 and Table 1). Pit 2 is the only pit that used cast blasts in 2005, while Pit 3 will start cast blasting in 2007. Average depth for the overburden in Pit 2 is about 45 metres. Due to the depth of Pit 2 it is not economically feasible to use a regular dragline back-cut, face-cut mining sequence. Therefore, the bench is prestripped and lowered using cast blasts and dozer-backhoe assistance. The cast blast method was used because of the higher overburden thickness which results in higher stripping ratio and the limited overburden capacity of the dragline 8750. By using cast blasting, the 8750 dragline only has to remove face-cut material (approximately 100 m pit length per day). The in situ stripping ratio is 4.25:1. Truck and shovels are used to pre-strip roughly 10 m of overburden (1.49:1 pre-stripping ratio). This reduces the amount of overburden that is needed to be moved by the dragline to an effective stripping ratio of 2.76:1. Even at this reduced stripping ratio the dragline capacity is over-extended and to improve the dragline efficiency, it is considered necessary to maximize the percentage of overburden cast directly into its final position.

Figure 7 Highvale Coal Mine active pits (fall 2004)

Table 1 Highvale Mine pits

Highvale pits	Status in 2005	Stripping ratio	Dragline
Pit 2	Active	4.25:1	8750
Pit 3	Not active	-	-
Pit 4	Active	4.35:1	1360
Pit 5	Not active	-	-
Pit 6	Active	-	-
Pit 7	Active	3.65:1	8050

2.3 Cast blasts

The cast blasts that were studied were all located in Pit 2 at Highvale Mine (Figure 7). Even though draglines are one of the lowest cost overburden removal equipment, their operating costs per cubic metre of moved material represents around 60% of a mine's total operating costs (Bucyrus-Erie, 1976). Therefore, the efficiency of the overburden removal process and the dragline employment in that process are very important to the economics of the mine.

After Shaw et al. (1978) made an engineering and economic evaluation of cast blasting and concluded that this method can be used cost-effectively to remove overburden, explosive casting started to gain increasing popularity. The introduction of the cast blast technique in strip coal mining is a result of increasing overburden depths, higher stripping ratios and increased costs of production (Sengstock & Kennedy, 1995).

When the overburden rocks are cast blasted and moved to the area where it does not need to be further handled by dragline/shovel, the dragline costs are reducing but at increased drilling and explosive costs. The economics of a cast blast are schematically shown in Figure 8. The explosive and drilling costs increase as the percent cast increases, while the responding digging costs decrease (Chiromis, 1980 and Tracy, 1985).

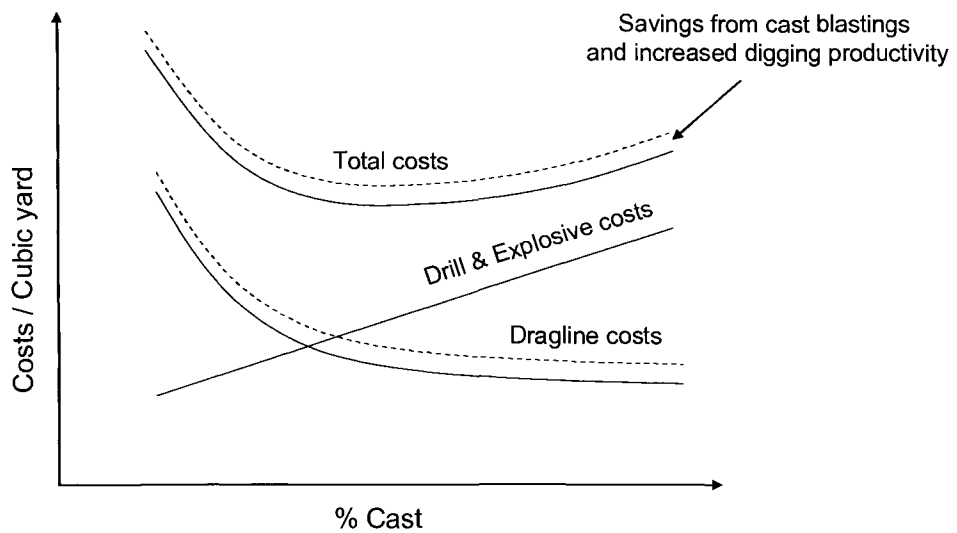

Figure 8 Economic analysis of cast blasting

Operation research optimization performed by Favreau (1994) using computer modeling showed that cast blasting reduces digging costs even more than might be expected just from reduced quantities of overburden that needed to be moved by a dragline. The further savings stem from the fact that overburden which has been strongly broken and displaced by the blast is more easily dug, so that the dragline has higher productivity and less wear thereby reducing the costs of displacing even the material which still has to be handled by the dragline (Figure 8). The quantitative analysis showed that savings from adopting cast blasting and its associated increased digging productivity in terms of total mining costs per BCM of excavated overburden is around 6%. Given that overburden removal is the largest cost component in mining the coal, the savings can be significant. Furthermore, a reduction in use dragline or shovels can sometimes mean that a mine can avoid or delay buying an additional dragline/shovel which is beneficial to overall cash flow.

The use of cast blasts in overburden removal is not limited to strip coal mining. Since many similarities exist between geological characteristics of overburden formations in coal seams and phosphate beds, some studies showed the applicability of cast blasting in mining multiple-bed phosphate ores with high overburden-to-ore ratios (Taqieddin, 1997).

The correct design of the cast blasting parameters is important to the performance of the blast. Cast blasts are designed to maximize the amount of overburden cast directly into a final spoil position (Figure 9). The objective is to leave less blasted material that needs to be transported with mechanical equipment, which reduces the total cost of mining. According to Petrunyak & Postupak (1983) up to 65% of the blasted overburden can be moved from a highwall to the spoil side in a cast blast, with only the remaining portion requiring removal by mechanical equipment. This can reduce the overall coal production costs by up to 35%. The explosive energy should be utilized in a way to move the overburden across the pit. The efficiency of a cast blast is a measure of the overburden volume thrown by the blast over the pit floor to the spoil pile as a percentage of the total volume of blasted overburden.

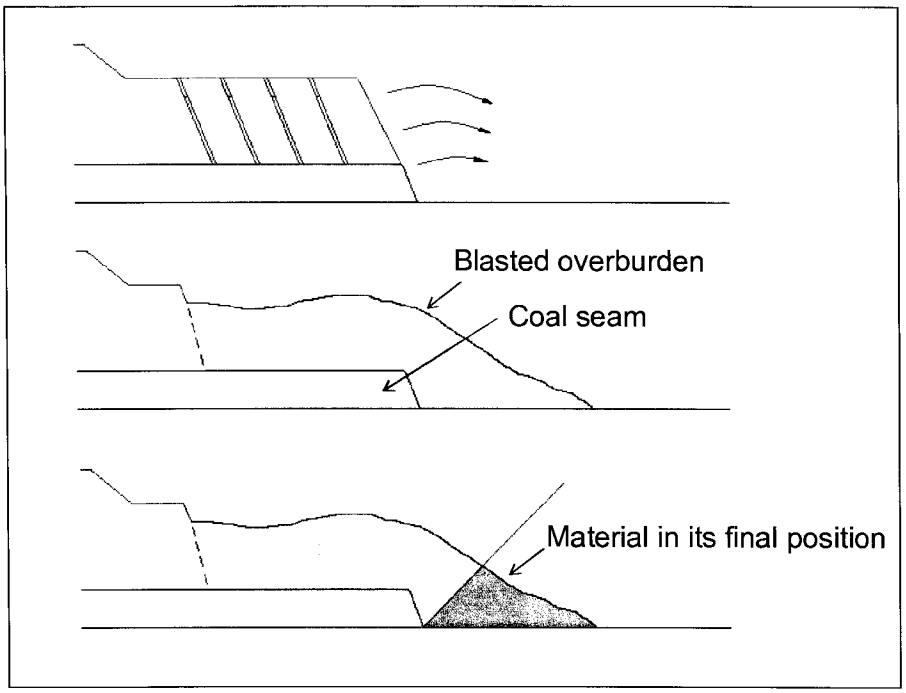

Figure 9 Cast blast sequence

Since draglines are the machines with high costs per hour of operation, it is clear that they can be considered as low-cost excavators of overburden only if high productivity is achieved. Workman (1995) showed that a dragline's productivity increases with greater fragmentation, so the cast blast shots should be designed not only to provide excellent displacement, but also to both improve fragmentation of material that is left behind for dragline removal.

In some cases, when a mine experiences higher than normal stripping ratios for a period of time, cast blasting may become necessary in order to move sufficient overburden to meet contractual commitments for coal delivery. Under this circumstance, overburden removal cost becomes a secondary factor because the costs associated with failure to deliver can be larger (Workman, 1995).

2.3.1 Cast blast design

Cast blast designs are largely based on local experience and experimentation as well as comparison with methods in use at other mines. Cast blast efficiency depends on the blast design linked to the pit geometry and height to width ratios. The wider the pit is,

the less effective a cast blast is in moving overburden into its final position (Martin & King, 1995). Cast blast designs consider the following elements:

Explosive selection: Explosive products are selected to meet basic site specific criteria, to maximize safety, and minimise costs. Ammonium nitrate and fuel oil (ANFO), emulsion for wet holes, and ANFO/emulsion blends are used throughout the coal industry. Highvale Mine frequently has wet holes but rather than using relatively expensive emulsion, they use blasthole liners and ANFO to minimize the explosive costs. Casting requires more energy input to the bank than is needed when material displacement is not priority, so the ANFO equivalent powder factor is in the range of 0.5 to 0.75 kg/m^3 (Sengstock & Kennedy 1995, Martin & King 1995).

Blasthole pattern: There are a variety of patterns in which the blastholes may be drilled. The staggered equilateral pattern is common at many Australian and American mines. The burden to spacing ratio (B:S) varies with the type of blast and with rock mass properties. For example, at Bulga Coal in Australia, the B:S ratio is 1:1.54 (Goswami & Keith, 2001). At Thunder Basin Coal's Black Thunder Mine in Wyoming, the burden equals 2.5 x the blasthole diameter, and B:S is 1:1.33 (Martin & King, 1995).

Front row location and toe burden: The location of the blastholes at the front row is very important in the cast blast design. To achieve maximum cast effect, adequate velocity off the bench face is required. Excessive toe burden can create confinement for the explosive gasses at the toe region. In such situation, the explosive gasses will try to crater rock upwards creating fly rocks or will enter into the coal seam below mixing overburden materials with the coal. In both cases, the cast blast efficiency will decrease. Highwall presplitting and angle drilling are common methods used to control toe distance and to achieve close to optimal burden over the full face height of the bench (Kanchibotla, 1999).

Blast length to pit width ratio: Better cast blast results are achieved with longer blasts. The presence of corners and the contact between the blasted and unblasted pit section are proportionally more significant for short lengths of blast section and reduce the overall cast efficiency. A longer blast section yields a more uniform blast profile. The optimum

design length for maximum cast efficiency should be 3 to 6 times the pit width (Workman, 1995).

Highwall height to pit width ratio: The highwall height to pit width ratio is very important to successful cast blasting. In shallow overburden pits (less than 18 m), the cast effectiveness is reduced, especially for wide pits. According to Workman (1995) cast blasting is not very effective if the overburden depth to pit width ratio is less than 0.6. A value greater of 0.8 is preferred for best results.

Delay timing: Adequate delay between detonation of successive rows of blastholes is essential to giving the burden time to be displaced away from the highwall by the explosive gases. The optimum delay depends upon the rock mass characteristics of the overburden rocks. To prevent cut-offs and misfires, down-the-hole delays are usually required when cast blasts are designed.

Presplitting: The use of presplitting helps to form a stable and safe highwall as well as reducing ground vibration experienced behind the highwall when the cast blast is fired. When creating a highwall at a steep angle by using a row of presplit blastholes, the front row burden for the next cast blast will be constant from crest to toe. This will improve the subsequent cast blast efficiency.

Blasthole depth: An inevitable trade-off using cast blasting in strip mining is an increased risk of damage to and contamination of the underlying coal. The coal loss associated with cast blasting must be considered when evaluating the economics of the blast. However, according to Martin & King (1995) the average increase of coal loss of 1.0% to 1.5% due to the use of cast blasts is overcome by the overall economic benefits of the cast blast. To minimize damage to the underlying coal, the toes of blastholes used for cast blasting are typicaly designed to be about 1 to 2 m above the coal seam.

2.3.2 Cast blast efficiency

Cast blast efficiency can be measured using different methods and tools. Percentage of the blasted overburden cast into its final resting position on a spoil pile is probably the

most universal definition of cast blast efficiency because clearly delineates the effectiveness of the casting effort. The cast blast efficiency E is defined as:

$$E = \frac{V_c}{V} \times 100 \qquad \text{Equation 1}$$

where V_c is the volume of the overburden cast into its final position on the spoil pile and V is the total volume of overburden involved in the blast.

At Highvale Mine, a surveying crew performs ground measurements on a regular basis to measure the cast blast efficiency. The ground representation of the pit section before and after a cast blast is created in computer drafting software. A pre-blast survey typicaly consists of 50 to 60 discrete ground points. The coordinates of the specific points, located at the bench crest, bench toe, spoil toe and spoil pile, are measured using a Trimble 5800 GPS receiver unit and mobile Concord Laser. A similar survey is performed soon after the blast, when approximately the same number of characteristic points of the overburden pile is measured. All points are stored into the GPS receiver and later exported into the computer software. AutoCad is used to generate cross-sections every 25 m across the blasted section of the pit. Volumes are computed using an end-area method (Kavanagh & Bird, 1989), while the efficiency of the blast is defined as a percentage of the material placed into the final location versus the total volume of blasted overburden. The cast blast efficiencies calculated using this technique at Highvale Mine Pit 2, Cuts 76 and 77 have been in the range of 17% to 36% (Oldach, 2006).

3 Photogrammetric Technique

3.1 Project workflow

A general description of the methodology and concepts used in the research are given in the flow chart in Figure 10. Prior to starting the fieldwork it is essential to plan the fieldwork so that delays or possible re-shooting of the images are avoided. The process to generate terrestrial models based on captured images involves two distinct procedures:

- field work, where image pairs are captured and the positional data are gathered, and
- processing of images, using Adam Technology's software package.

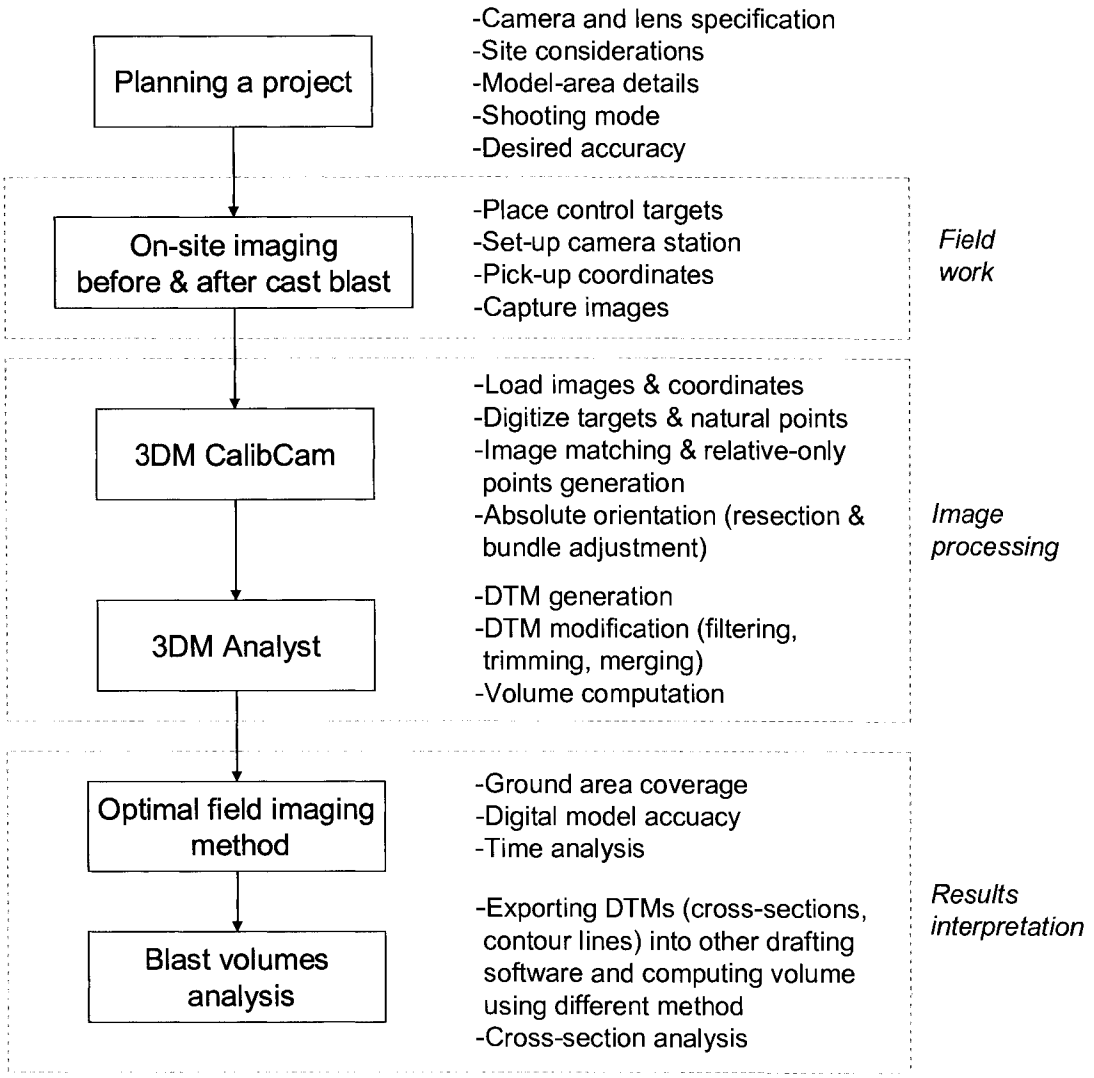

Figure 10 Project workflow

3.2 Camera and lens

All photographs were taken with a Canon EOS 1Ds Mark II digital camera (Figure 11), which is considered the best 35 mm digital single lens reflex camera on the market. The camera is equipped with a full-frame 36 x 24 mm 16.7 mega pixel CMOS sensor. Size of each pixel on the sensor is 7.21 x 7.21 μm. Further technical specifications for the camera are provided in Appendix E. All images were captured using the maximum provided resolution of 4992 x 3328 pixels in RAW format. The images were converted to 50 megabyte uncompressed TIFF files at 24-bit colour depth.

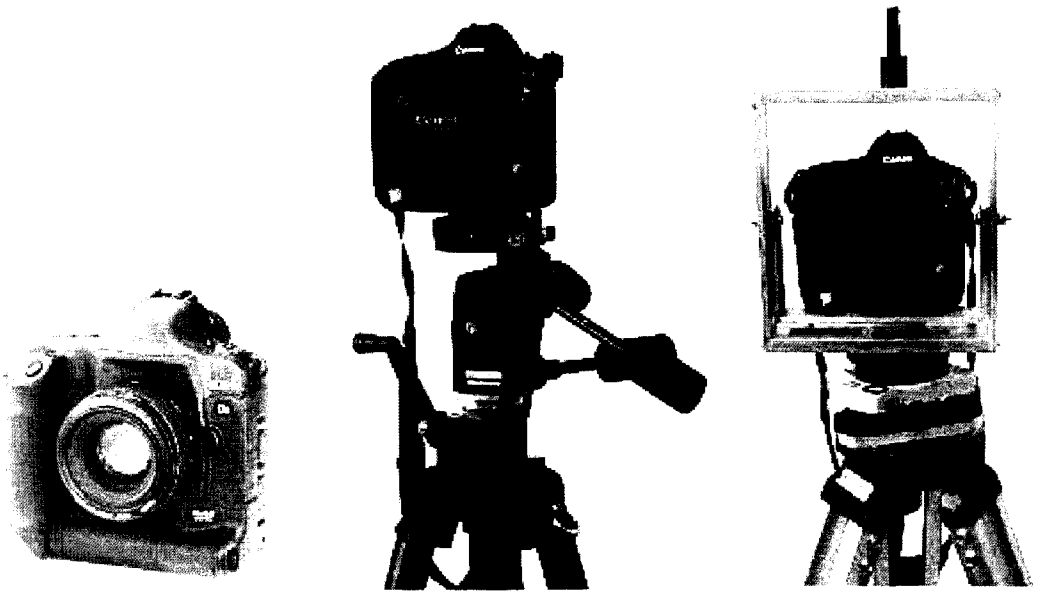

Figure 11 Canon EOS 1Ds Mark II, photographic tripod, and camera frame & surveying tripod

A Canon EF 35 mm f/1.4L USM lens was used on the Canon camera. Further technical specifications for the lens are provided in Appendix E. According to tests performed by Castleman (2005) this lens is free of significant linear distortion and possesses good central image sharpness with no central chromatic aberration. Significant coma in edges of the field occurs in applications when the aperture is set at f1.4 or f2.0. By stopping the lens down to f2.8 or more this effect can be almost completely corrected.

To maximize the accuracy of the digital terrain models generated from captured images, it is important to choose optimal camera and lens settings, and to ensure that these settings remain constant at all times. All images acquired at the Highvale Mine were

captured with fixed camera optics settings. The aperture, which controls the amount of light entering the lens, was set to f8.0. This aperture results in the sharpest image. At larger apertures (smaller f-stops), the image will lose sharpness due to lens aberration, while at smaller apertures (larger f-stops) the image will lose sharpness due to light diffraction (Adam Technology, 2004d).

While a fixed focal length lens was used to acquire the images, the true focal length of the lens does vary slightly as the focus on the lens is changed. Since the true focal length is one of the most important parameters when conducting photogrammetry work, the focus on the lens was manually set to infinity for all photographs. Given the object distances in the field were greater than 15 m, a focus set at infinity was appropriate for this lens.

The camera/lens combination was previously calibrated at the University of Alberta as a part of another research project. The 35 mm lens was calibrated for three different distance/base ratios 2:1, 3:1 and 7:1. The pit geometry and restrictions on locations for setting up the camera stations created distance/base ratios that were compatible with two of the three calibration files that were available (7:1 and 3:1 distance-to-base ratios) and these were used when processing the images. These elements of interior orientation determined during the calibration process are given in Appendix A.

3.3 Camera setup

The 3D spatial coordinates of the camera's focal point or camera/lens projection centre are required in order to process the images using the photogrammetry software. Before capturing images, the location of the camera was determined using a Trimble 5800 GPS receiver. Highvale Mine has its own GPS base station that provides error correction enabling the GPS receiver to measure coordinates with an approximate error of ±20 mm. Images of the pit were captured from camera locations on the bench crest and spoil side of the pit. The first four cast blasts were photographed using the camera mounted on conventional photographic tripod (Figure 11), while fifth and sixth blasts were captured using an aluminium camera frame (Figure 11) mounted on a survey tripod. The camera

frame was specially designed and built for photogrammetric applications. Both camera and frame can be easily levelled and rotated around a vertical axis, which provides operational convenience and time savings. At the top of the camera frame is an attachment hook for the GPS receiver.

In cases where images were captured with a conventional tripod setup, the coordinates of the camera perspective centre were determined indirectly. First, the absolute coordinates of the ground point that falls directly under the perspective point were determined using the GPS receiver mounted on a rod. The vertical distance between the ground point and the camera focal point was measured and added to the ground point elevation to obtain the elevation of the camera perspective centre (Figure 12).

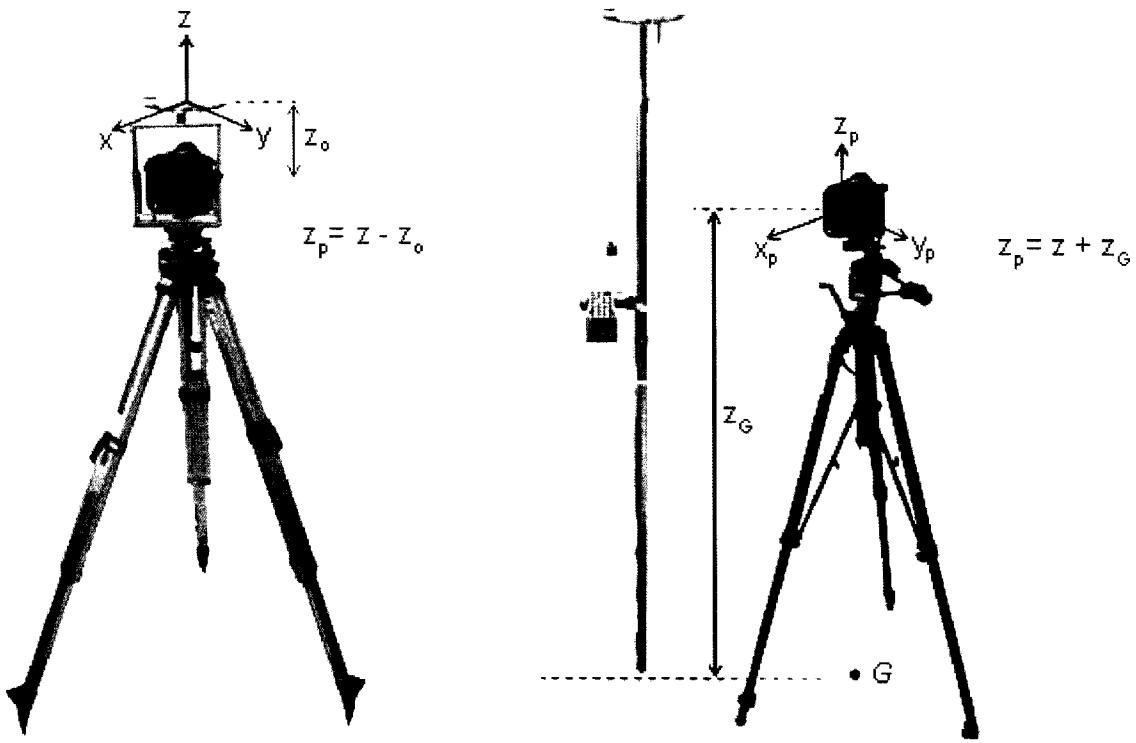

Figure 12 Camera setup and elevation of the lens nodal point

For the setup when the camera was mounted on the aluminium camera frame and the surveyor tripod, the camera coordinates were determined from the GPS receiver attached directly above the camera on top of the frame. The final elevation of the camera perspective center was obtained by subtracting a vertical offset distance from the *z*-

coordinate GPS reading (Figure 12). Compared to the conventional photographic tripod, this technique has the following advantages:

- Less time spent for each camera setup as there is no need to measure the vertical camera-ground distance since the vertical offset is a constant value, and can automatically be subtracted from the GPS elevation readings.
- Better overall accuracy, since there is one less measurement.
- Using the bubble level on the surveyor tripod, the camera can be oriented around a vertical axis that helps when taking fan shots.

The best results in generating 3D models during the post-processing phase can be achieved if the photographed area is close to perpendicular to the camera axes, which is the case for the pre-blast images (Figure 13). In this application, the bench face forms roughly a flat plane oriented perpendicular to the lens axis.

Figure 13 Camera located at the spoil pile

The photographs taken after the cast blasts involved taking images of muck piles that were spread between the highwall and the spoil pile. The cast blasted overburden is thrown by the explosive energy to the pit floor and spoil side of the pit, while a considerable portion of the material volume remains at the bench side. In general, the bulk of blasted overburden creates an irregularly shaped pile covering the bench, pit floor

and spoil side areas (Figure 14). The muck pile surface was far from being perpendicular to the lens axis and this creates problems as will be discussed later.

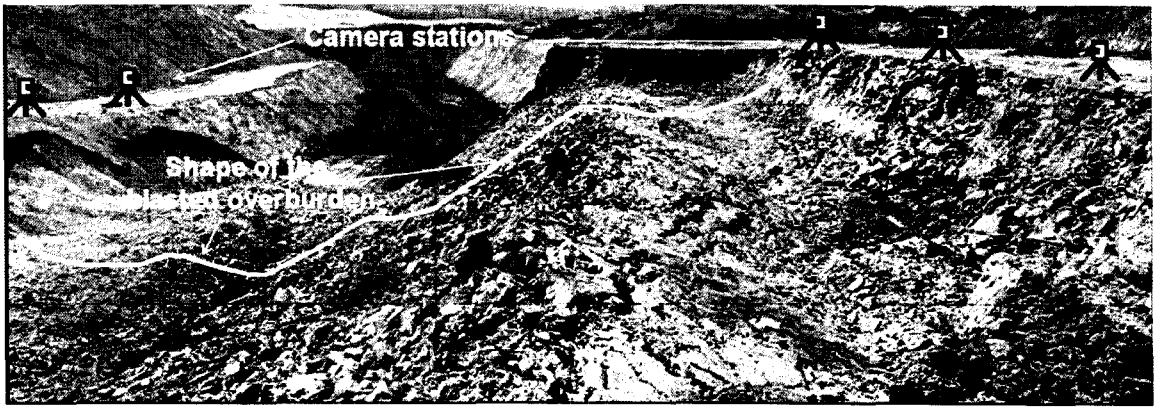

Figure 14 Shape of the overburden muckpile

3.4 Control targets

The simplest way to establish the relationship between the images and a mine coordinate system is to supply the 3DM CalibCam software with 3D coordinates of a series of object points in the images, known as control points. Circular white targets were used for the control points and their coordinates were determined using a GPS survey. The coordinates of the target centre were determined indirectly through the coordinates of the underlying ground point (Figure 15). The use of surveyed targets allows the coordinate system used by the Highvale Mine to be integrated into the image models and generated DTMs. The target coordinates are stored in an ASCII file with each control point defined on a separate line.

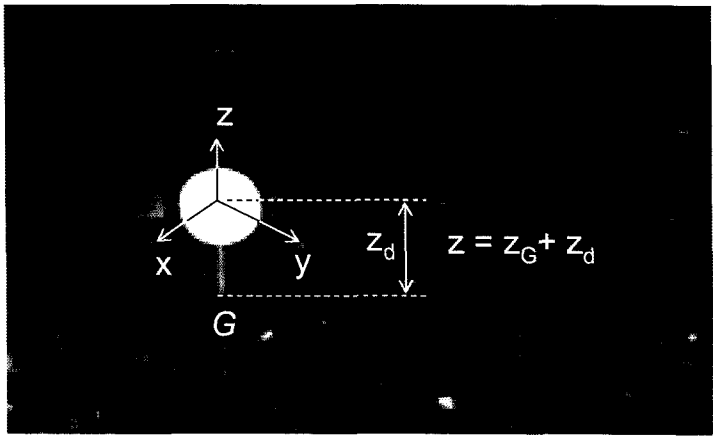

Figure 15 Control point coordinates and elevation correction

To ensure that at least one control target was captured on each pair of overlapped photos, 8 to 10 targets were spread around the imaged site area. Control target placement was dependant upon the site accessibility. Figure 16 shows some targets placed in the field. Typical locations for the targets were on the

- bench crest, so they are visible from the spoil side of the pit,
- spoil piles, so they are visible on images taken from the bench, and
- pit floor, which was the most optimal location since the same targets are included in images acquired from both sides of the pit.

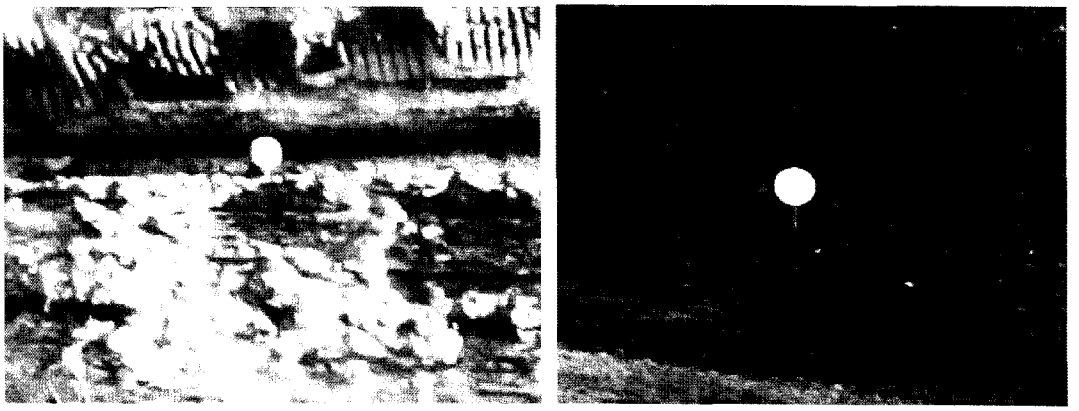

Figure 16 Control targets placed on the bench crest and pit floor

The centre of the target on images was determined with sub-pixel accuracy in the photogrammetry software. The use of a white circle on a contrasting background enabled 3DM CalibCam to locate the centre of the target very accurately (within 1/10 of a pixel) using special centroiding algorithm. It is required that the entire target should occupy a

width and height of at least 30 pixels on an image (Adam Technology, 2004b). The minimum size of the target for use in the field is calculated using:

$$T_s = 16 \times PS_g \qquad \text{Equation 2}$$

where,

T_s is a diameter of the circular target in centimetres, and

PS_g is the pixel size on the ground in centimetres.

3.5 Image acquisition modes

In order to generate a digital model of the terrain surface, the photogrammetric software requires a pair of images called models (Figure 17). The image pairs must overlap each other to create the digital model. Ideally, the camera axes should be parallel or slightly skewed to preserve point correlation between the images. The ratio between camera base separation and object distance is also important for the correlation between images. For successful digital model generation, it is desirable for the photographed object to be oriented roughly perpendicular to the camera axes. For objects that posses large depth of the field, the object distance is calculated as average value for nearest and furthest object points.

Photogrammetric software requires a network of control points (targets) in order to provide ground orientation to the models. The control targets should be stable and clearly visible and facing directly to the camera without obstruction. Even though the recommendation is to use minimum two control points per model if camera station coordinates are known (Adam Technology, 2004b), additional targets will increase redundancy and stabilize the models.

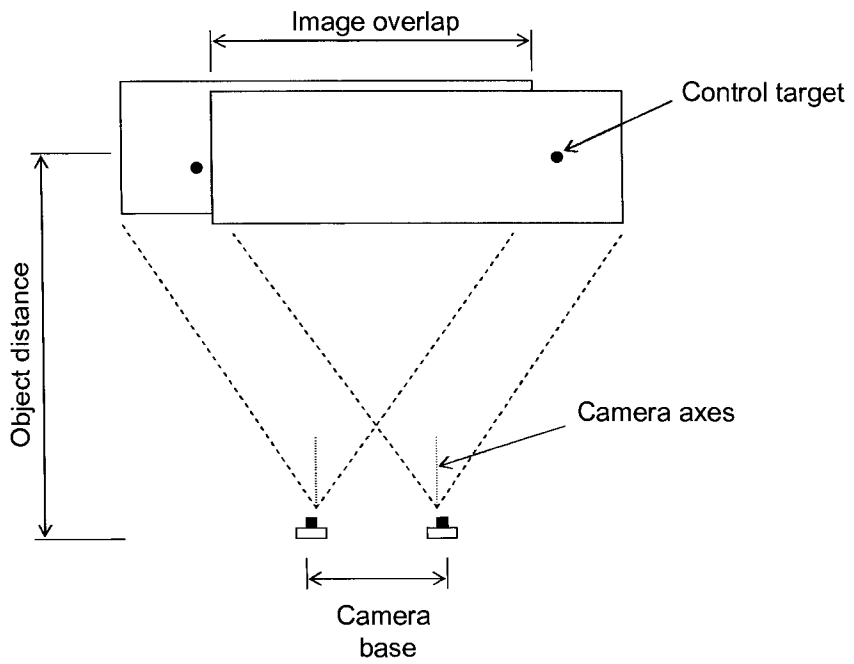

Figure 17 Image pair elements

To generate a DTM from acquired images, the fundamental photogrammetric requirement is that the same scene appears on at least two distinct images taken from different locations. If the camera is pointed roughly at the same object with almost 100% overlap in the image area for the two images, the method is known as a convergent photography (Figure 18).

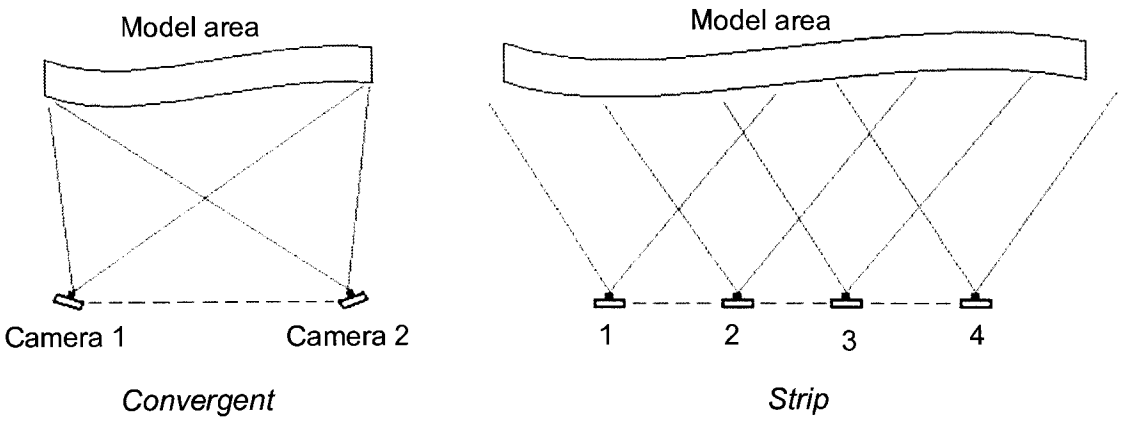

Figure 18 Convergent and strip shooting modes

For larger terrestrial applications, like photographing bench faces or stock piles where the width of the area of interest is large, the alternative approach is to capture the images in a

strip mode (Figure 18). In this mode, the camera axes are approximately parallel to each other and at the same time orthogonal to the object. Each image should overlap the image before and after in the strip for approximately 60% in horizontal direction (Figure 17). The desired 60% overlap ties all of the images together and allows orientation information to be spread along the strip without requiring each model to have a control point (Adam Technology, 2004c).

Another technique that allows multiple images to be captured from one camera station and merged together into one panoramic image is called fanning (Figure 19). This method of covering large terrestrial areas from only two camera stations became possible with the release of 3DM CalibCam v2.2, which allows merging of multiple images from a single camera location. CalibCam version 2.2 was released after the 3rd cast blast was photographed, and hence the technique used for the subsequent cast blasts took advantage of this feature. This is advantageous as it reduces the number of camera stations and therefore reduces the time spent capturing images.

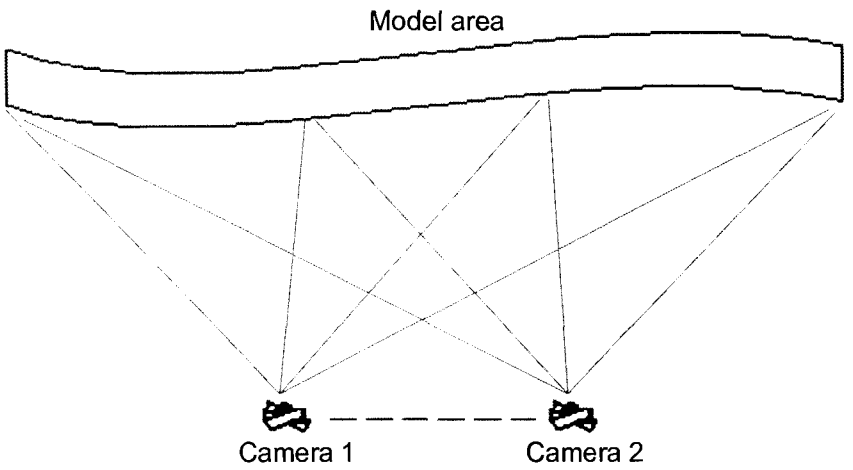

Figure 19 Fan mode

3.5.1 Strip mode

The number of camera stations and photos (one photographic image corresponds to one camera location when using the strip mode) needed to cover the whole area affected by each cast blast was determined using an object distance calculation spreadsheet (Adam Technology, 2004e). The typical object distance was 95 m when acquiring the images.

For this object distance, the ground coverage area obtained for the 35 mm lens is 98 x 65m. Using the recommended overlap between images of 60%, the size of one model (overlapped image pair) on the ground is:

$$H_o = 0.6 \times G_w \qquad \text{Equation 3}$$

Where,

H_o is horizontal overlap on the ground in metres, and

G_w is ground coverage of image (width) in metres.

The minimum number of subsequent photos in the strip can be obtained from:

$$I_s = \frac{W_a}{G_w \times \left(1 - \frac{60}{100}\right)} + 1 \qquad \text{Equation 4}$$

Where,

I_s is the number of images per strip, and

W_a is the width of the pit affected by the cast blast.

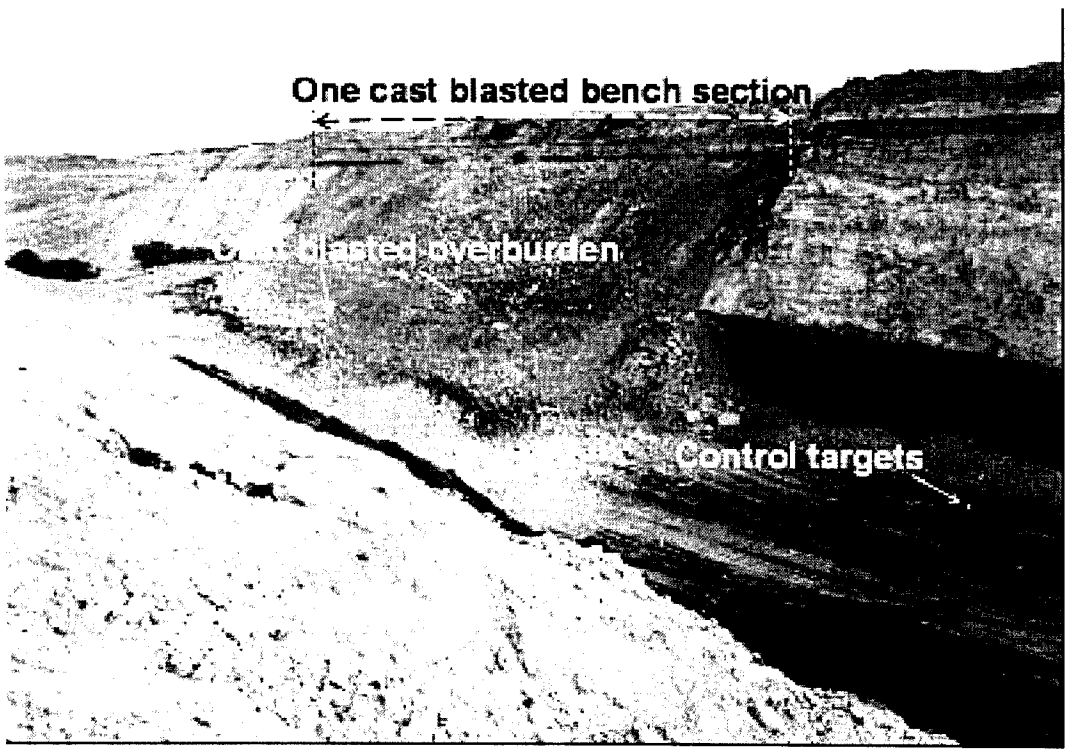

Figure 20 Typical cast blasted section

This relationship is plotted in Figure 21 for two different lenses.

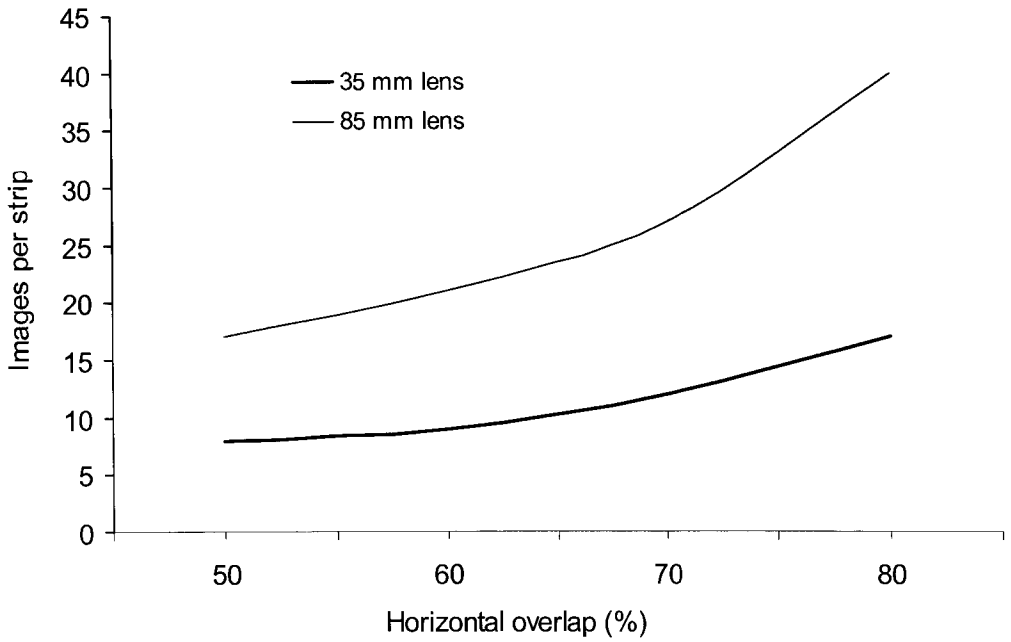

Figure 21 Number of images in a strip for 60% overlap assuming 95 m object distance and 310 m area width

Camera separation distance B can be obtained from the following equation:

$$B = G_w \times \left(1 - \frac{60}{100}\right) \qquad \text{Equation 5}$$

where ground coverage of image G_w depends upon the ground pixel size PS_g and the total number of pixels on the camera sensor N_p:

$$G_w = N_p \times PS_g \qquad \text{Equation 6}$$

At the distance of 95 m using a 35 mm lens, one pixel size of 7.21 μm will cover a terrain area of 19.6 mm.

Figure 22 shows how the camera base distance and the number of images are dependent upon the object distance.

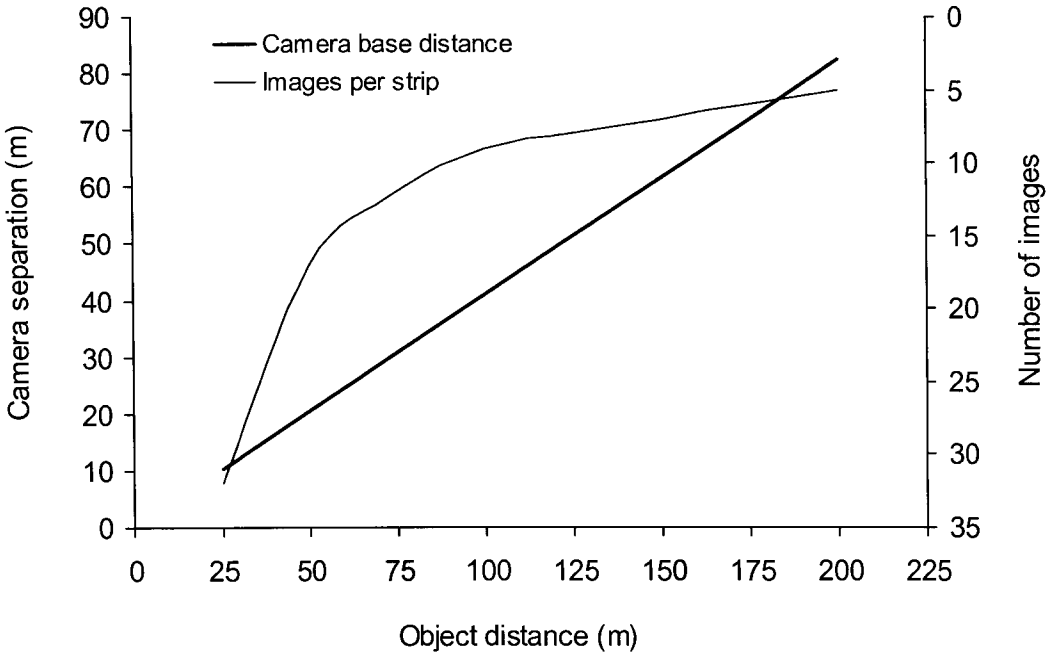

Figure 22 Horizontal parallel photos – strip mode

3.5.2 Convergent and fan modes

Another camera set-up mode used in acquiring images of the highwall and the muck pile is the convergent mode. In this mode, a single digital model is developed from one pair of overlapped images taken from two camera locations (Figure 23). Camera axes are inclined and pointed at the same object location. The photogrammetric software can cope with inclination angles of up to 30°. At higher inclination angles the ability to successfully match features in each image reduces significantly which results in no 3D points formed over unmatched areas.

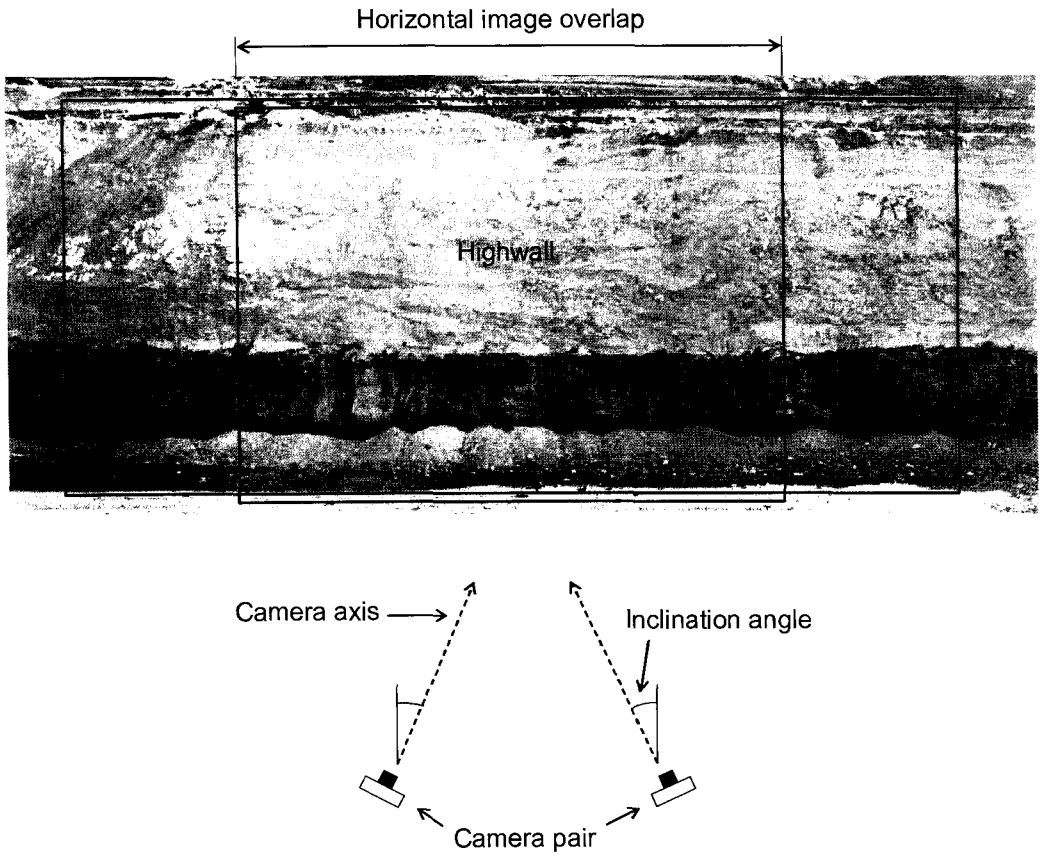

Figure 23 Camera stations for convergent mode

The required number of convergent camera pairs (models) and the optimal camera station separation distance were determined for an object distance of 95 m and 40 m. The results are given in Table 2. For a 95 m object distance, the camera base distance can vary from 36 m for 10° inclination angle, up to 110 m for 30° angle. According to instructions and recommendations provided by Adam Technology (2004b), the object distance should be no less than 3 and no more than 10 times the base distance. Considering that the furthest object points were expected to be located around 150 m away from camera and the closest were about 40 m away, the camera pair separation should be within a range of 15 to 35 m. This camera base distance range should be suitable for capturing and matching all points lying within a depth of the field from 40 to 150 m.

Table 2 Multiple convergent shooting mode camera separation distances

Camera-to-object distance: 95 m			
Inclination angle	Camera separation (m)	Horizontal overlap (m)	Number of models required for 300 m long terrestrial area with 10% overlap
10°	36	91	3.5
20°	70	93	3.4
30°	110	101	3.2
Camera-to-object distance: 40 m			
Inclination angle	Camera separation (m)	Horizontal overlap (m)	Number of models required for 300 m long terrestrial area with 10% overlap
10°	15	38	9.6
20°	29	39	9.4
30°	46	42	8.5

To capture large terrestrial areas like the extended highwall and spoil piles it is necessary to use multiple convergent models with at least 10% overlap between models (Adam Technology, 2004a). Therefore, at least four pairs of camera stations are required for capturing a highwall face length of 300 m at an average object distance of 95 m. To ensure that object points located closest to the camera will also be covered, the number of camera pairs increases to ten, which greatly magnifies the amount of fieldwork.

The third technique used in acquiring images in the field is the fan shooting mode. The major benefit of this technique is that it allows multiple images to be captured from individual camera stations, which are later merged into one large image. It was necessary to take at least five consecutive images from a camera station to cover the full 300 m long highwall face when using the 35 mm lens at an average object distance of 95 m (Figure 24). Since there are no specific recommendations for calculating the camera base distance when using the fan mode, the criteria and results obtained using the strip and convergent modes were applied. The main restriction of the fan mode is that it is

typically best used when the camera station is located at large distances from the object (Adam Technology, 2004a).

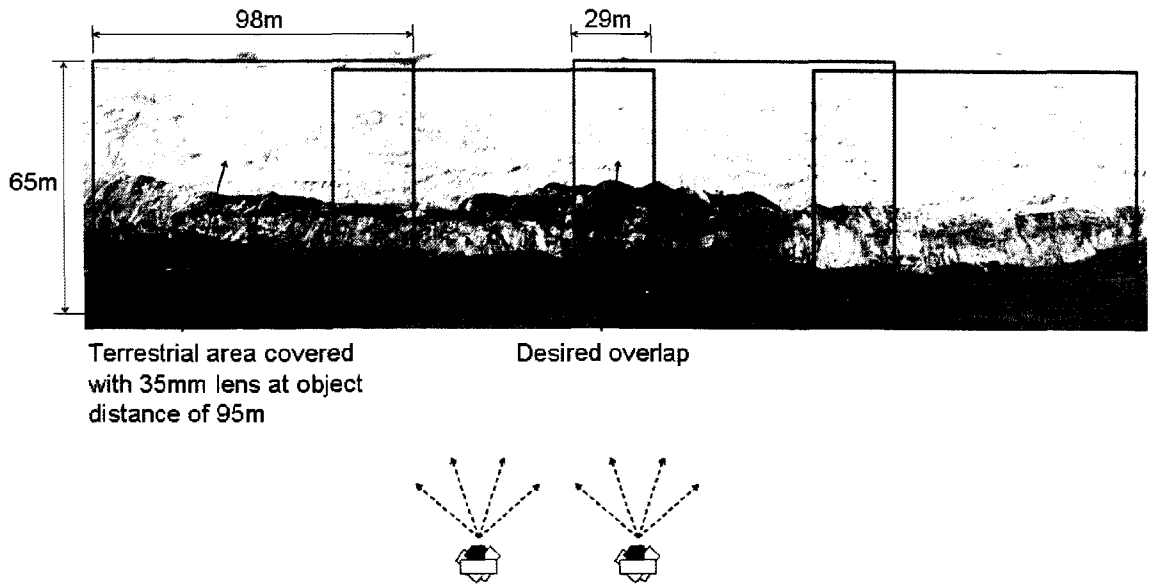

Figure 24 Area coverage using fanning mode

The fieldwork that was conducted at the Highvale Mine was able to partially evaluate the usefulness of all three image acquisition modes.

4 Fieldwork

4.1 Introduction

Digital photographs were taken for six overburden cast blasts in the Pit 2 at Highvale Mine between April and September 2005. The first set of images was obtained in Cut 76 on April 28, and the last set on September 1, 2005 in Cut 77 (Figure 25). A series of pictures of the bench face and spoil side of the pit were taken from known camera locations. Pre-blast and post-blast images were used to generate two types of digital terrain models – one representing the terrain surface before and one after the overburden blast. Optimal data analysis (volume computation and overburden displacement) based on finalized DTMs requires that both models are fully developed and cover the whole blasted area.

The first step in planning the fieldwork is to determine the location of camera setups and the image acquisition mode. Definition of these parameters for the first monitored blast at the Highvale Mine was based on an overview of the field trial performed at BMA's Goonyella coal mine, Queensland, Australia (Adam Technology 3, 2004). The purpose of that trial was to demonstrate the suitability of ADAM Technology's photogrammetric software for pit wall mapping and geotechnical data collection. A digital surface model of a 700 m long pit wall was generated from 108 images captured from 36 camera stations using a 5.9 mega pixel Nikon D1x camera. All camera locations and 52 control points were previously surveyed using a total surveying station.

A similar approach was employed as a starting point for generating the first 3D model of a cast blast section of the pit at the Highvale Mine. The size of the first cast blast section is 310 m long and 35 m high. Parallel photos taken in a strip mode were used. Camera stations were aligned and oriented orthogonal to the opposite side of the pit. The digital terrain model of the spoil side of the pit was generated from photographs taken with the camera located at the bench crest. Similarly, a digital terrain model of the pit wall face was based on images captured from spoil side of the pit (Figure 13).

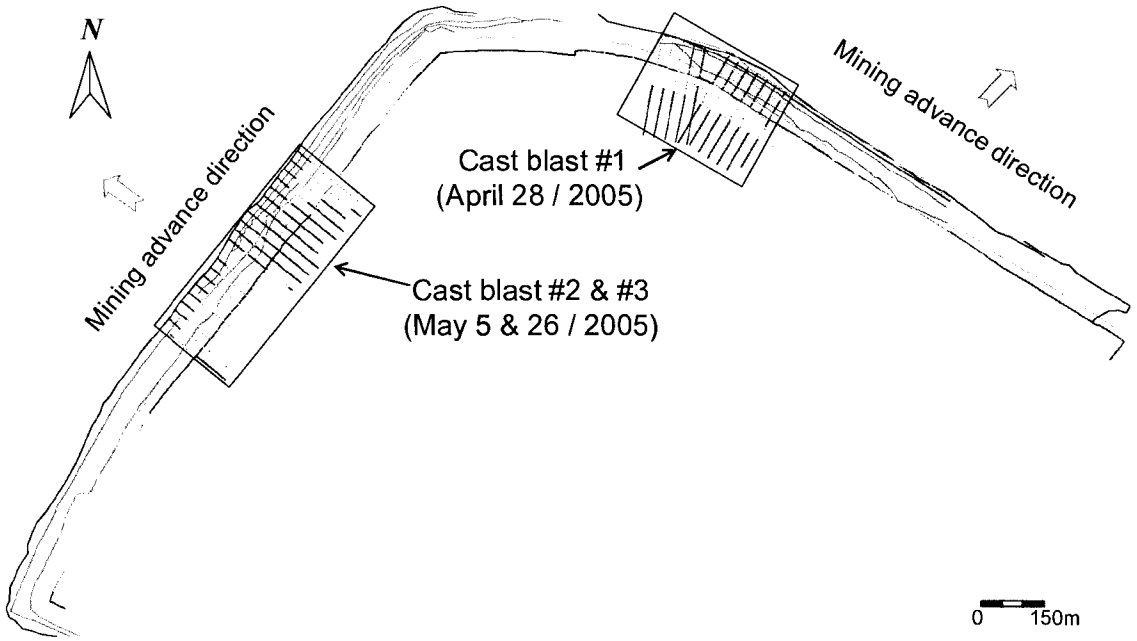

(a)

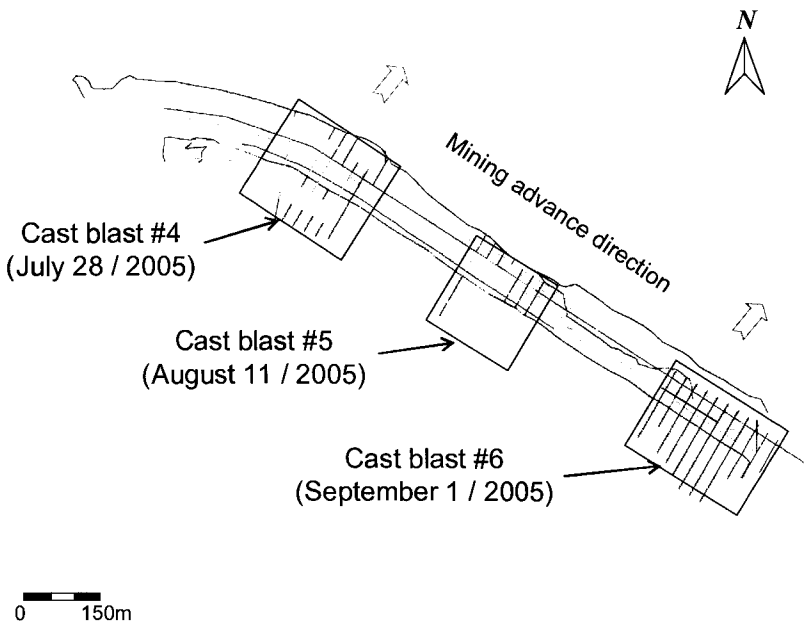

(b)

Figure 25 Highvale Mine Pit 2 (a) Cut 76 and (b) Cut 77

4.2 General cast blast design

The generic cast blast design pattern used in Pit 2, Cuts 76 and 77 will be described using the blast that occurred on May 26, 2005, which can be considered as a typical cast blast

(Figure 26). The specific blasthole pattern is slightly different for each individual cast blast, and is adjusted to suit the bench geometry and pit configuration.

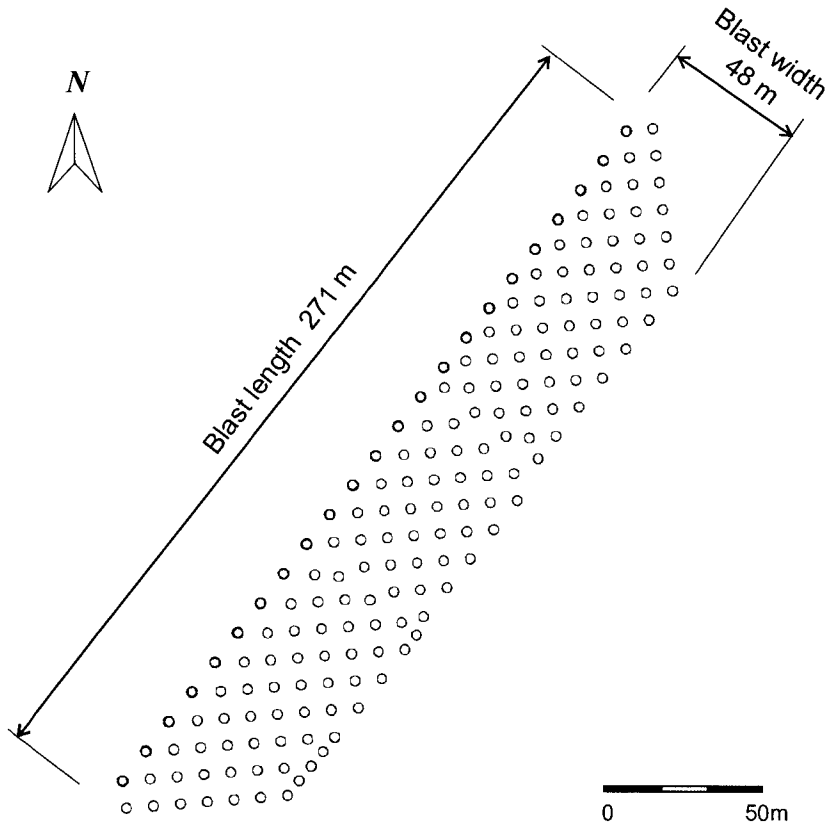

Figure 26 May 26, 2005 cast blast design (blast #3) – plan view

A staggered equilateral drill hole pattern was used. The cut is designed with an overall highwall angle of 55°, while the designed pit width is 45 m. The blast section is 271 x 48 m (Figure 26) and consists of eight rows with 19 to 24 blastholes per row. The blasthole diameter is 343 mm, and hole spacing to burden ratio is 1.9. Figure 27 shows the blasthole burden and spacing.

The blastholes are drilled with a 60° plunge towards to pit, while the last row is drilled with an increased plunge of 70° (Figure 28).

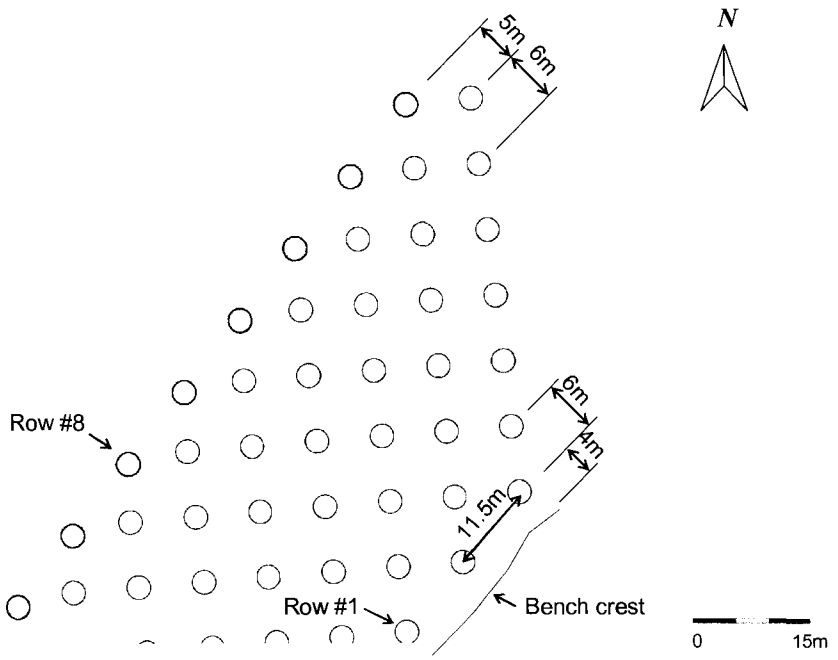

Figure 27 Staggered blasting pattern

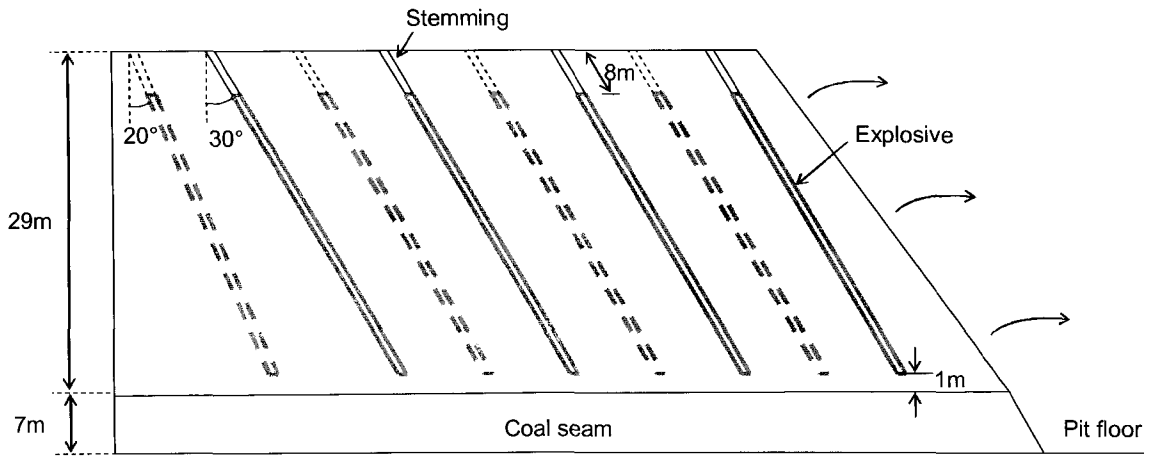

Figure 28 Bench cross section

The explosive used was an ANFO mixture (94% ammonium-nitrate and 6% fuel oil). The design powder factor was 0.625 kg of explosive per cubic metre of blasted overburden. Since all drill holes are wet at the bottom due to ground water inflow, plastic borehole liners were used to keep the ANFO dry. The millisecond delay timing was as follows: 800 ms down-the-hole delay; nine milliseconds delay between holes along a row; and 400 ms delay between rows. The blast was also designed to minimize environmental concerns like ground vibrations, fly rock and noise (Christensen, 2005).

4.3 Cast blast #1

The first cast blast that was monitored using the photogrammetry technique occurred on April 28, 2005 in Pit 2, Cut 76. A summary of the cast blast design is given in Figure 29.

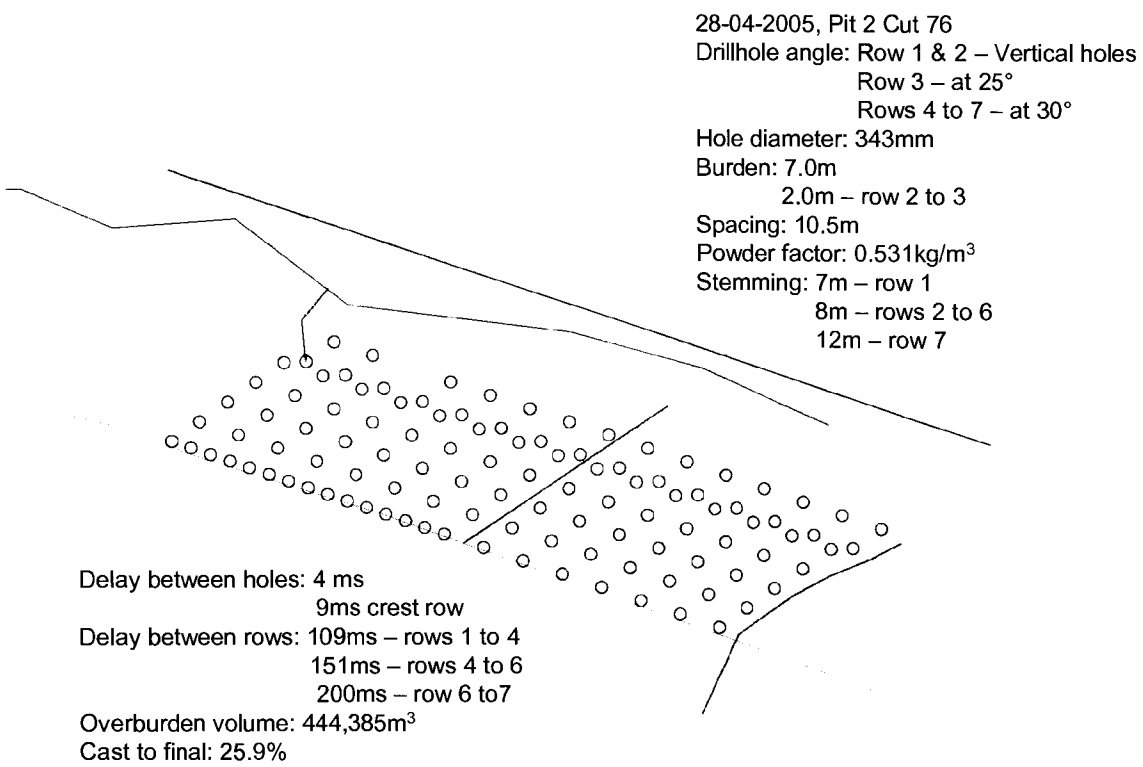

Figure 29 Cast blast design summary – blast #1

The photogrammetric fieldwork used for the first cast blast was guided by the work done by Adam Technology at the BMA's Goonyella coal mine in Australia. A strip mode was used to acquire the images. Two final digital terrain models were built from all captured images. The pre-blast DTM was based on 17 images, nine captured from the bench side and eight from the spoil side of the pit. After generating 15 single models (Figure 30), with an average number of around 40,000 digital points, they are merged together into one single DTM of the pit section.

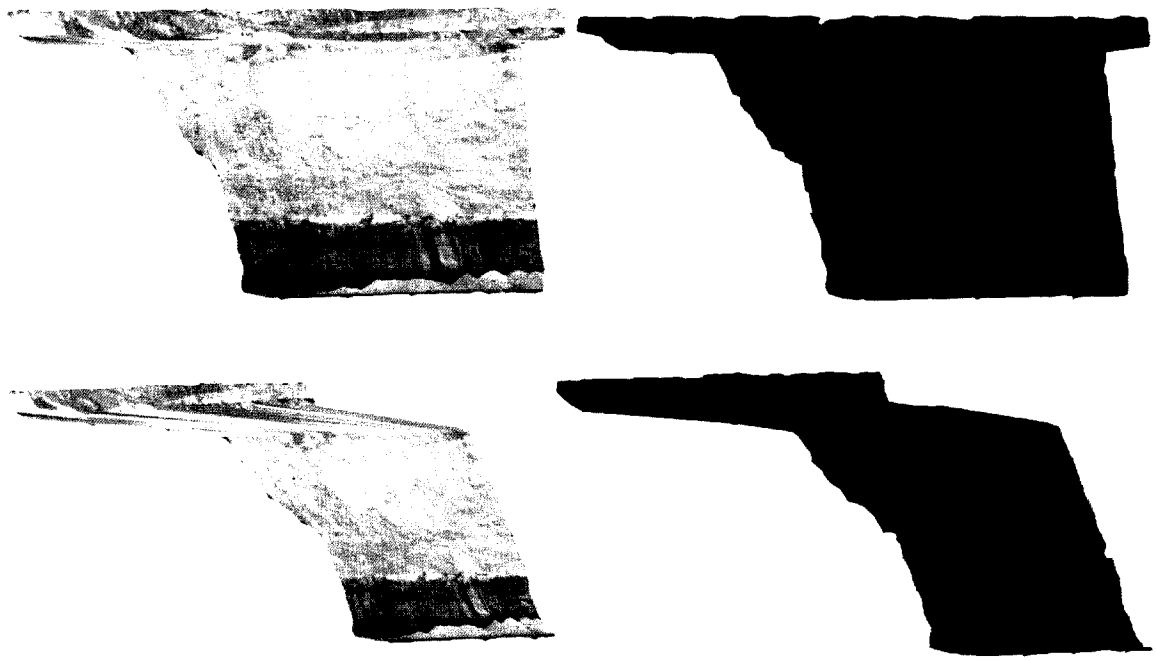

Figure 30 Single DTM model showing textured and triangulated surfaces

The triangulated final DTM (Figure 31) contains around 650,000 points and 1,300,000 triangles which provides reliable surface representation, and covers 100% of the pre-blasted area.

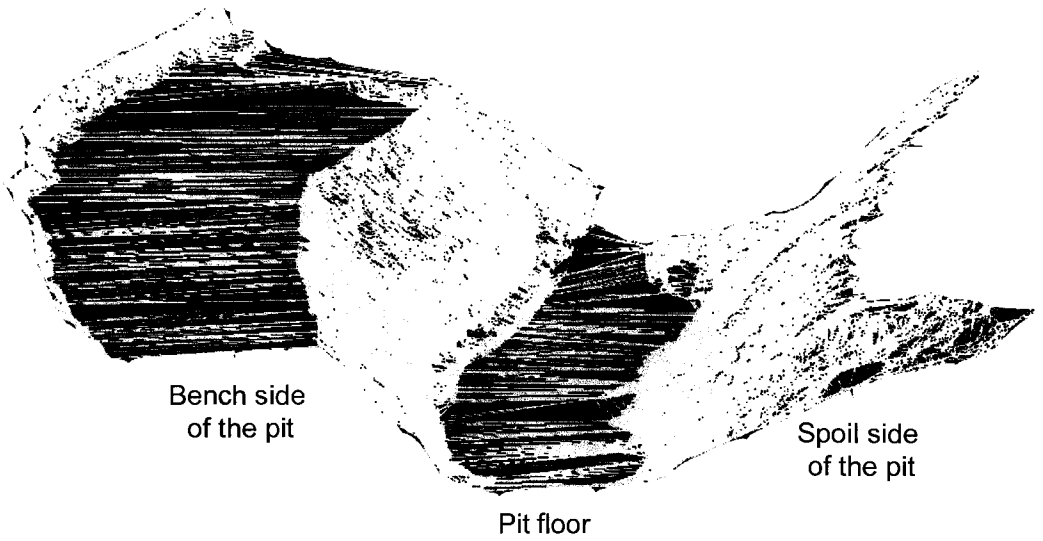

Figure 31 Final pre-blast DTM of cast blast #1

The post-blast model is generated using 18 strip-mode images of the blasted overburden from 18 known camera stations (nine at each side of the pit). Altogether 16 single DTMs were merged into the one digital representation of the pit surface (Figure 32).

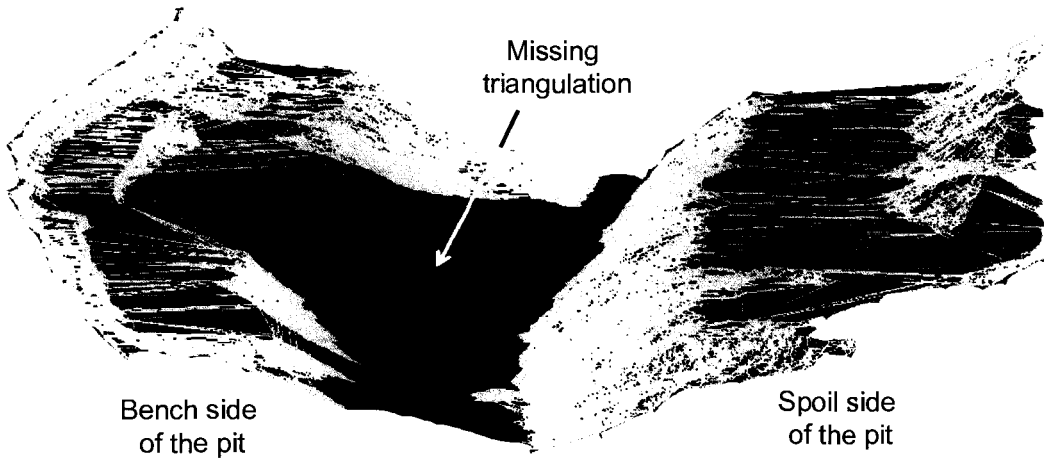

Figure 32 Final post-blast DTM of cast blast #1

The final post-blast DTM consists of 370,000 points and more than 740,000, triangles and covers 61% of the blast-affected area in plan view (Figure 33). Therefore, this model is not good and reliable representation of the pit surface, and can not be used for accurate final volume computation.

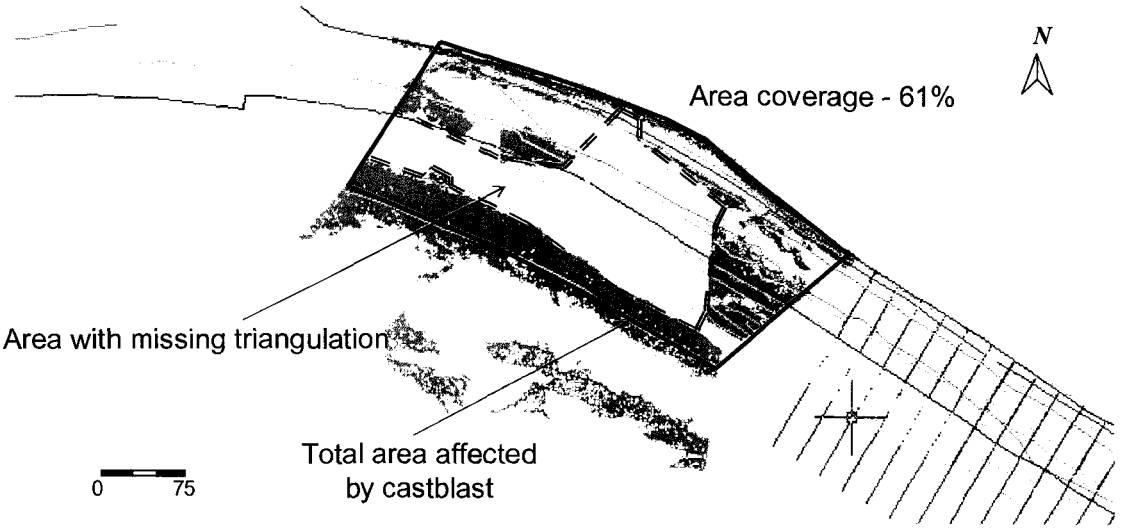

Figure 33 Plan view of DTM points in the post-blast pit section for cast blast #1

The missing points and triangulation in the middle of the pit area has two causes:

- The camera stations were set up too close to the photographed object. This is because of the site limitations and inability to relocate the cameras further and higher from the object.
- The surface of the overburden pile extends across the pit from the last row of drill holes on the bench side to the bottom of the spoil piles. The shape of the pile is irregular and extended, causing a large depth of the field from the new crest to the camera positions.

The problems encountered when trying to generate a 3D model of a relatively flat and spread out pile occurs during the post-processing phase and image matching operation, when software is trying to identify and digitize all natural points that appear on image pairs. When object points are too close to the camera stations they tend to appear more dissimilar on each image. The software algorithm will not recognize object points due to the large parallax angle. This can be compensated somewhat by reducing the default tolerance setting use to automatically identify objects. Objects that are further away from the camera and close to perpendicular to camera axes, like the bench crest, spoil pile tops and other background objects were easily digitized and covered by the triangulation mesh.

4.4 Cast blast #2

The second cast blast that was monitored was also located in Cut 76. Cast blast design parameters are given in Figure 34. The fieldwork for the second cast blast was focused on overcoming the types of problems encountered in processing post-blast images from the first cast blast. This time the pile of the blasted overburden was photographed from the lateral face of the blasted zone (Figure 35). Cameras were set up on the bench and spoil side, and pointed toward the pile of material. Shooting was performed using a convergent mode, where overlap between left and right photos is close to 100% and camera axes are not parallel to each other. Due to site limitations and limited ability to view the whole muck pile, the average camera base distance was reduced to 19 m.

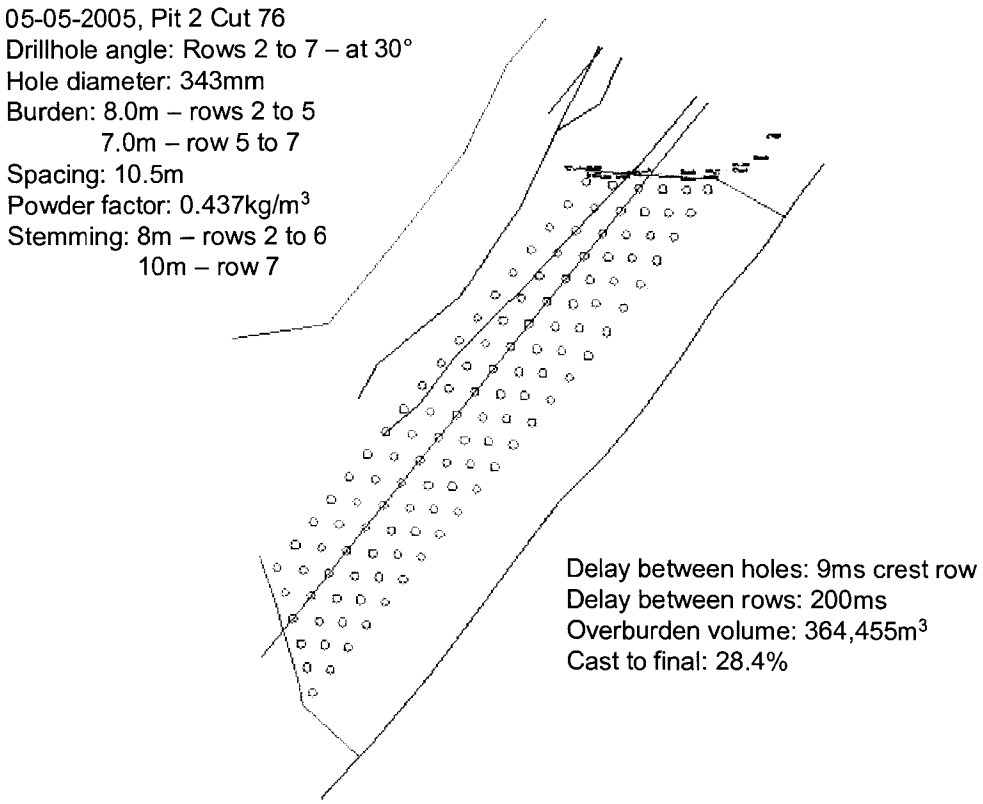

Figure 34 Cast blast design summary – blast #2

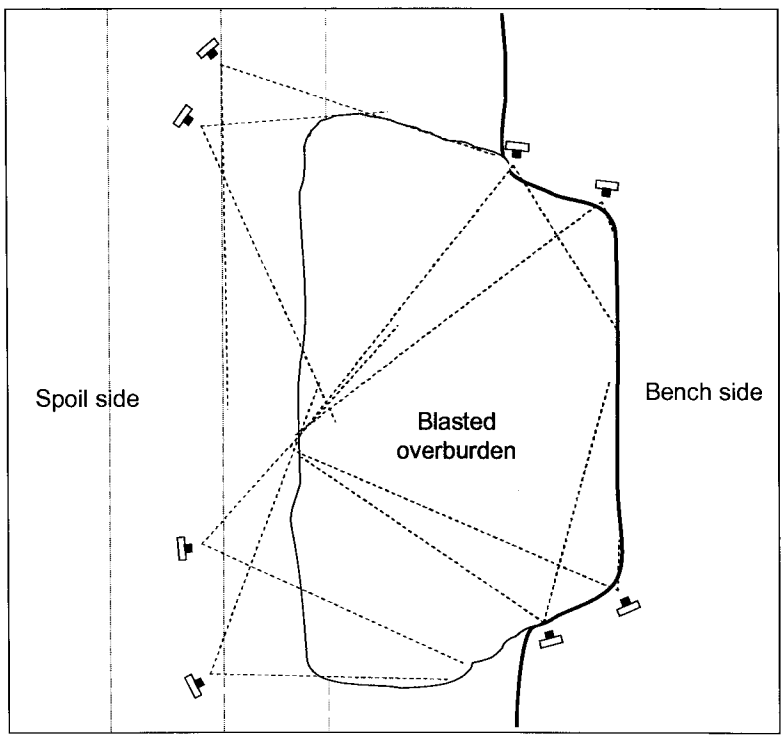

Figure 35 Convergent mode camera setup for cast blast #2

Even though using a convergent mode to capture images of large features is not recommended because of reduced accuracy when approaching the edges of the model (Adam Technology, 2004b), the primary concern during second cast blast was to be able to generate a post-blast DTM that covered the whole pile surface.

Creation of the pre-blast digital terrain model of the pit was again fully successful using strip imaging and the same image acquisition mode used for cast blast #1. Seventeen strip images were used to generate 15 individual DTMs. After merging them together into one single model of the pit, the final surface coverage was 100%.

The post-blast digital model was created using only three camera stations set up in a convergent mode. The final model was based on overlapped images acquired from two camera pairs; combining images from stations C35 and C36, and stations C36 and C41 (Appendix C – Cast blast #2). The images taken from the other camera stations were not usable for DTM generation, because there was poor image correlation in the near-field area of interest. These camera stations needed to be placed further from and higher relative to the blasted overburden but site limitations preclude this option. Two digital terrain models from each good camera pair were merged into one, which covers only 19% of the imaged area (Figure 36). The software was able to generate only those 3D surface points that were located furthest from the cameras stations.

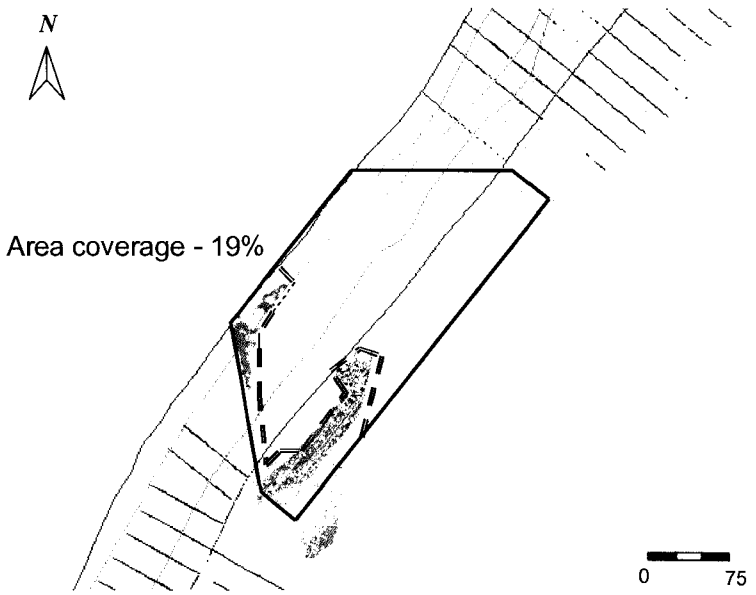

Figure 36 Plan view of DTM points in the post-blast pit section for cast blast #2

4.5 Cast blast #3

The third cast blast was used to test the efficiency of DTM generation using a strip mode to acquire the images but with reduced camera base separation. This trial was based on the method used in the first cast blast where cameras were aligned parallel to each other and oriented orthogonal to a base line. Detailed description of the blast design parameters is given in Section 4.2.

The pre-blast DTM of the pit section was again fully developed using images obtained with a standard strip mode with 17 camera stations and average base distance of 28 to 30 m. For both pre- and post-blast images, the camera separation was reduced 30% from the strip mode settings used during the first cast blast (Figure 37).

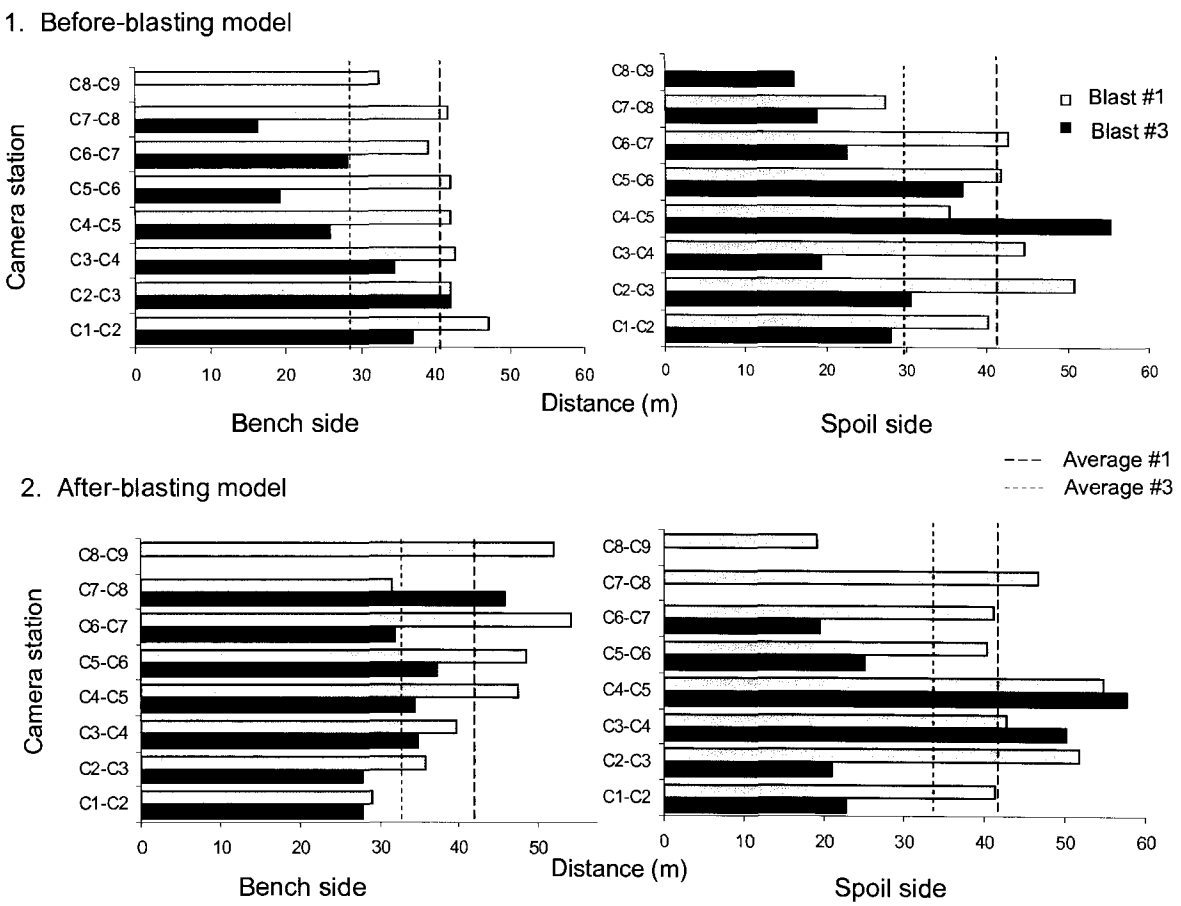

Figure 37 Camera base separation – Strip mode

The reduced camera spacing resulted in much better but still incomplete 3D point and triangulation coverage of the post-blast overburden pile compared to results obtained

from the first and second cast blasts. The post-blasting DTM was generated from 13 merged models from both sides of the pit with average camera separation of 33 m. Processing of the images was not able to generate points or triangulation in the middle portion of the pile located along the length of the blasted section. The post-blast model coverage by the triangulation was 82% (Figure 38).

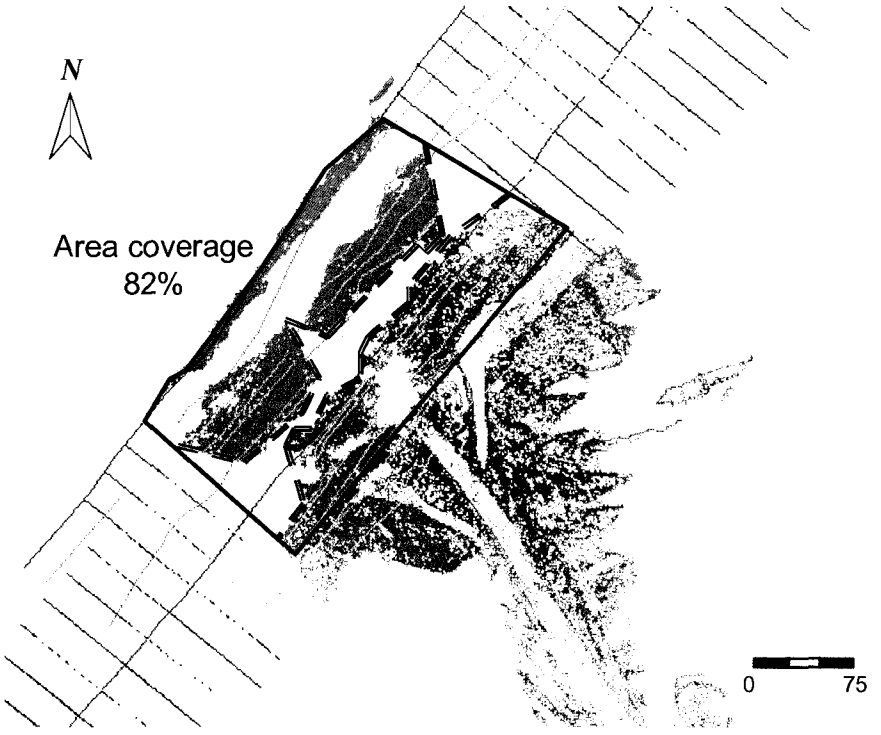

Figure 38 Plan view of DTM points in the post-blast pit section for cast blast #3

4.6 Cast blast #4

The fieldwork for the fourth cast blast introduced the image fanning acquisition mode in an attempt to further increase triangulation coverage of the post-blast overburden pile while also reducing the effort required in the field. The fanning technique allows multiple images to be captured from individual stations, which are then merged into an extended ortho-corrected panoramic image. It was decided to consider this methodology for two main reasons:

- To overcome previous problems with post-blast DTM surface coverage.

- To reduce the time spent at the site. The biggest advantage of the fan mode is that it reduces the number of required camera stations. Therefore, the time spent on camera set-up, surveying, and image capturing decreases.

Cast blast design description and blasthole layout are given in Figure 39.

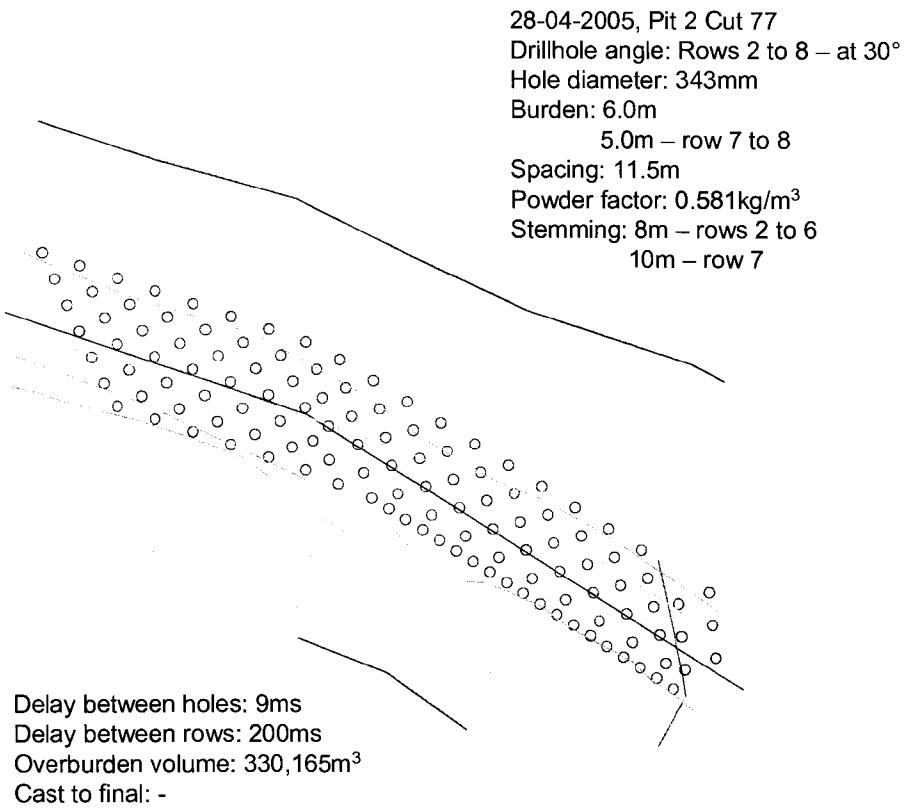

Figure 39 Cast blast design summary – blast #4

The pit surface before the cast blast was captured with a combination of strip and fan modes. The spoil side of the pit was imaged using two camera stations on the bench crest. Cameras were placed 58 m apart, and five images were captured from each station. With 30% overlap between fanning images, five photos was enough to cover nearly 200 m of the spoil side. The highwall face was captured from six camera locations, and two images taken from each location (Figure 40), which was more than enough to build a representative digital terrain model. The full DTM of the pre-blast pit was generated from two spoil-side and five bench-side DTMs merged together into one model. The final model contains more than 390,000 3D points and 780,000 triangles.

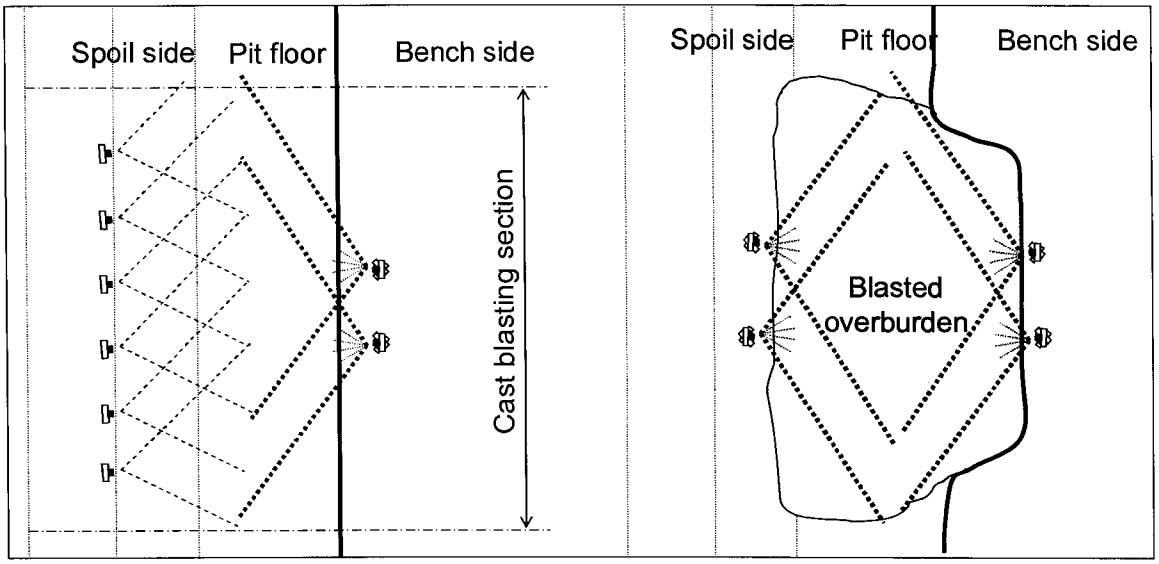

Figure 40 Image capturing modes for cast blast #4

The surface of the pit section after the blast was imaged using a fan mode from four camera locations (Figure 40). Two camera stations were set-up on the bench and two on the spoil side. The camera separation distance was 43 and 50 m respectively. Five images taken from each camera station were used to create one panoramic image. The merged images in TIFF format were cropped to cover the area of interest. It was possible to create panoramic images up to a size of 240 MB. When these images are used for DTM generation, the whole process failed due to memory limitations in the software/computer. After unsuccessful attempts to generate a DTM from the images, it was concluded that size of the panoramic image was too big to be handled by the 3DM Analyst software.

To reduce the size of the merged image, only three photos at a time were merged such that two panoramic images were generated for each camera station with the 'middle' or 3rd photograph in each fan used twice. This reduced the size of the merged TIFF files to a range of 78 to 153 MB. This allowed the 3DM Analyst software to generate a DTM from the image pairs. The final post-blast DTM was created from four single models, two from each side of the pit. The model contains 235,000 3D points and 470,000 triangles. The terrestrial coverage of this model in plan view is about 70% (Figure 41).

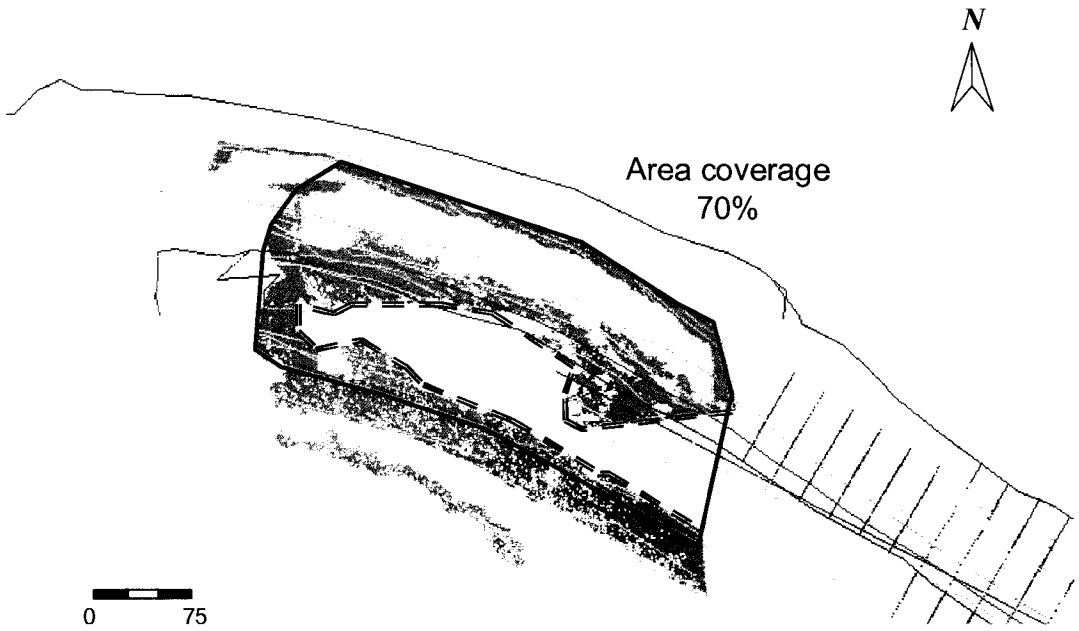

Figure 41 Plan view of DTM points in the post-blast pit section for cast blast #4

4.7 Cast blast #5

At the fifth cast blast, both pre- and post-blasting photographs were shot using a shorter camera base distance and the fan mode. Photo coverage of the pit before the cast blast was done from two camera station pairs, one on each side of the pit, while after the blast the photographs were taken from eight camera locations (Figure 42).

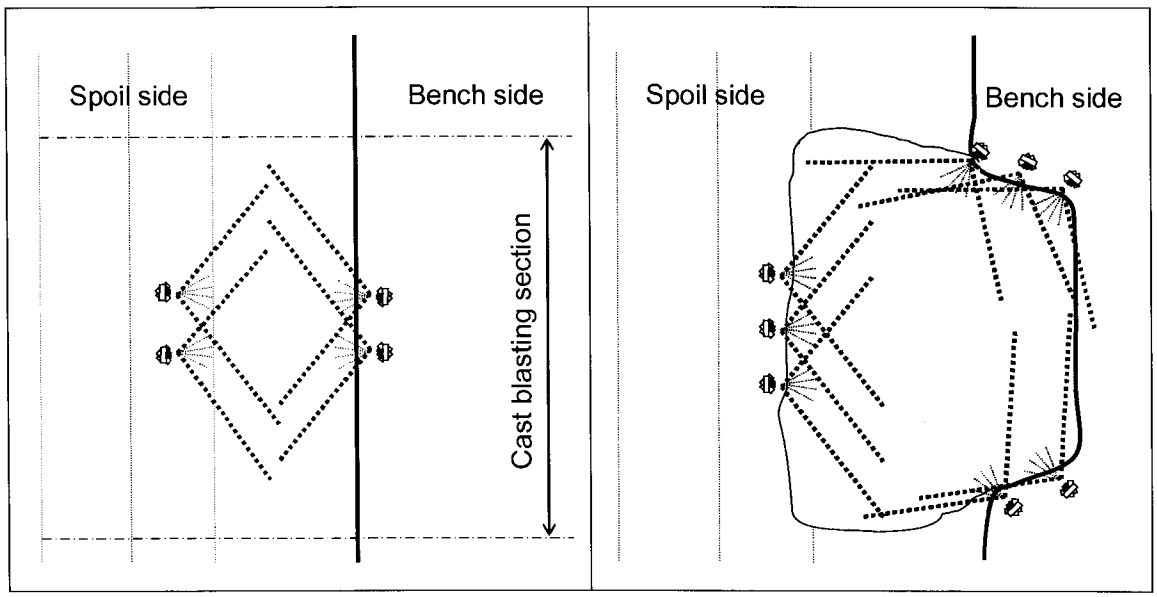

Figure 42 Image capturing modes for cast blast #5

The blast design elements are given in Figure 43.

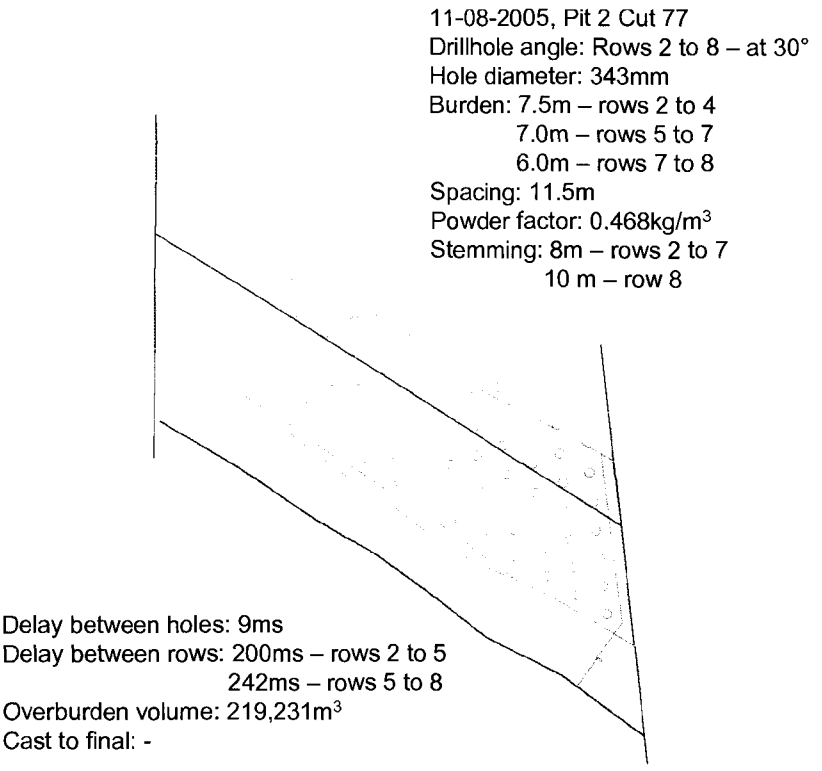

Figure 43 Cast blast design summary – blast #5

Unfortunately, most of captured positional coordinates of the camera locations and control targets were accidentally deleted from the GPS receiver after they were picked up at the mine site and this information was lost. Therefore, the pre-blast model was completely lost for future analysis, while some of the post-blast coordinates were preserved. Using the available post-blast survey data, two single DTMs were generated; one from spoil-side camera pair and one from three bench-side camera location. In cases, when coordinates of control targets and camera locations are lost, it may be possible to utilise the acquired images by matching common features between images with and without control coordinates. In this way survey control can be passed from images containing control points to images without control points. When these images are acquired from opposite sides of the blast section, generation of common natural points was precluded. Therefore, lost coordinates of the third fan camera pair and corresponding targets made generation of a third single DTM impossible. After

generating and merging the two available DTMs, the final triangulated surface model managed to cover over 90% of the blasted overburden pile (Figure 44).

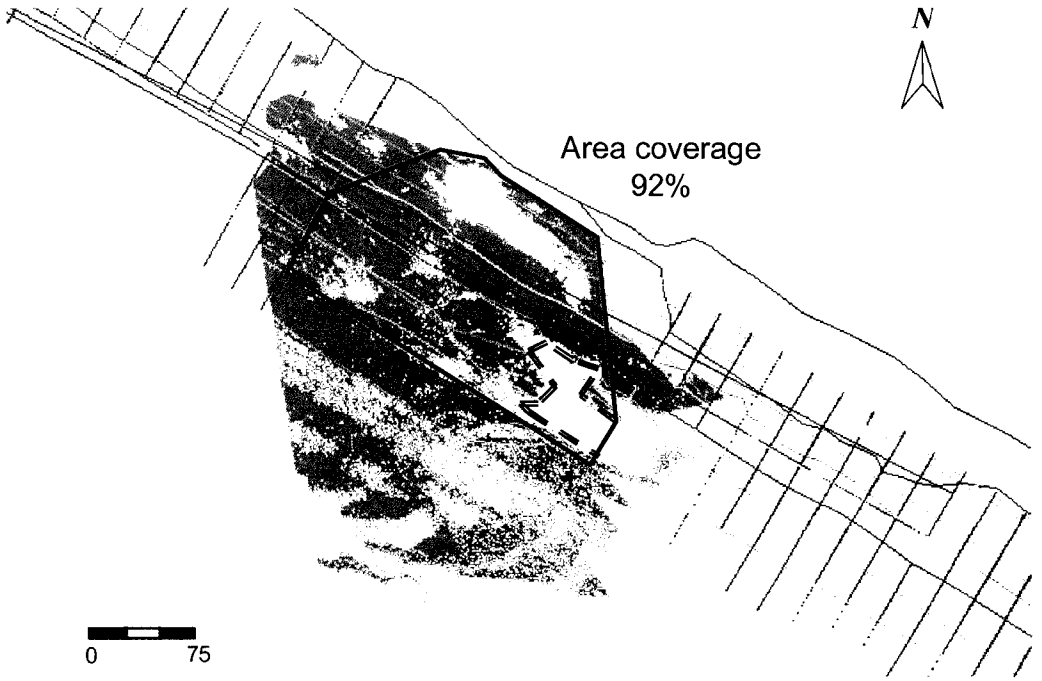

Figure 44 Plan view of DTM points in the post-blast pit section for cast blast #5

4.8 Cast blast #6

The sixth cast blast was the last cast blast scheduled for the summer period in Cuts 76 and 77. The blast design layout is shown in Figure 45.

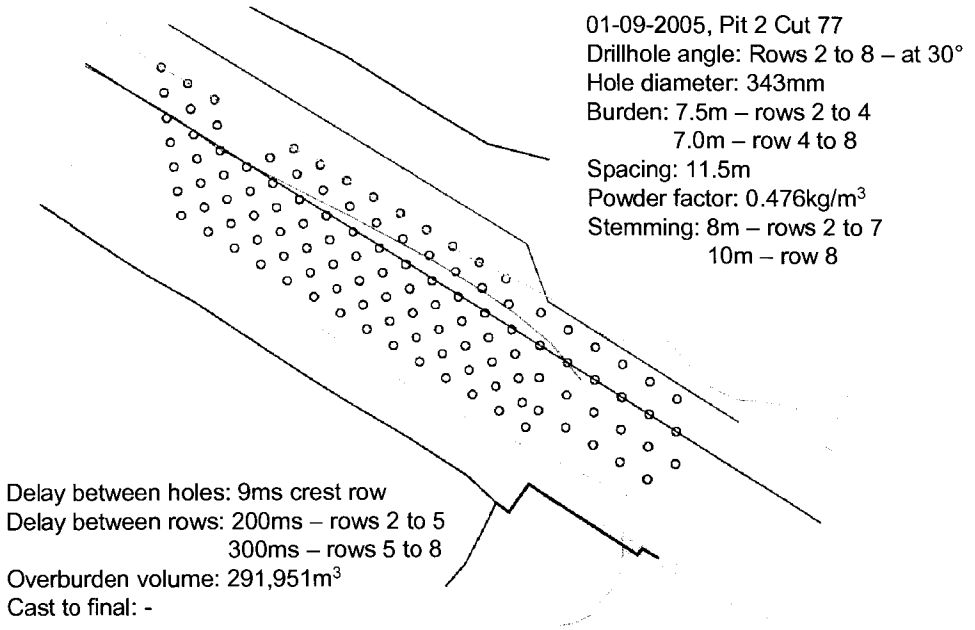

Figure 45 Cast blast design summary – blast #6

A fan mode with reduced camera distance between stations and multiple pairs of stations were used again due to very good results obtained from previous cast blast. The locations of all camera stations and control targets in both cases are shown in the point-cloud plan view of the model in Figure 46. Pre-blast images were captured from eight locations, with full coverage of the highwall face, spoil side and pit floor. The post-blast DTM was generated using images captured from five camera pairs – two located on the bench and three on the spoil side of the pit.

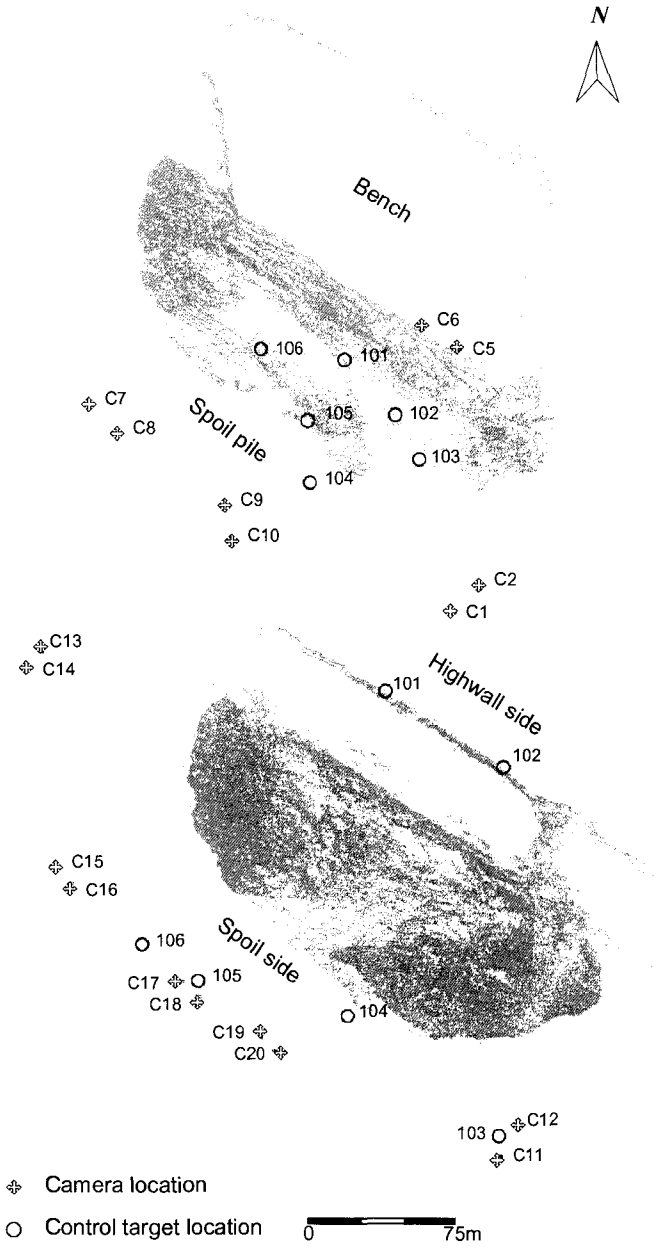

Figure 46 Pre- and post blast camera and control targets layout – blast #6

The digital terrain model of the pit before the blast was fully developed and consisted of more than 133,000 3D points and 267,000 triangles, while the post-blast triangulated mesh covers 99% of the surface area (Figure 47). Screen captures of the DTM before and after blasting showing triangulated and textured surfaces are shown in Figure 48.

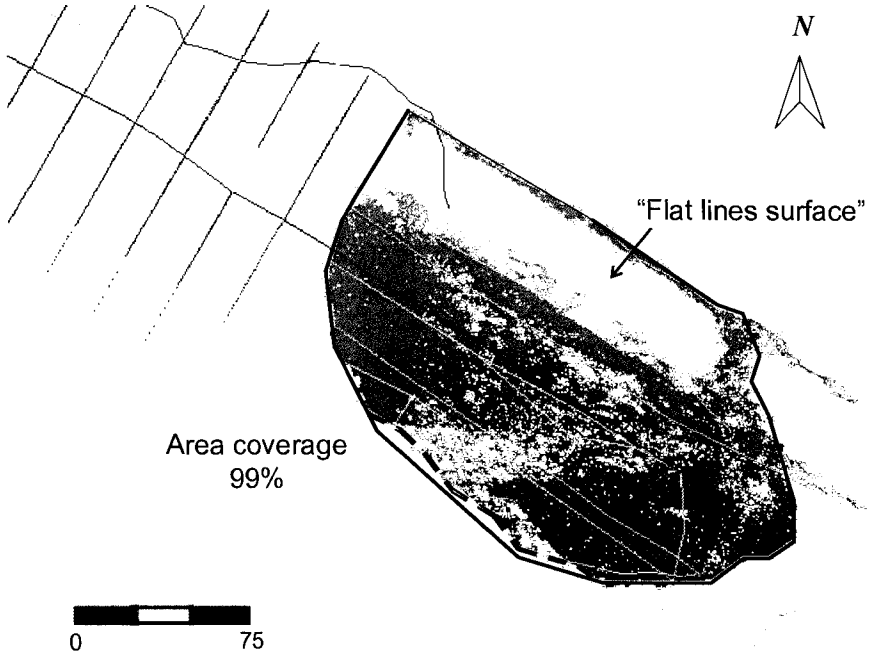

Figure 47 Plan view of DTM points in the post-blast pit section for cast blast #6

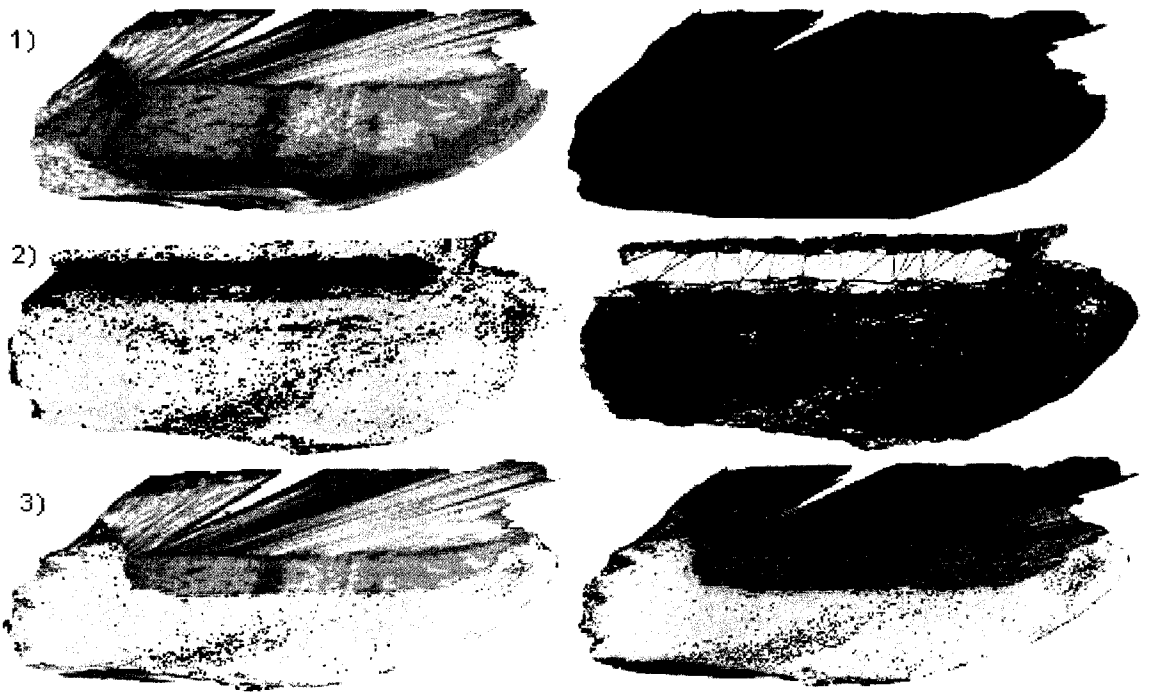

Figure 48 Terrain models: 1) pre-blast (textured and triangulated DTM); 2) post-blast (triangulated DTMs): 3) pre-blast DTM overlapped with post-blast DTM

4.9 Discussion and summary

Fieldwork to obtain digital images for construction of digital terrain models of six overburden cast blasts at the Highvale mine were conducted over the summer of 2005. Different image acquisition techniques were used as the work progressed in an attempt to improve and optimize the field effort required and the coverage of the eventual digital terrain models generated from the images.

Two common problems occurred when processing the images to generate the 3D points. Zones or bands of surface area failed to be covered by the 3D points and triangulation for the post-blast models. For example, Figure 47 shows two bands with little or no 3D points. The band on the upper part of the model occurs because the ground surface in this 'power trough' was lower than, and was obscured by, the top of the blasted overburden when the photographs were taken (Figure 49). If a feature cannot be seen from the location of the camera, no 3D data will be available for the feature. Unfortunately, the camera stations could not be set up at a higher elevation to overcome this problem.

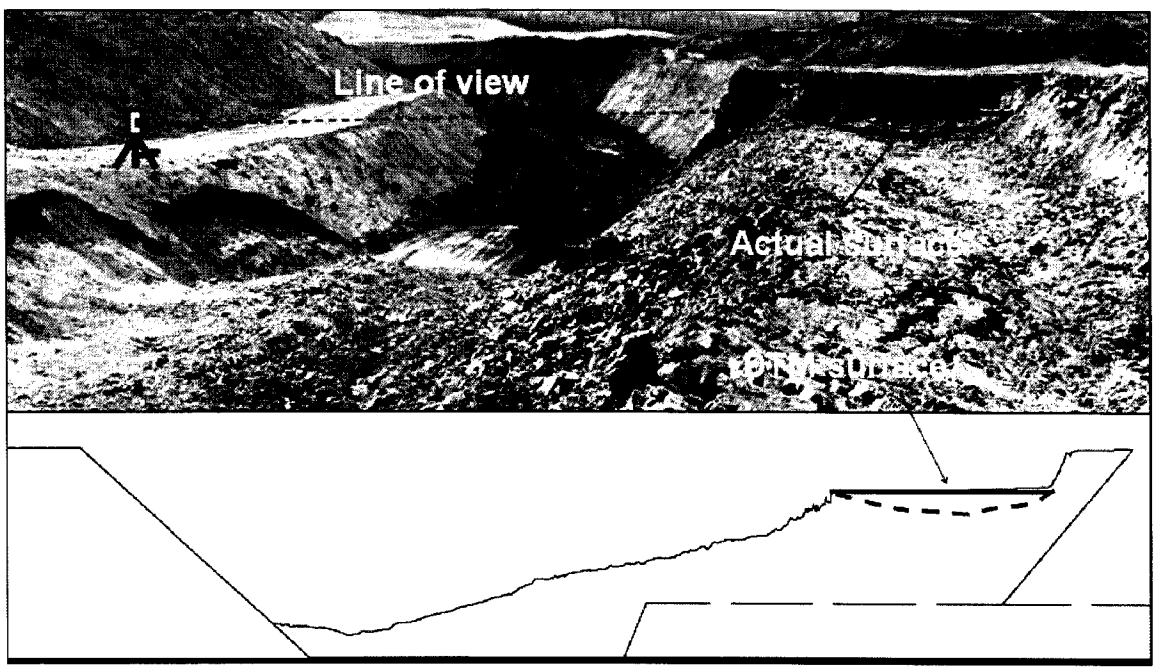

Figure 49 Volume differences: actual and DTM surface of the pile

The other problem can be seen in missing 3D points for areas near the base of the spoil piles. For example, the band of missing 3D points outline by a bold dashed line on

Figure 38 was created because of an image-matching problem. When the photogrammetry software creates the 3D point coordinates it does so by automatically conducting image matching between the images taken from two different camera stations. For the pre-blast models, the ground topography and camera station placement enabled 100% coverage of 3D points for all six blasts. After a cast blast, the geometry was less favourable (Figure 50). Some portions of the cast overburden that appear in the images were too close to the camera base line. These areas look quite different on both images due to a large parallax angle and the image matching was unsuccessful thus causing missing 3D points and triangulation (Figure 51). The solution to this problem is to either place the camera stations closer together, which would increase the total number of camera stations and the fieldwork involved, or to move the camera stations further away (and hopefully higher) from the object. These options were not practical and lack of 3D points in the lowest elevations of the post-blast model was simply accepted.

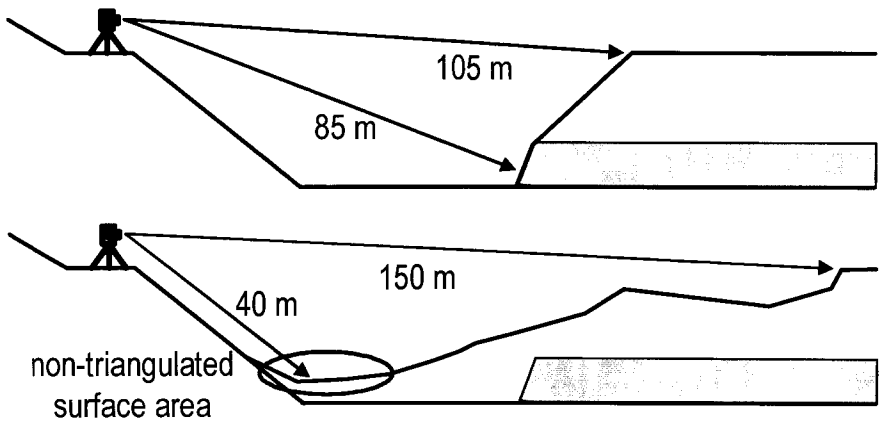

Figure 50 Pre- and post-blast geometry.

Figure 51 Missing 3D coordinates in image portion too close to the camera base line.

Some preliminary conclusions can be made as a reference for future applications of photogrammetry in coal mines.

- The pre-blast models of the pit were fully developed using either strip or fan modes. The relative ease in developing pre-blast models is due to favourable object (pit surface) orientation. The ground surface was closer to being perpendicular to the camera axes and the depth of field was approximately constant and not too large as seen in the upper cross-section shown in Figure 50. Preference should be given to the fan mode due to fewer camera set-ups and shorter overall time spent in the field.
- Even though the post-blast DTMs of the overburden pile did not provide complete coverage in the first four trials, progress was made to understand the causes of poor coverage and to increase the triangulation surface coverage for subsequent blasts. The main consideration was the closeness of the camera stations to the photographed subject. The poorest results were achieved in post-processing convergent image pairs where the object (blasted overburden) covered a wide depth of view. This significantly reduced the correlation between portions of the images corresponding to the near field were the angle of convergence was high as seen in the lower cross-section shown in Figure 50. A possible solution to this problem is to further reduce camera separation and use multiple convergent camera pairs to surround the photographed object. On the other hand, the field effort in acquiring images will increase significantly.
- The fan mode for capturing images shows that it is possible to capture the same terrestrial area from only two camera locations. It is important to note that the time

savings in this case is large compared to the strip mode. Nevertheless, this capturing mode, first applied at cast blast #4, did not provide triangulation of the object points lying close and in between cameras. Also, the lateral extents of the overburden pile were left uncovered.

- Combining images taken from multiple pairs of camera stations used in the fan mode ensures better coverage of the object. Reduced distance between cameras in each pair improved triangulation in the area near the cameras.

A summary of the image capturing modes, camera setups, control targets, and other DTM elements is given in the following tables.

Table 3 Photo-capturing modes used at the Highvale Mine

Blast	Date	Location	Image acquisition mode	
			Before blasting	After blasting
# 1	April 28 / 2005	Pit 2 Cut 76	Strip mode	Strip mode
# 2	May 5 / 2005	Pit 2 Cut 76	Strip mode	Convergent mode
# 3	May 26 / 2005	Pit 2 Cut 76	Strip mode*	Strip mode*
# 4	July 28 / 2005	Pit 2 Cut 77	Strip & fan mode	Fanning mode
# 5	August 11 / 2005	Pit 2 Cut 77	Fan mode*	Multiple fan mode*
# 6	September 1 / 2005	Pit 2 Cut 77	Multiple fan mode*	Multiple fan mode*

* Reduced camera separation distance

Table 4 Number of camera stations

Blast	Area width (m)	Camera stations			
		Before blasting		After blasting	
		Bench side	Spoil side	Bench side	Spoil side
# 1	310	9	8	9	9
# 2	242	8	9	5	4
# 3	274	8	9	8	7
# 4	192	2	6	2	2
# 5	124	2**	2**	5	3
# 6	205	4	4	4	6

** Control points coordinates lost

Table 5 Camera base distance

Blast	Average camera separation (m)			
	Before blasting		After blasting	
	Bench	Spoil pile	Bench	Spoil pile
# 1	40.4	41.1	42.3	42.3
# 2	41.2	37.9	19.6	96
# 3	28.4	30.0	32.7	34.3
# 4	58.3	33.1	43.0	50.1
# 5	-	-	8.2	18.4
# 6	18.7	19.5	9.0	14.2

Table 6 Control targets

Blast	Control targets			
	Before blasting		After blasting	
	Targets	Location	Targets	Location
# 1	5	Bench	4	Bench
	5	Spoil pile	5	Spoil pile
# 2	8	Pit floor	4	Bench
# 3	10	Pit floor	5	Bench
			5	Spoil pile
# 4	5	Bench	4	Bench
	4	Pit floor	4	Spoil pile
# 5	8	Pit floor	4	Bench
			4	Spoil pile
# 6	6	Pit floor	1	Pit floor
			3	Bench
			2	Spoil pile

Table 7 Number of images

Blast	Number of acquired images			
	Before blasting		After blasting	
	Bench side	Spoil side	Bench side	Spoil side
# 1	9	8	9	9
# 2	8	9	8	8
# 3	8	9	8	7
# 4	10	12	10	10
# 5	10	10	15	15
# 6	12	10	12	28

Table 8 Size of digital terrain model

Blast	Size of final DTM			
	Before blasting		After blasting	
	No of points	No of triangles	No of points	No of triangles
# 1	649,132	1,298,242	370,619	741,208
# 2	633,902	1,267,783	15,063	30,103
# 3	912,842	1,825,671	428,637	857,257
# 4	391,359	782,691	234,855	469,642
# 5	-	-	485,016	970,003
# 6	133,157	266,266	382,052	764,073

Table 9 Final digital terrain models

Blast	Image points accuracy A_p (pixel)		Area coverage (%)		Models successfully constructed	
	Before DTM	After DTM	Before DTM	After DTM	Before DTM	After DTM
# 1	0.183	0.174	100	61	✓	×
# 2	0.142	0.205	100	19	✓	×
# 3	0.232	0.166	100	82	✓	×
# 4	0.208	0.341	100	70	✓	×
# 5	-	0.697	-	92	-	×
# 6	0.163	0.230	100	99	✓	✓

5 Optimal Field Measuring Technique

One of the research objectives was to determine optimal field imaging techniques that would be appropriate for measuring cast blast efficiency. Definition of the optimal fieldwork method is based on an analysis of a three different parameters that affect the efficiency of the fieldwork:

- degree of coverage of the final digital terrain model,
- accuracy of the digital terrain model, and
- time and effort spent in the field.

5.1 Model coverage

A primary concern was the need to completely cover the area of interest with digital points and hence triangulation (Figure 51). Without points, a DTM cannot be created. Unfortunately the site conditions and accessibility forced the camera stations to be located closer to the area of interest and at a lower elevation than desirable.

Different image acquisition modes and different camera setups were used for the cast blasts in order to achieve the highest possible terrain coverage with the digital terrain models. The different set-ups and modes of image acquisition are discussed in Chapter 4, and the summary of the model coverage results is given in Figure 52.

All pre-blast models obtained 100% coverage of the area of interest, with the exception of cast blast #5 which could not be built due to accidental deletion of the GPS coordinates. The percentage of surface coverage for the post-blast digital terrain models differs from blast to blast and depends upon the image acquisition mode and camera setup. Progress in developing better post-blast models is noticeable through the change from strip to fan modes, and with decreasing distance between camera stations. The findings indicate that the use of multiple pairs of camera stations in a fan mode combined with camera separation limited to about 20 m provides maximum coverage in case of large terrestrial applications.

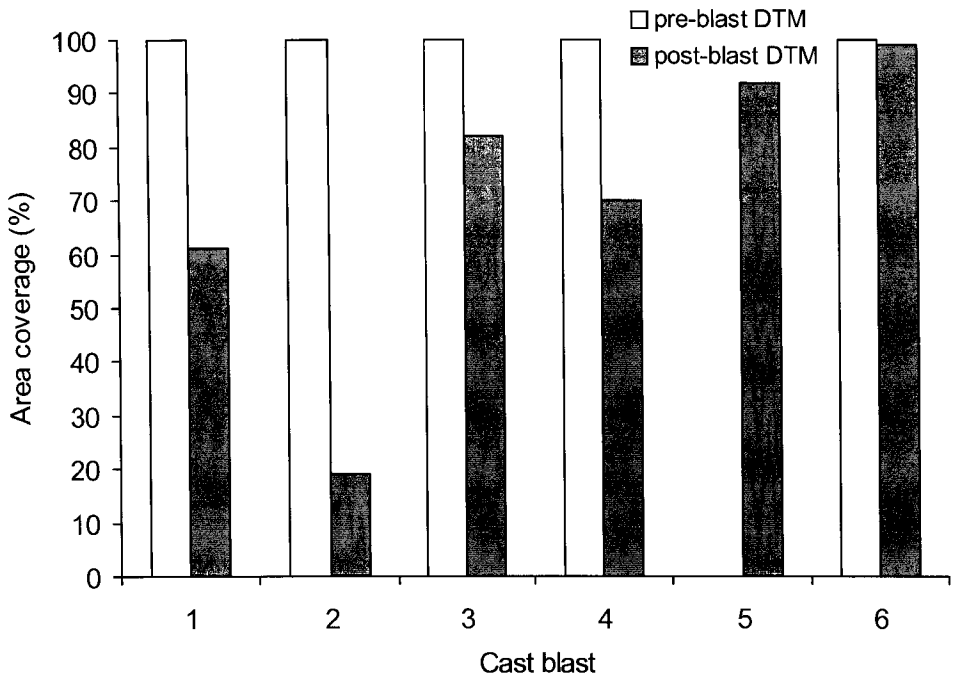

Figure 52 Digital terrain model coverage

5.2 Digital terrain model accuracy

Digital terrain models generated using photogrammetric software should be a reliable and accurate representation of the photographed terrain surface. Since the final model is obtained as a result of different measurements and computations, the total accuracy of the model will be influenced by the:

- accuracy of the camera and target coordinates using the GPS receiver,
- accuracy of the measured vertical camera to ground distance, and
- accuracy of the photogrammetric software measuring system.

Extensive analysis of errors caused by the first two factors was not conducted because standard surveying practices were used in the field and greater accuracy would require an effort that would not be typically performed in a mining environment. According to the information obtained from the mine surveyors, the control point measurement error using the GPS receiver in combination with the ground-base control network is within two centimetres. Also, all vertical camera offsets were measured using a measuring tape.

Therefore, the surveyed camera and control target coordinates are estimated to be accurate within ± 30 mm given a combined source of errors.

Analysis of the accuracy of the digital terrain models is focused on how the field imaging techniques and the software tools affects the accuracy. A digital terrain model is a set of 3D points that are connected with lines to form a triangulated surface. Generation of the 3D data points is based on epipolar images (Figure 1). These images are produced from the original photographs acquired in the field plus the camera stations, control points and lens calibration data. The epipolar images are generated in the 3DM CalibCam software after the absolute orientation bundle adjustment procedure is successfully completed. According to Cooper and Robinson (2001) the least-square bundle block adjustment algorithm is a complex non-linear set of equations that has to be solved in order to determine the unique values of absolute orientation parameters – position and orientation. Once the bundle adjustment procedure is finished, a generated report shows all errors and residuals related to camera and image points. The image point error summary (A_p) is an indicator of the control point accuracy measured in pixels (Adam Technology, 2004b).

A change of the camera base distance, while the camera's focal length and object distance remains fixed will affect the overall accuracy of the generated terrain model (Adam Technology, 2004b). The following formulas are used for calculating ground accuracy given the camera's focal length, the object distance and the camera separation. Overall accuracy can be divided into plan and image depth accuracy. The estimated accuracy in the image plane (plane parallel to the image sensor in the camera) is calculated as follows:

$$A_{plan} = A_p \times PS \times \frac{D}{f} \qquad \text{Equation 7}$$

Where,

A_p is the accuracy in the image in pixels,

PS is the size of a pixel on the image sensor in millimetres (0.00721 x 0.00721 mm),

D is the distance from the camera to the area being imaged in metres (95 m), and

f is the focal length of the lens in millimetres (35 mm).

For targets digitized using Adam Technology's centroiding algorithm accuracy is 0.1 pixel; for points digitized using the least-squares matching option 0.3 pixel; and for points picked manually accuracy range is 0.5 to 1.0 pixel (Adam Technology, 2004b).

The depth accuracy of generated models is calculated from the plan accuracy and the distance/base ratio:

$$A_{depth} = A_{plan} \times \frac{D}{B} \qquad \text{Equation 8}$$

Where,

B is the distance between the two camera positions in metres.

Combining plan and depth accuracy, the overall accuracy is:

$$A_{overall} = \sqrt{\left(2A_{plan}{}^{2} + A_{depth}{}^{2}\right)} \qquad \text{Equation 9}$$

The image point accuracy A_p is defined separately for the pre- and post-cast blast digital terrain models. The final digital model is created by combining and merging together two DTMs, one representing the spoil side and the other representing bench side of the pit. Each of those models are also created by merging individual DTMs covering limited terrestrial areas of highwall or spoil pile. The accuracy estimation of the merged DTM for each side of the pit is based on image point accuracy A_p, determined as an average of image point errors of a set of photos taken from each side of the pit. The higher of those two averaged values is adopted and considered in assessing the overall accuracy of the final pre- and post-blast digital terrain models.

Using the image point accuracy values A_p (Table 8) retrieved from the bundle adjustment reports (Appendix B), and an average object distance of 95 m, the ground accuracy of the various digital terrain models is obtained using the following figures.

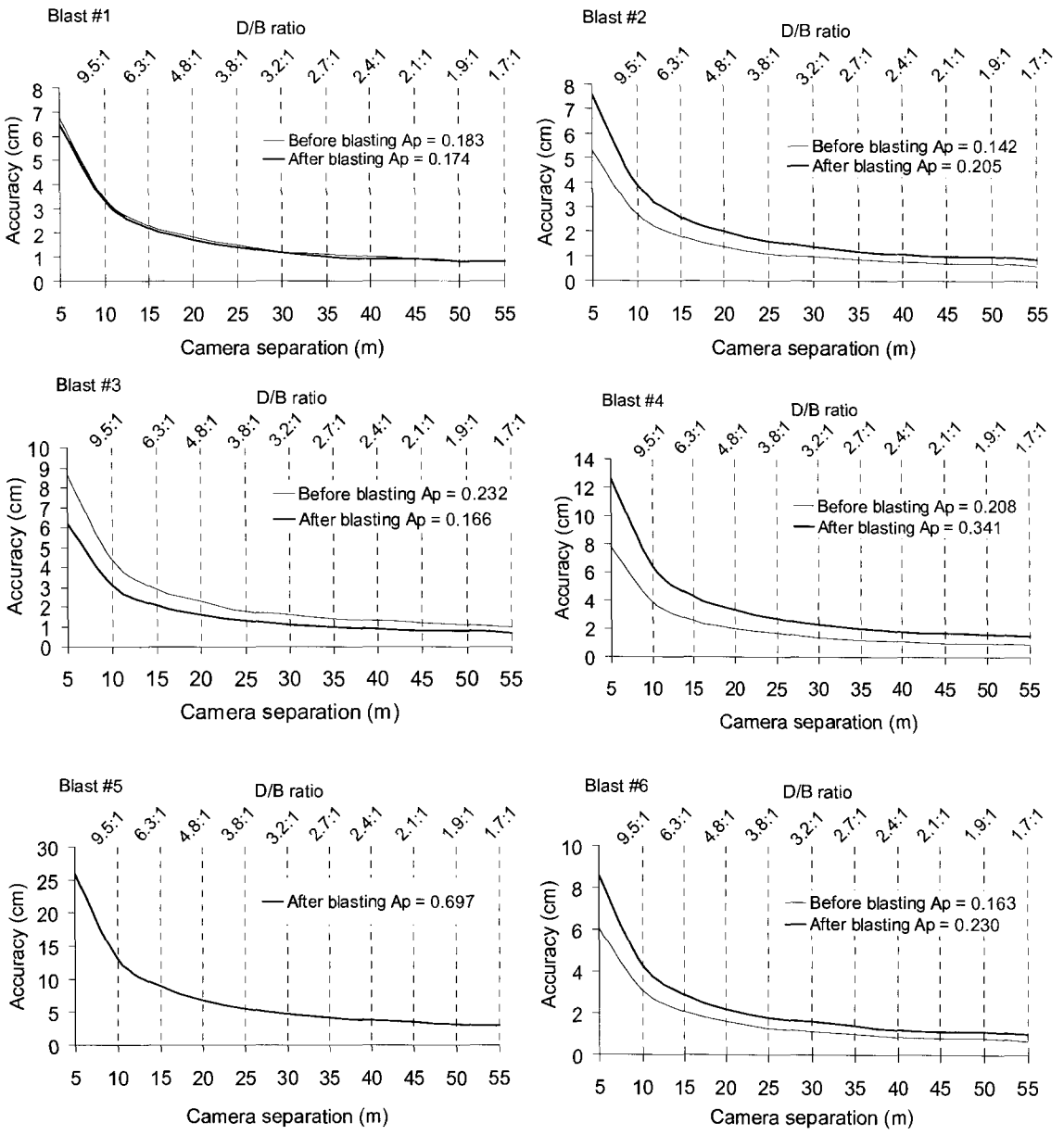

Figure 53 Model accuracy as function of camera separation using the image point error summary for each model

The plots show that better DTM accuracies occur at the lower distance/base ratio values (or wider camera separation for a fixed object distance). Besides the camera separation, the target digitizing method used for the ground control points affects the overall accuracy values as well. The accuracy results computed for each cast blast model are given in Figure 54.

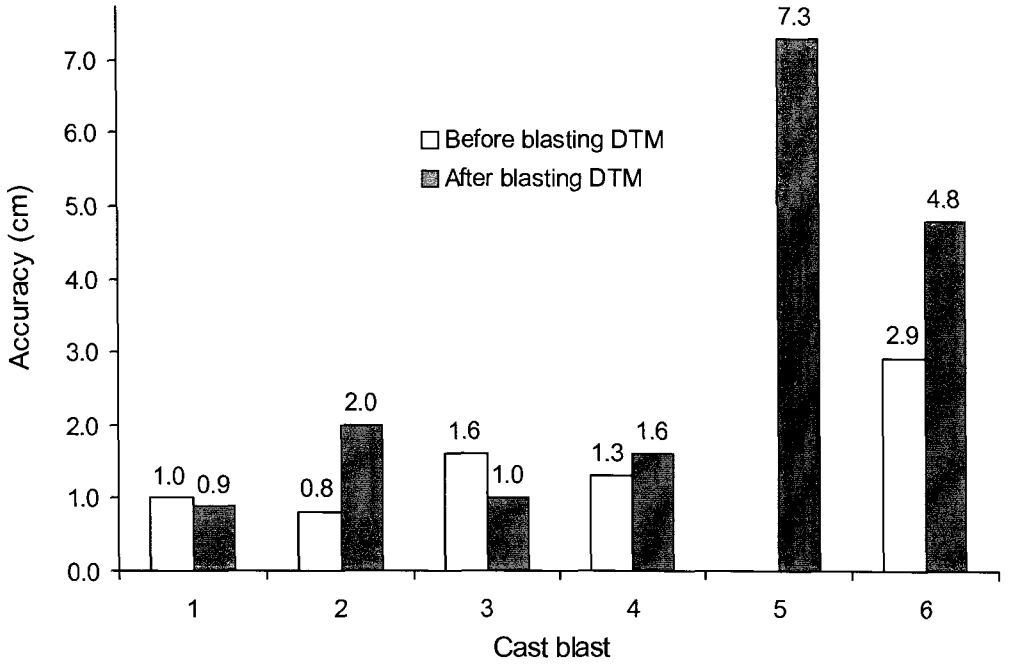

Figure 54 Ground accuracy of digital terrain models

Figure 54 shows that the best accuracy was achieved using a strip mode with average camera separation of 40 m (cast blast #1). Slightly higher error is obtained in the cast blast #3 model, where camera base separation was reduced to around 30 m while using the same shooting mode. On the other hand, DTMs obtained using the fan mode with smaller camera separation, and distance-base ratios ranging from 5:1 to 9:1 (cast blast #5 & #6), gave less ground accuracy than the strip mode. The highest model error is present in the DTM for cast blast #5. The digital terrain model for blast #5 was developed from incomplete field data with only one ground control target, and the cameras were separated less than 10 m. The accuracy of point coordinates in a DTM obtained with a fan mode is in the range of ±30 to 75 mm, which is considered more than adequate for the purposes of assessing cast blast efficiency.

The tables of control point residuals (Appendix B) lists the average root mean square residual error for the control targets used to construct each DTM from a set of photographs. The error represents the difference in coordinates for the control target surveyed by the GPS and those determined within the DTM. The average residual error on the control targets ranged from 2 to 44 centimetres. These residual errors are typically higher than the image residuals that are obtained from the natural points shown in Figure

54. This shows that the dimensional accuracy of the overall digital terrain model is better than the absolute coordinates of the control targets. The photogrammetric software creates a very accurate DTM, but the coordinate system for the DTM can be slightly shifted/rotated relative to the mine coordinate system due to survey errors introduced by the GPS survey of the camera locations and control targets.

5.3 Time analysis

The time and effort required in the field to acquire the images is important. Taking the pre-blast images and control target surveying must be finished at least 45 minutes to one hour before the cast blast due to safety requirements. Similarly the post-blast fieldwork must be completed before dozers or other mobile equipment start working on the blasted overburden. The beginning and the end of a day shift are other limitations that need to be followed. Another goal of the research is to show that the photogrammetry method consumes less time than conventional surveying.

The total time spent on the site acquiring images and collecting data can be divided into:

- Control target time: time to setup control targets and GPS survey their coordinates,
- Camera station time: time to setup cameras, acquire images and GPS survey their coordinates, and
- Other time, which is time spent to arrive and leave the mine site, change pit sides and collect targets at the end.

All site measurements were conducted with a crew of two people, one person carrying the photographic equipment (camera and tripod) and capturing images, and the second person carrying the GPS receiver and collecting coordinates. The total time spent on fieldwork before and after each blast is given in Figure 55.

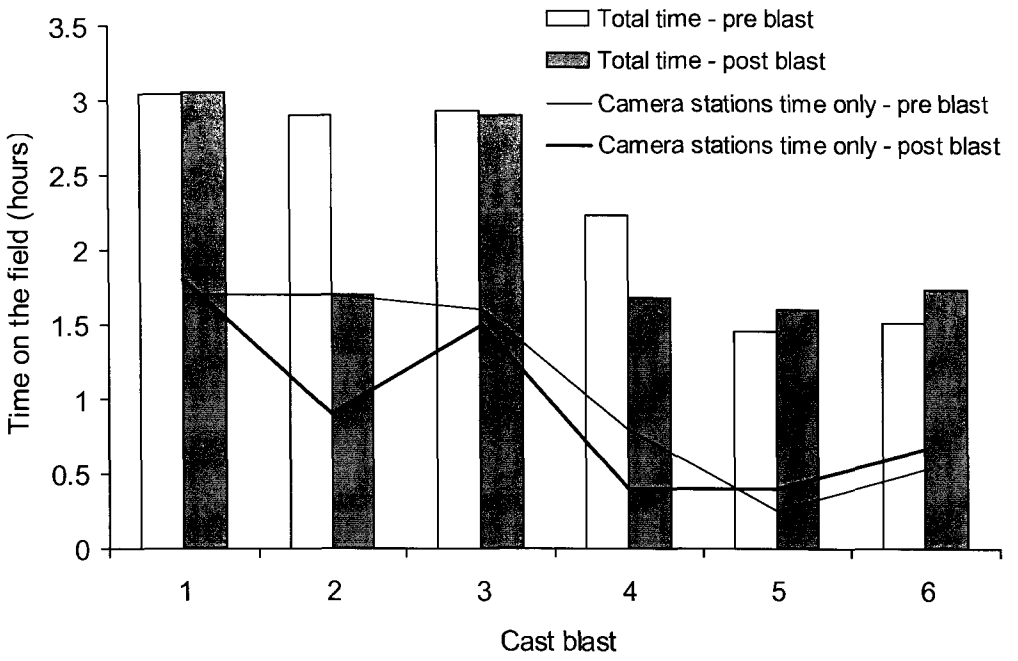

Figure 55 Fieldwork time

Figure 55 shows that first three blasts required around three hours to complete the fieldwork. All these trials were performed using the same strip mode with different setups, with the exception of second post-blast covered with convergent mode. The fourth cast blast was covered using combined strip-fan modes, and last two models are generated with a fan capturing mode. When using a fan mode for image acquisition, the time spent capturing images was between 1.5 and 2 hours. The fan acquisition mode required less fieldwork and less time compared to the strip mode.

If only camera station time is considered in both pre- and post-blast scenarios (Figure 55), it can be seen that the fluctuation of overall time is mostly caused by the fluctuation of camera station time. The time required for the control targets and other time does not change significantly, and their participation in total time is more or less constant. The reduction in camera station time when using a fan mode is due to:

- Fewer camera stations. The strip imaging modes in the first three blasts consists of 15 to 19 stations per final model, while in the fan mode that number is four to ten.
- Shorter camera setup time. The first four blasts were photographed using a standard photographic tripod with an average setup time of six minutes per station. The last two blasts were captured using a camera frame mounted on surveyor tripod with an

average setup time of four minutes. The camera frame incorporated a mount for the GPS receiver which shortened the overall time needed at a camera station because the GPS survey was quicker and more convenient.

Based on the time analysis, use of the fan mode combined with an integrated GPS mount on the camera frame is a good choice to minimize the time spent in the field.

The office time required to process the images to obtain digital terrain models is 3 to 5 hours, and depends upon factors like, camera station and control targets data entry, number and quality of the acquired images, number of individual models that needs to be merged into a final one, and editing of the final digital terrain model. Even though the model generation is relatively effective and largely automated in the software, manual work by the operator is indispensable in order to control the whole process, correct triangulation errors, filter, trim and edit the digital models. It is important to note that one of the most beneficial properties of the digital terrain models is the terrain texture that provides visualization that is crucial for correct interpretation and handling of the digital models.

5.4 Summary

Recommendations for the best image acquisition technique are based on the fieldwork conducted for six cast blasts, including separate pre- and post-blast image acquisitions. The analysis is based on three criteria: model coverage, accuracy, and time spent in the field. In terms of model coverage, the fan mode with multiple camera pairs surrounding the object of interest was the best choice. The time analysis shows that the fan mode using a camera frame is the quickest technique to acquire the images. On the other hand, the fan mode yields the lowest model accuracy because the distance between camera pairs is relatively short. The longer separation between camera stations used in the strip model increases DTM accuracy but results in loss of DTM coverage closer to the camera stations. For the purposes of calculating volumes and cross-sections to assess cast blast efficiency, the lower accuracy (±30 to 75 mm error on coordinates) of the DTMs obtained with the fan mode is deemed insignificant.

6 Overburden Volumes and Cast Blast Efficiency

6.1 Introduction

The digital terrain models created from the images acquired in the field can be used for various purposes. In this chapter, the pre- and post blast DTM obtained from cast blast #6 are used to demonstrate how the DTMs can be used to calculate volumes and to then calculate the cast blast efficiency. Cast efficiency is calculated only for blast #6 because it is the only cast blast in which both the pre- and post-blast digital terrain models covered essentially all of the area of interest. The digital terrain models covered most of blasted area, so they are suitable for the volume computation. The exception is a small piece of the post-blast model that remained triangulation-free (Figure 51), which will be approximated in the computations.

6.2 Volumes and efficiency calculated using 3DM Analyst

The total volume of blasted overburden is computed in 3DM Analyst using the pre- and post-blast digital terrain models. The digital terrain models were trimmed and limited only to the area affected by blast. The overburden volume is attained by summing individual volume portions (Figure 56). Each portion is calculated separately by trimming and cutting the pre- and post-blast digital terrain models (Figure 85) into smaller models. Using these models, the volume portions are calculated by:

- comparing the difference between the post-blast DTM and the pre-blast DTM to obtained V_1, and
- calculating the volume of a single DTM down to a specified elevation (V_2 and V_3).

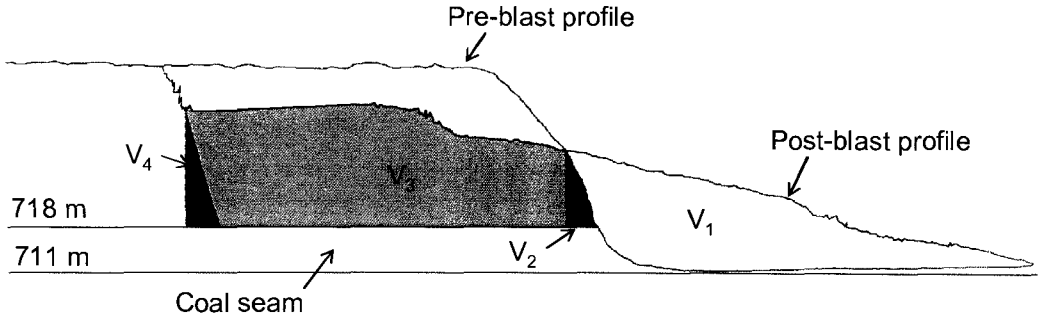

Figure 56 Overburden volume – cross section

The base elevation used in the volume computation is the upper plane of the coal seam, at an elevation of 718 m. Volume portion V_3 is corrected (reduced) for "flat-line surface volume" (Figure 49) and volume V_4. The total volume of the blasted overburden is given by:

$$V = V_1 + V_2 + V_3 - V_4 \qquad \text{Equation 10}$$

Volume 1 is calculated as a difference between the upper surface DTM, which is the post-blast model, and the lower surface from the pre-blast DTM. Both surfaces are extracted from the full DTMs by manually drawing a closed polyline over the intersection between the two models (Figure 57).

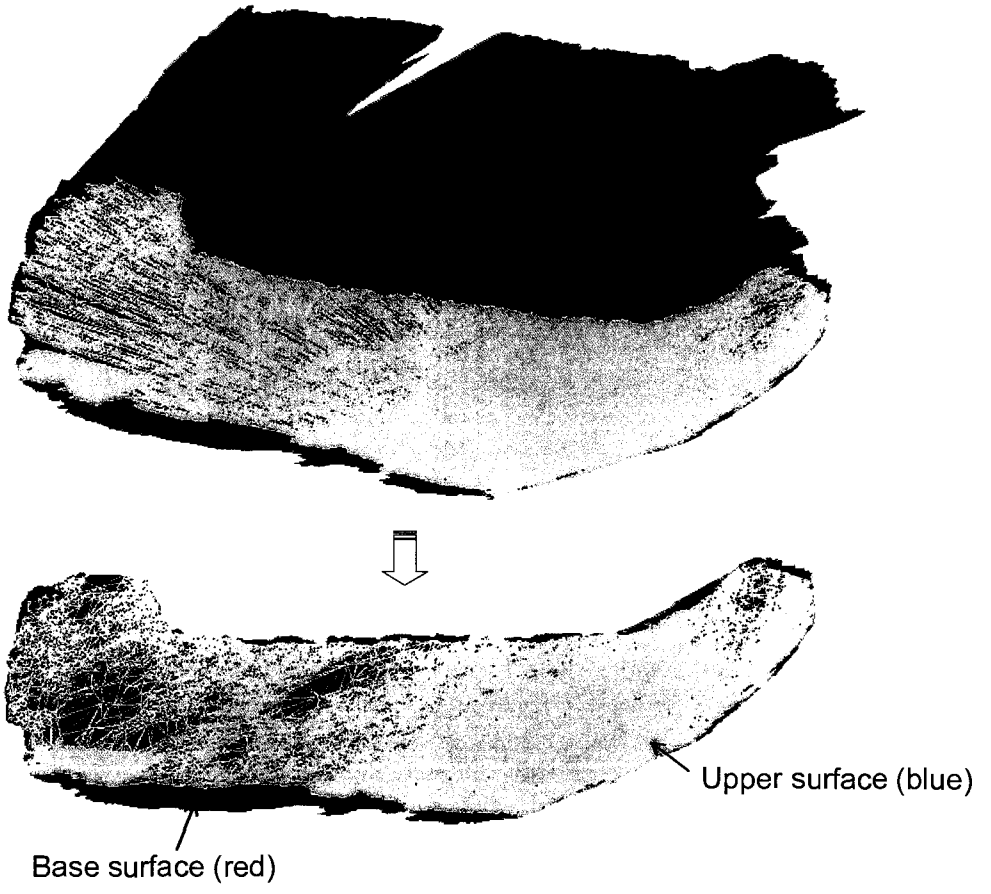

Figure 57 Portion of volume V_1 between two surfaces

Volume 2 is calculated using a clipped segment of the pre-blast digital terrain model. This volume of material is equal to the overburden that lies beneath the highwall slice down to the upper surface of the coal seam at an elevation of 718 m (Figure 58).

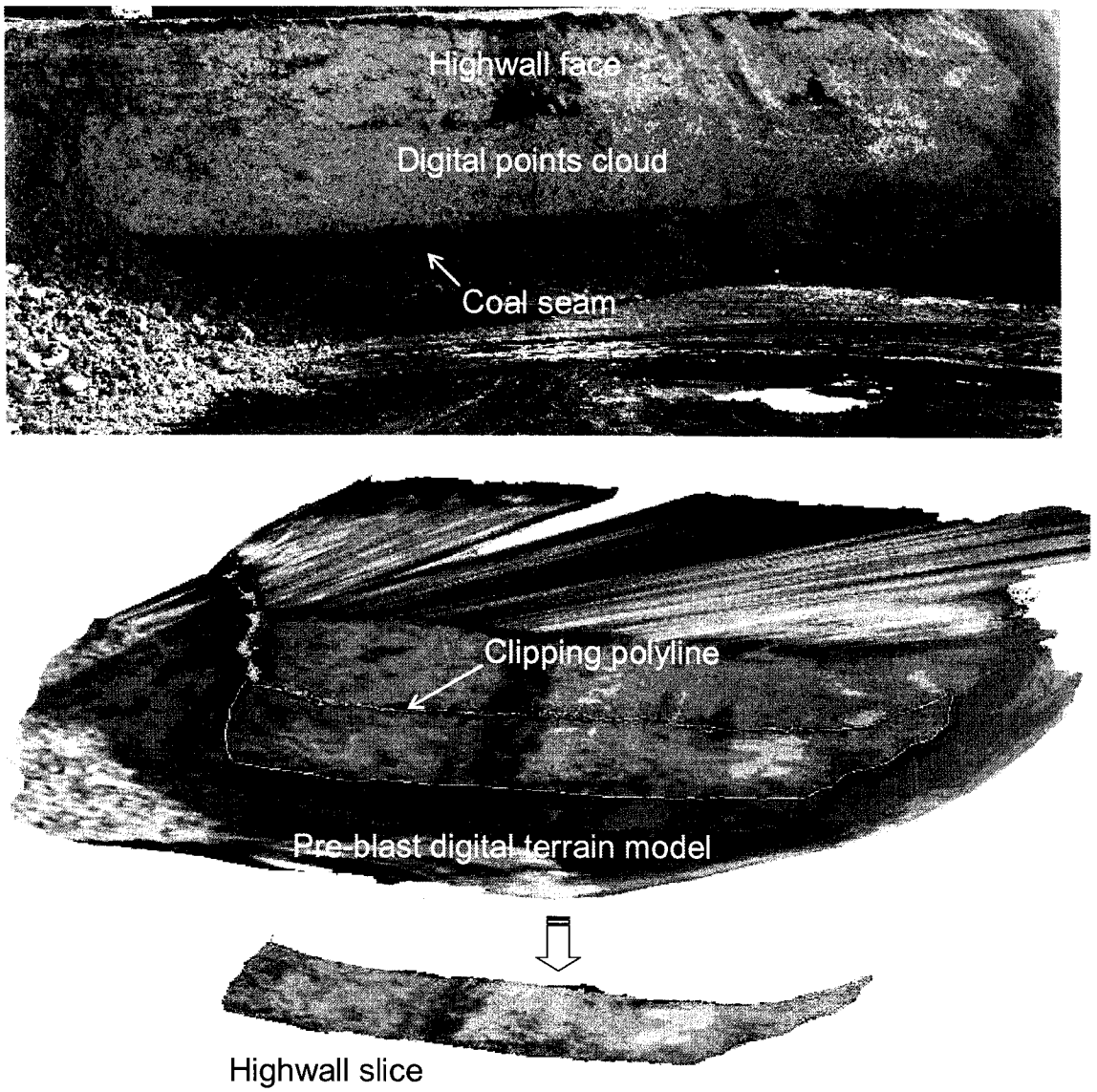

Figure 58 Portion of volume lying under the highwall slice (V_2)

Volume 3 lies between the post-blast surface constrained with a bench cut-off and an intersection line and the bottom horizontal plane at an elevation of 718 m (Figure 59).

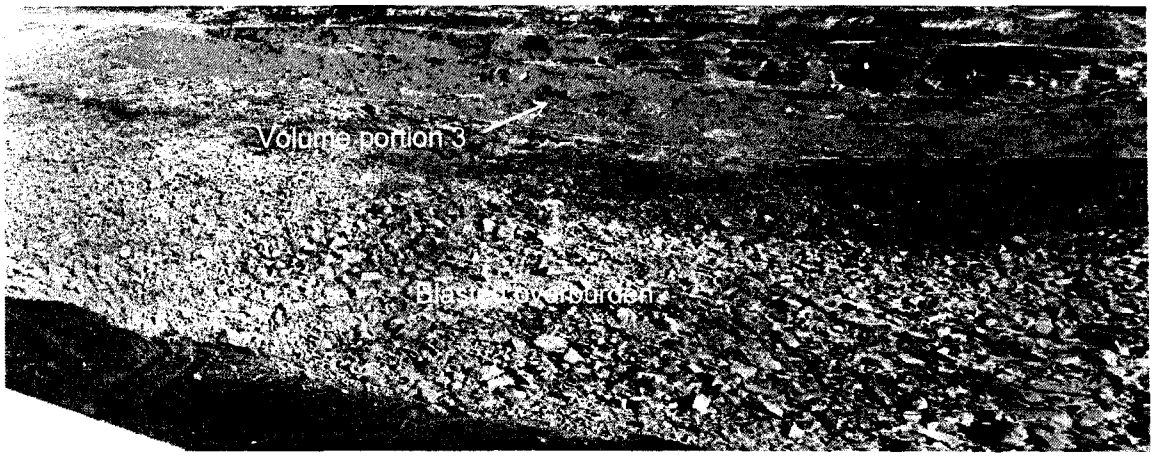

Figure 59 Volume portion #3

According to Favreau (1994), the cast blast efficiency E is given by the volume of overburden cast into its final position on the spoil pile as a percentage of the total volume of blasted overburden (Equation 1). The spoil limit (Figure 60), which determines the volume of material in the final position V_C, is defined through the mine design process. The toe of the spoil pile is assumed to start at the base of the previously mined out coal seam. Highvale Mine spoil piles are designed with a slope of 34° (Oldach, 2006).

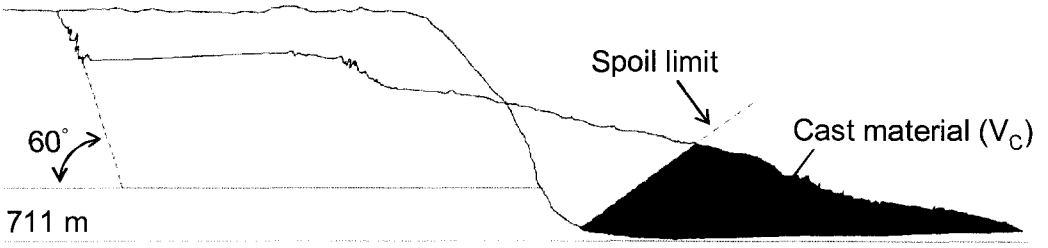

Figure 60 Volumes used for determining cast blast efficiency

The volume of overburden lying in its final position V_c can not be computed directly from the pre- and post-blast models. Besides the two existing overlapped surfaces from the DTMs, determination of volume portion V_c requires introduction and creation of third surface – a plane with dip direction angle of 34° (which is the designed spoil limit angle), and oriented along the pit cut. If a 34° dipping plane could have been superimposed over the DTM then it would have been possible to determine V_c by the portion of V_1 lying below the cutting plane. However, this plane could not be generated in 3DM Analyst since this software package is basically photogrammetric software with limited design

capabilities. Therefore, it was decided to calculate the volume of casted material V_c using cross sections and the end-area method. The volume V_c is thus the same when calculating cast efficiency using digital terrain models and through cross section analysis.

The individual volumes calculated from the pre- and post-blast DTMs and the resulting cast blast efficiency for the sixth blast are listed in Table 10.

Table 10 Overburden volumes and blast efficiency for blast #6

Volumes by 3DM Analyst	Volumes by average end area
$V_1 = 89{,}278\ m^3$	$V_1 = 8{,}913\ m^3$
$V_2 = 7{,}861\ m^3$	$V_2 = 26{,}862\ m^3$
$V_3 = 189{,}825\ m^3$	$V_3 = 37{,}737\ m^3$
$V_4 = 30{,}063\ m^3$	$V_4 = 39{,}851\ m^3$
	$V_5 = 39{,}612\ m^3$
	$V_6 = 37{,}700\ m^3$
	$V_7 = 34{,}801\ m^3$
	$V_8 = 32{,}212\ m^3$
	$V_9 = 16{,}262\ m^3$
Total volume $V = 256{,}901\ m^3$ Material into the final position $V_C = 64{,}863\ m^3$ Cast blast efficiency E = 25.2 %	Total volume $V = 273{,}950\ m^3$ Material into the final position $V_C = 64{,}863\ m^3$ Cast blast efficiency E = 23.7 %

6.3 Volumes and efficiency calculated using end area method

Another method used to verify results of the volume computation is the average end area method. Ten cross sections of the overlapped digital terrain models were generated at 25 m spacing (Figure 61). It is assumed that the volume between successive cross sections is the average of their areas A_i multiplied by the distance l between them:

$$V = \sum_{i=1}^{9} V_i = \frac{l}{2} \sum_{i=1}^{9} (A_i + A_{i+1}) \qquad \text{Equation 11}$$

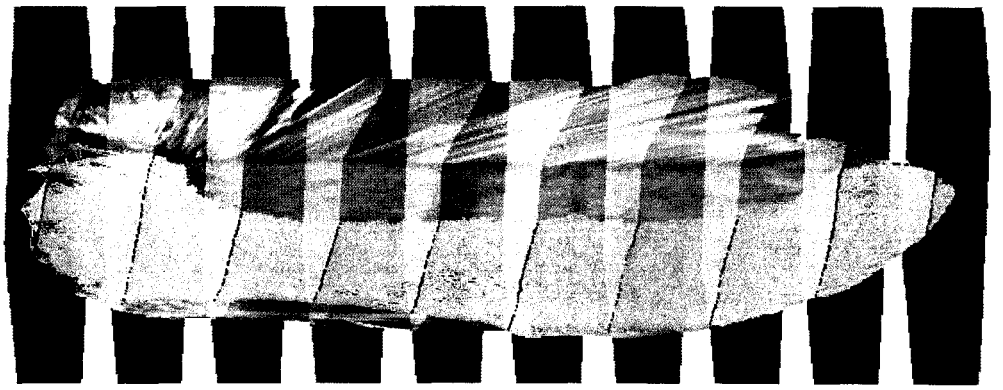

Figure 61 Cross sections through overlapped digital terrain models

Computation resulted in nine subsequent individual volumes. The sum of these volumes gives the total amount of overburden involved in blast #6. The efficiency of the blast was computed using the same volume percentage method.

The final results of the volume and blast efficiency computation are given in Table 10. The overburden volume obtained using the end area method is 6.6% higher than the volume obtained by subtracting digital terrain models. The volumes obtained using the DTMs are likely more reliable than simply using cross-sections cut through the DTMs and the difference of nearly 7% between the two methods is indicative of the error that can be introduced if only cross-sections are used to compute cast blast efficiency.

6.4 Cross section analysis and comparison

Surveyors at the Highvale Mine use a conventional GPS-based method to pick up about 50 to 60 coordinates of along the highwall and spoil pile that are then used to generate cross sections (Figure 62) through the pit. The surveyors attempt to measure the coordinates along the base and top of slopes. These points are connected to define breaks in slope and then cross-sections are constructed through the pit at 25 m spacing.

The cast blast efficiency is computed for each cross section, as a ratio between the material in final position and the total face cut material. This method is slightly different than the efficiency calculated using 3DM Analyst (Equation 10) because the total volume of blasted overburden in the denominator is computed using the design bench face cut volume increased by a swelling factor S_w:

$$E' = \frac{FinalPosition(LCM)}{S_w \times TotalFacecut(BCM)} \times 100 \qquad \text{Equation 12}$$

The swell factor for blasted overburden at each cross section location is calculated as follows (Oldach, 2006):

$$S_w = \frac{BlastedOverburden(LCM)}{BlastedFacecut(BCM)} \qquad \text{Equation 13}$$

Cross section volumes (areas) used to calculate E' and S_w are shown Figure 62.

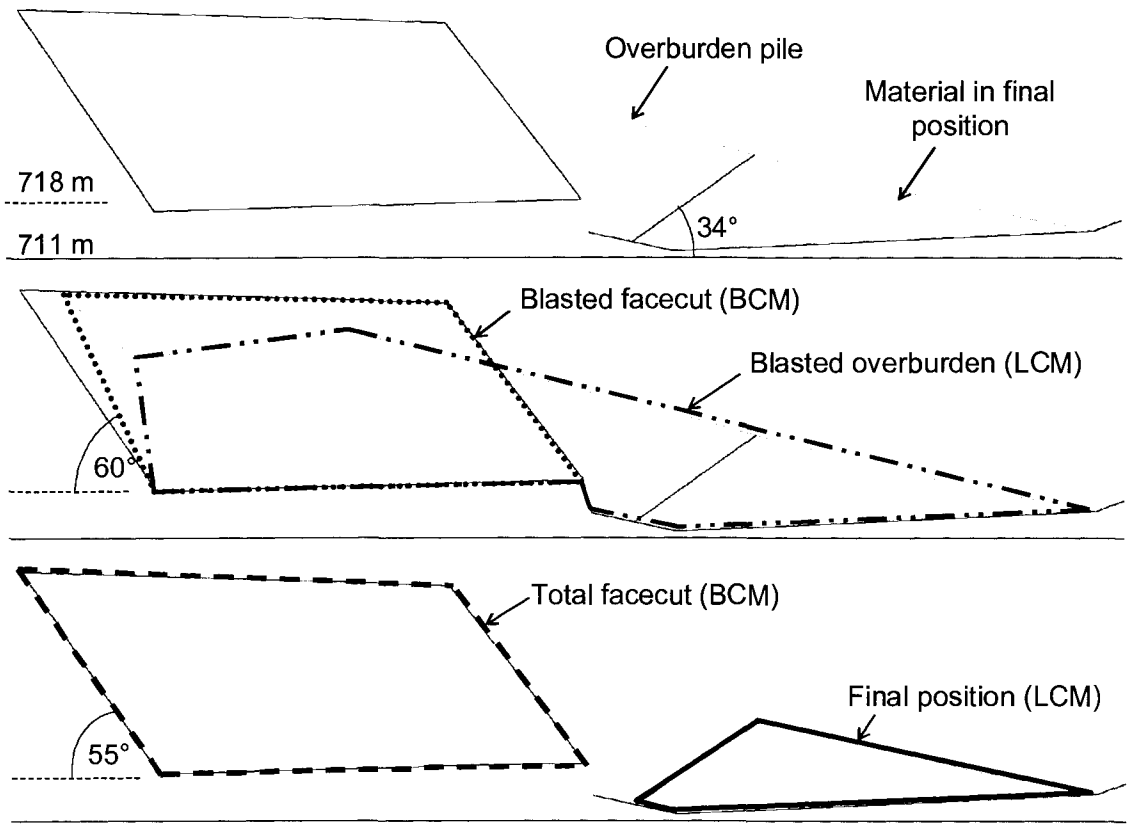

Figure 62 Typical pit cross section for cast blast #6 based on conventional survey coordinates (outlined areas are used to calculate S_w and E')

The results of cast blast efficiency obtained using cross sections taken through the digital terrain models are compared with the results obtained by the Highvale surveyors. The comparison is made using five cross sections of cast blast #6 located in the middle portion of the blast. The cross sections based on conventional survey coordinates were overlapped at the same location with the cross sections generated from the digital terrain

model. Cast blast efficiencies computed using Equation 10 and Equation 12 are given for each cross section in Figure 63.

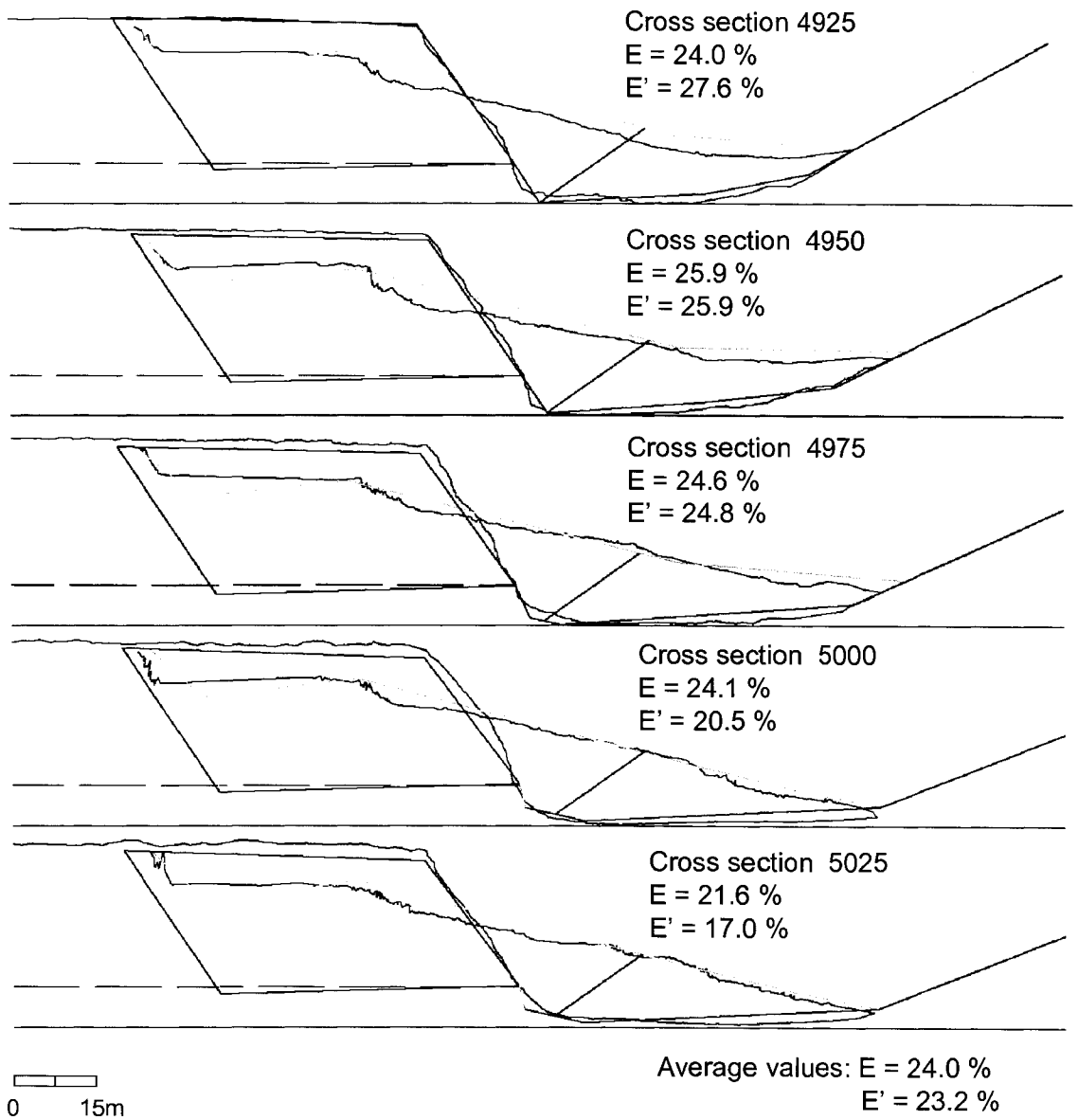

Figure 63 Cast blast efficiency calculated for overlapped cross sections of blast #6

Figure 63 shows that both cross sections are fairly similar even though they were created with different data acquisition methods. The cross-sections obtained from the conventional surveys are very simple and clearly cannot capture subtle differences in the topography that are seen in the cross sections cut from the digital terrain model. In addition, the conventional cross sections are based on extrapolation of out-of-plane coordinates that may create errors at a specific cross-section location.

6.5 Discussion

If it is considered that cast blast efficiency measured in Pit 2 Cut 76 and 77 ranges from 17 to 36%, the 25.2% efficiency achieved for blast #6 can be considered as a standard efficiency. Other coal mining operations are experiencing similar level of cast efficiency. For example, according to Goswami & Keith (1999) at the Bulga Coal operation, an average of 27.4% of material is cast into final position.

In deep stripping Australian mines, overall cast blast efficiency ranges from 16 to 28%. Efficiency of around 16% is achieved in cases where 25 metres of overburden are prestripped by shovel/truck, and then 35 metres of overburden is cast blasted. In operations without prestripping, where the total overburden thickness of 60 metres is cast blasted, the cast blast efficiency is 28% (Sengstock & Kennedy, 1995).

At the Cordero Rojo coal mine, Wyoming, where annual coal production is 45 millions of tons of coal, all overburden is moved using cast blasting and draglines. Cast-to-final efficiency in this mine was reported to be a range from 22.5% to 27% (Pereira, 2001).

One method to increase cast blast efficiency is to keep the depth to width ratio high. Cast effectiveness is always higher in narrower pits, and is most effective when the overburden height is 25 metres or greater. Finally, Workman (1995) concluded that at least 20 to 25% efficiency is needed to generate cost savings compared to conventional techniques.

7 Conclusions and Recommendations

7.1 Conclusions

Terrestrial photogrammetry is a valuable tool that can deliver digital terrain models with coordinate accuracy in the range of ± 75 mm for the types of applications documented in this thesis. This accuracy is considered more than adequate for the purposes of assessing cast blast efficiency. The field trials at the Highvale Mine demonstrated that digital photogrammetry can offer an effective solution for measuring detailed surface topography and for subsequent cast blast efficiency estimation. The pre-blast DTMs covered 100% of the area of interest. However, there were some problems concerning the field imaging technique required to photograph the blasted overburden, from vantage points that are close to the area of interest (short object distances).

The two most common problems associated with the post-blast DTMs resulted in incomplete DTM coverage over the area of interest after the blasts. One problem was caused by obscured views from the camera station. If a portion of the ground cannot be seen from the location of the camera, no 3D data can be generated. The obvious solution is to take the photographs from a higher elevation, but higher vantage points were often not available when using a ground-based camera mounted on a tripod. The other problem was associated with large depths of field for the blasted overburden resulting in a portion of the ground surface of interest being located too close to the cameras for image matching to work in the software. Areas close to a camera station will look quite different on images taken from two different stations that are relatively widely spaced due to a large parallax angle. The solution to this problem is to either place the camera stations closer, which would increase the total number of camera stations and the fieldwork involved, or to move the camera stations further away (and hopefully higher) from the object. Neither option was practical given the site limitations and available equipment for the field situations encountered at Highvale Mine.

It was found that a fan image acquisition mode using multiple pairs of camera stations worked best in the field. This method requires the shortest time to capture images and

minimizes the number of camera stations that are needed. Using more than one pair of camera stations generates multiple DTMs that can be merged to give complete and secure coverage of the whole terrestrial area affected by blasting.

The fieldwork needed to acquire images and survey control using a fan mode is less than two hours, which is similar to that currently used for a conventional GPS/laser surveys while generating approximately 5000 times as many 3D coordinates.

The cast blast efficiency and overburden volumes were calculated by comparing and subtracting final pre- and post-blast digital terrain models. The results were verified with volume computation methods using cross-sections and independent survey results obtained from the Highvale Mine surveyors. The use of cross-sections alone creates errors in the computed volumes in the order of 10% and hence the calculated cast blast efficiencies probably contain a similar degree of error.

Some advantages of the photogrammetric technique versus a conventional GPS/laser survey are:

- All computations and measurements are based on digital terrain models generated from images obtained remotely from safe distances.
- The greater spatial resolution of observed 3D points makes measurements more accurate.
- Volume analysis can be done in three dimensional space with 3D models instead of using 2D cross sections.
- It is possible to isolate one blasted section from adjacent areas, and precisely calculate the volumes and efficiency of each blast.
- Acquisition of the field data is quick.
- Flexibility of capturing images combining different modes and merging generated single models.
- Allows user to easily visualize the object in 3D from any angle.

The photogrammetric approach is subject to several limitations that need to be considered:

- The accuracy of the 3D coordinates created using photogrammetry depends on the quality of the images, including the resolution of the camera, the spatial (geometric) relationship between the camera positions and the object being photographed, and the spectral and spatial variation of the object.
- The image quality and spectral and spatial variation within the image will depend on the lighting conditions and shadows. The best images occur under light overcast skies that reduce shadows and generate uniform lighting conditions.
- Survey control is required, which typically means a GPS receiver must be used in conjunction with the photography equipment to survey the locations of the control targets and camera.
- The optimal number and placement of control targets is typically not known in advance of the fieldwork resulting in the need for extra targets for redundancy.

7.2 Recommendations

The usefulness of the photogrammetry technique, the ease of the subsequent image processing, and the coverage and accuracy of the generated digital terrain models would be improved if the camera could be significantly elevated with respect to the existing ground surface at the Highvale Mine. Therefore field work to determine a cost-effective means to take photographs from a higher elevation is recommended. A number of potential options exist to accomplish this. In increasing order of capital and operating costs, some potential options for raising the camera above the ground are:

- kite
- telescoping mast
- permanent camera mounted on top of a dragline boom
- tethered hot air or helium-filled balloon
- motorized helium-filled balloon
- helicopter

Two inexpensive and easiest to deploy options are the use of a telescoping mast or a kite. From a practical perspective, a telescoping mast could probably elevate the camera up to

15 m above the ground whereas a kite would best operate in the range of 20 m to perhaps as much as 150 m above the ground.

The maximum ground area to be covered by a DTM of a cast blast (and the surrounding undisturbed area) would be about 400 m by 250 m in size. Assuming the camera could be positioned vertically above the centre of this area, with a 35 mm lens, the camera would have to be 400 m above the area to capture on one vertically-shot image the complete area. While it may be possible to fly a kite to suspend a camera this high, remote control of a camera to take images is currently limited to about 100 to 150 m from the ground. Therefore, when using a kite, the camera height is limited to about 150 m and many camera positions would be required to cover the area of interest and this would probably be impractical.

However, it is not necessary to take vertically-shot images. In fact, when imaging the steep highwall, vertical images are not desired. A better approach would be to take the images from a position above the spoil pile with a lens with a shorter focal length (and wider field of view) as seen in Figure 64. In this manner, the complete area of interest could be covered in one photograph and the kite could be positioned at two locations about 20 to 30 m apart along the length of the spoil pile to give stereo coverage.

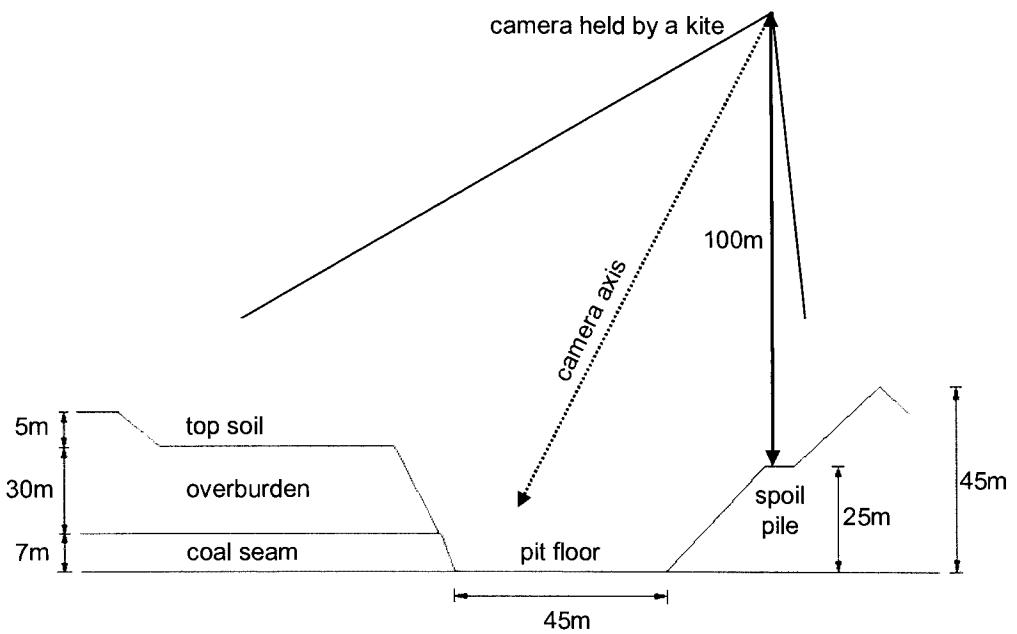

Figure 64 Oblique aerial photography using a kite to suspend the camera

When using a kite, the precise location of the camera can not be measured when the photographs are taken. To compensation for this, additional survey targets would be required on the ground. The photogrammetry software would then be able to determine the camera locations and orientations using the digitized targets in the images. Using a single pair of images to create a full DTM greatly reduces the image processing effort.

The other cost-effective option of using a telescoping mast to take images would improve the coverage of the post-blast DTMs by avoid situations involving an obscured view and would also help to position the camera further from the area of interest. However, given the large size of the area affected by a cast blast, multiple images would be needed, probably acquired in a fan mode. The use of a mast would reduce the number of camera stations needed compared to a tripod. It should be possible to image the complete pre-blast area with one pair of camera stations located above the spoil pile assuming the camera elevation achieved with the mast is at least 5 m higher than the back cut. For the post-blast DTM, it is likely that two pairs of camera stations would be needed, one above the spoil pile and the other above the newly created highwall.

It should still be possible to mount a GPS receiver on the mast along with the camera such that the precise camera location is measured. This would minimize the number of control targets needed in the field.

While the work presented in this thesis demonstrates that digital photogrammetry can be used to create detailed, sufficiently accurate, digital terrain models there is still opportunity to improve the fieldwork involved. Future applications of photogrammetry for measuring surface topography before and after cast blasts or other similar applications at Highvale Mine should evaluate techniques to raise the elevation of the camera.

Digital terrain models were used to calculate cast blast efficiency. However, there are numerous other uses for these models that should be evaluated. Some examples include:

- Measure stock pile and pit volumes
- Measure bench face geometry to calculate actual burden and design better blasts
- Slope monitoring and spoil pile stability assessment
- Developing geological models of the overburden and/or coal.

References

Adam Technology (2004a). 3DM CalibCam 2.1 Camera calibration and block adjustment software: *User's manual.* Belmont, Australia.

Adam Technology (2004b). 3DM Analyst 2.1 3D measurement software*: User's manual.* Belmont, Australia.

Adam Technology (2004c). 3DM Analyst 2.1 trial at BMA Coal's Goonyella Mine. Queensland, Australia.

Adam Technology (2004d). Image capturing quick start guide. Belmont, Australia.

Adam Technology (2004e). Object distance calculation spreadsheet.

Alberta Geological Survey. (2005). Earth Sciences Report 1959-01: *Coal Reserves for Strip-Mining, Wabamun Lake District, Alberta.* Retrieved September 25, 2005, from http://www.ags.gov.ab.ca/publications/ABSTRACTS/ESR_1959_01.shtml

Birch, J. (2005). 3DM Analyst Case Study. *Adam Technology.* Belmont, Australia.

Bitteli, G., Dubbini, A. and Zanutta, A. (2004). Terrestrial laser scanning and digital photogrammetry techniques to monitor landslide bodies. *20th International Society for Photogrammetry and Remote Sensing Congress* (Vol. 35). Istanbul, Turkey.

Bucyrus-Erie Company. (1977). *Surface Mining Supervisory Training Program.* Prepared and published by Bucyrus-Erie Company.

Canon. (2005). *Canon EOS-1Ds Mark II Specification Sheet.* Retrieved February 2, 2006, fromhttp://www.easydigitalcameras.com/specs/Canon/EOS-1Ds%20Mark%20II

Canon. (2006).*Canon EF 35 mm f/1.4L USM Download Library.* Retrieved February 2, 2006, from http://consumer.usa.canon.com/ir/controller?act=DownloadDetailAct

Castleman, W. (2005). *Evaluation of the Canon EF 35 mm f/1.4L USM lens.* Retrieved July 25, 2005, from www.wlcastleman.com/equip/reviews/35mm/)

Chiromis, N.P. (1980). Casting overburden by blasting. *Coal Age* (Vol. 85, No 5), 172-180.

Christensen, J. (2005). Personal communication. Highvale Mine, Luscar Ltd.

Cooper, M.A.R. and Robson, S. (2001). Theory of close range photogrammetry. In K. B. Atkinson (Ed.), *Close Range Photogrammetry and Machine Vision* (pp. 9 – 51). Caithness, UK: Whittles Publishing.

Favreau, R.F. (1994). Optimization of overall excavation costs in a coal strip mine. *Information Systems & Operational Research Journal* (Vol. 32, No 3), 187-201.

Fryer, J.G. (2001). Introduction. In K. B. Atkinson (Ed.), *Close Range Photogrammetry and Machine Vision* (pp. 1 – 7). Caithness, UK: Whittles Publishing.

Goswami, T., and Keith, G. (1999). Practical aspects of cast blasting at Bulga Coal Australia. *Twenty-fifth Annual Conference on Explosives and Blasting Technique* (Vol. 2). International Society of Explosives Engineers. Nashville, Tennessee, 207-214.

Greewe, C.W. (Ed.). (1996). Digital photogrammetry: an addendum to the Manual of photogrammetry. American Society of Photogrammetry and Remote Sensing. Falls Church, VA.

Isaacs, K.I. (1997). Mensuration of aggregate quantities. *CGC: Innovation, Conservation and Rehabilitation* (No. 97). Toronto, ON, 1-6.

Kanchibotla, S.S. (1999). Coal loss due to cast blasting – Implication on mine economics. *Twenty-fifth Annual Conference on Explosives and Blasting Technique* (Vol. 2). International Society of Explosives Engineers. Nashville, Tennessee, 221-229.

Kavanagh, B.F. and Bird, S.J.G. (1989). Surveying: Principles and Applications (2nd ed.). Englewood Cliffs, New Jersey: Prentice Hall Inc.

Lyatsky, H.V. and Lawton, D.C. (1988). Application of the surface reflection seismic method to shallow coal exploration in the plains of Alberta. *Canadian Journal of Exploration Geophysics* (Vol. 24, No 2), 124-140.

Martin, L.K. and King, M.G. (1995). The efficiencies of cast blasting in wide pits. *Twenty-first Annual Conference on Explosives and Blasting Technique* (Vol. 2). International Society of Explosives Engineers. Nashville, Tennessee, 176-185.

Moffitt, F.H. and Mikhail, E.M. (1980). Photogrammetry (3rd ed.). New York, NY: Harper & Row Publishers.

Oldach, K. (2006). Personal communication. Highvale mine, Luscar Ltd.

Pereira, P.R. (2001). Post-blast cast profile shape predicition at large coal surface mines. *Twenty-seventh Annual Conference on Explosives and Blasting Technique* (Vol. 1). International Society of Explosives Engineers. Orlando, Florida, 31-38.

Petrunyak, J. and Postupak, C. (1983). Explosives energy is challenging mechanical energy for overburden removal. *9th Annual Conference on Explosives and Blasting Techniques*. Society for Explosives Engineers. Dallas, TX, 176-198.

Sengstock, G.W. and Kennedy, B.J. (1995). Australian open cut coal mine blasting practices and trends. *Twenty-first Annual Conference on Explosives and Blasting Technique* (Vol. 2). International Society of Explosives Engineers. Nashville, Tennessee, 136-154.

Shaw, D.E., Case, J.B. and Gusek, J.J. (1978). Engineering and economic evaluation of explosive casting of overburden for surface mining, *U.S. Department of Energy Report.*

Stylianidis, E., Patias, P., Tsioukas, V., Sechidis, L. and Geogiadis, C. (2003). A digital close-range photogrammetric technique for monitoring slope displacement. *11th FIG Symposium on Deformation Measurements* (Sec. E5). Santorini, Greece.

Tannant, D.D., Radmanovic, J. and Jiang L. (2006). Digital photogrammetry for surface mining applications. *CIM Mining Conference & Exhibition.* Vancouver, B.C. 12 p.

Taqieddin, S.A. (1997). Theoretical evaluation of blast casting technique in strip mining multiple phosphate rocks. *Twenty-third Annual Conference on Explosives and Blasting Technique.* International Society of Explosives Engineers. Las Vegas, Nevada, 255-266.

Tracy, J.M. (1985). Increased production through cast blasting in surface coal mines. *A.M.C. Coal Convention*, Pittsburgh, U.S.A.

Transalta. (2003). *Highvale Mine.* Retrieved October 5, 2005, from http://www.transalta.com/website2001/tawebsite.nsf/AllDoc

University of Vienna. (1999). The Aerial Archive: Introduction to photogrammetry. Retrieved January 22, 2005, from http://www.univie.ac.at/Luftbildarchiv/wgv/intro.htm

Workman, J.L. (1995). The design, implementation and optimization of cast blast in strip mining. *Twenty-first Annual Conference on Explosives and Blasting Technique* (Vol. 2). International Society of Explosives Engineers. Nashville, Tennessee, 155-167.

Appendix A: Theory of Photogrammetry

Introduction

The methodology used to determine the size and shape of any 3D object from photographic images of the object is called photogrammetry. This technique uses a pair of 2D photographic images of the object of interest which are then observed with stereo photogrammetric equipment or processed with computer software to create a three dimensional model of the object. This is an indirect measurement method, which means that object dimensions can be measured "without being touched". Therefore, the term 'remote sensing' is used by some authors instead of photogrammetry (University of Vienna, 1999).

Photogrammetry can be divided into far range photogrammetry (with camera focus set to infinite), or close range photogrammetry (with camera focus set to finite values) (Figure 65). Another grouping can be aerial photogrammetry, which is mostly far range photogrammetry, and terrestrial photogrammetry.

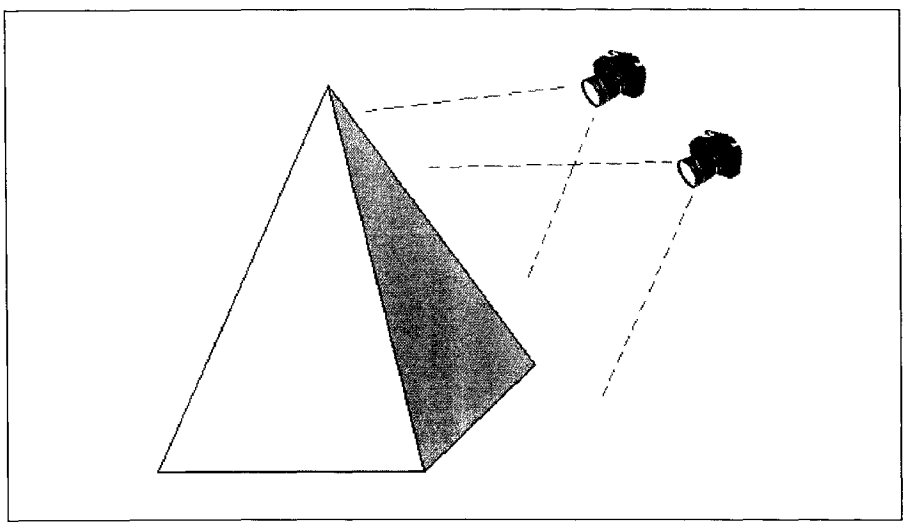

Figure 65 Close range photogrammetry

Aerial photogrammetry uses photographs obtained from specially equipped light aircraft. With a port hole in the floor of the airframe through which a highly calibrated metric camera is pointed directly vertical to acquire vertical aerial images of the object (Isaacs,

1997). This method can be very expensive if performed on a regular basis. For a measurement of 3D objects in many cases close range photogrammetry is more appropriate. According to Atkinson (2001) the term 'close range photogrammetry' describes photogrammetric technique where the extent of the measured object is less than about 100 m, and cameras are positioned close to the object.

Recent technology developments have enabled photogrammetry to be used more frequently for solving engineering problems. Extensive development in digital technologies has resulted in a switch from conventional film-based photogrammetry to high-resolution digital photogrammetry techniques. The aim remains the same, to build a 3D object model from two dimensional photographic images. Digital photogrammetry provides tremendous benefits in extraction, editing and quality control of Digital Terrain Models (DTM). Also, digital modeling offers superior stereo viewing and operator comfort. Digital photogrammetry simplifies the classical photogrammetric workflow and makes results more accurate, reliable and flexible. Creation of the final DTM model from terrestrial digital images is now much faster and straightforward, which together with accuracy benefits increases overall productivity and reduces costs (Greewe, 1996).

Background theory

The background theory of photogrammetry is in mathematical description of depth perception from a pair of overlapping photographs, which is known as a *stereoscopic vision.* The term describes the phenomenon of viewing the object in three dimensions when looking at two photographs of the same object from two viewpoints. Moffitt & Mikhail (1980) explain that two basic principles are involved in stereoscopic vision. The first is the *double-image* phenomenon; when viewing an object from two different viewpoints there will be two images of the object. "Left" image is formed from the first (left) viewpoint and "right" image from the second (right) viewpoint. If the distance between viewing points and observed object increases, there would be somewhere, at a certain distance, a position of the object where the object would be seen as a single image from both viewpoints. This is called *depth of stereoscopic vision*, and by quantifying this phenomenon the amount of depth can be determined.

The second stereoscopy principle is *paralactic angles*. The relative angles ϕ_1 and ϕ_2 formed between the lines joining at different distances from the viewpoints are called *paralactic angles* for those two viewpoints (Figure 66). The impression of the distance $d_2 - d_1$ results from a difference in paralactic angles $\phi_1 - \phi_2$. Stereoscopically viewing, the four marks that appears on a plane surface are actually two marks (points) in three dimension space, separated by depth $d = d_2 - d_1$.

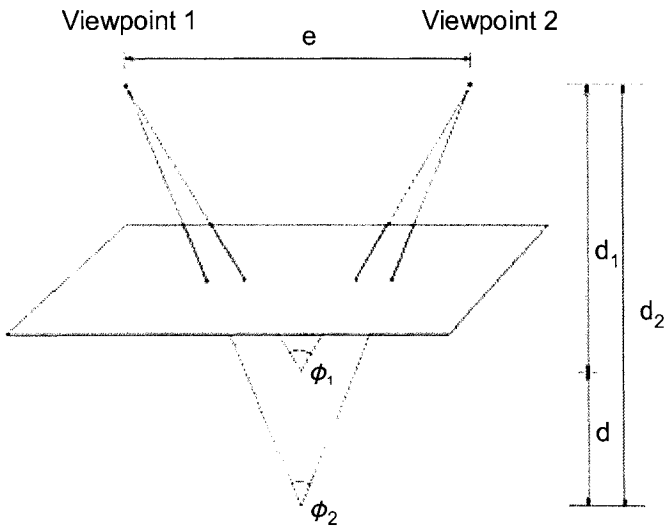

Figure 66 Depth perception and parallactic angles

The depth perception at specific object distances will depend on the viewpoint separation *e*. If the same principle is referred to photography acquisition, the depth of the field perception will increase with increased separation distance between camera stations.

Single camera geometry

The starting point for building any functional photogrammetric model is single camera geometry. Three-dimensional object points are projected onto a projection plane (sensitized film or charged coupled device) through one point inside camera lenses called *perspective centre*. A point *A* in three dimensional object space is projected onto the projection plane by a straight line *AOa* passing through the perspective center *O* (Figure 67). The *perspective axis pO* is orthogonal to the projection plane and intersects it at the *principal point p*. Distance *c* from the perspective centre to the plane of projection is

known as *principal (focal) distance.* To define the functional relationship between object point *A* and its projection *a*, two Cartesian coordinate systems are introduced.

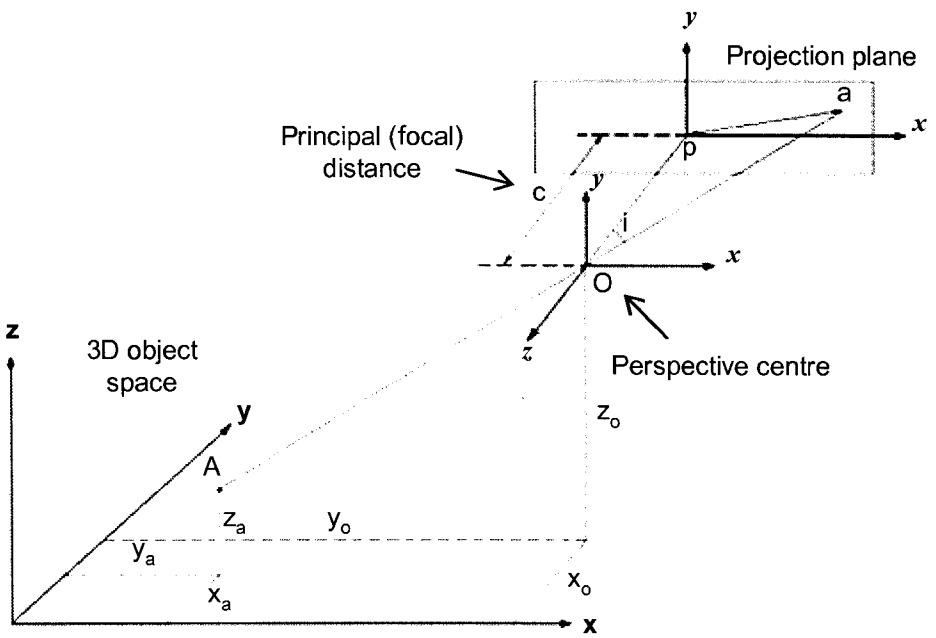

Figure 67 Single camera geometry

Object coordinates. A three dimensional right-handed Cartesian coordinate system (*x, y, z*) is used as a reference for the object space. In this system coordinates of the object point *A* are x_a, y_a and z_a while coordinates of the perspective centre are x_o, y_o and z_o. A common orientation of the object space coordinate system for terrestrial and close range photography is defined by ground survey system such that the *y*-axis is directed toward north (Moffitt & Mikhail, 1980).

Image coordinates. The projection plane is a two-dimensional representation of a generally three-dimensional object space. The location of image point *a* can be determined with a two-dimensional *x* and *y* coordinate system. However, a third axis *z* is employed to generalize geometry of the photography. The *z*-axis of the system is directed away from the plane of projection, while *x* and *y* are directed so as to complete a right-hand system. In terrestrial photography the *x*-axis is taken to be horizontal, or nearly horizontal. The principal point *p* is taken as an origin of image coordinate system. The coordinates of point *a* on the secondary system are x_a, y_a, *0*. In many

photogrammetric operations, the principal point is assumed to fall at the intersection of x and y axis, and consequently $x_o = y_o = 0$. However, precise position of the principal point within image coordinate system is often determined through the camera calibration process.

Interior and exterior orientation

Interior orientation refers to the parameters inside the camera that are not affected by the camera's position in the object space. Geometric elements of the interior orientation are x_o, y_o and c, and they represent the position of the perspective centre within the image coordinate system (Figure 68). Strictly speaking, lens distortion is accounted for when determining the elements of the interior orientation, and can be eliminated through the camera calibration process.

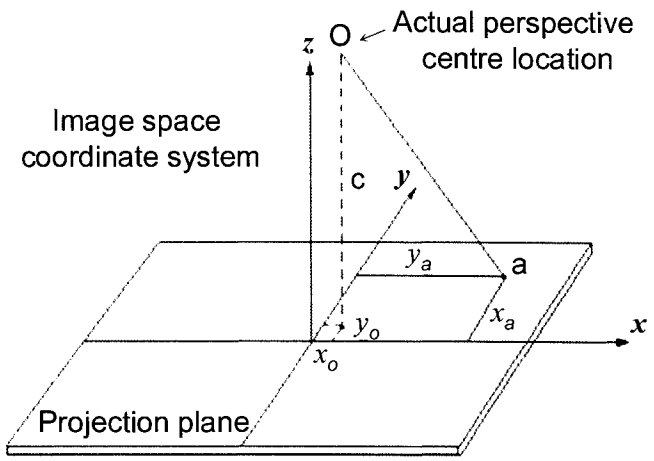

Figure 68 Interior orientation elements

Exterior orientation defines image plane position and orientation in object space at the moment of exposure. The position of the projection plane of the camera is determined by the object-based coordinates of the perspective center O (Figure 69). Conversion between the object-space coordinates and the image coordinate system is possible through coordinate transformation. The final orientation of the camera's perspective centre at the moment of image exposure is expressed as a resultant of three independent rotations (ω, ϕ, κ) (Figure 68).

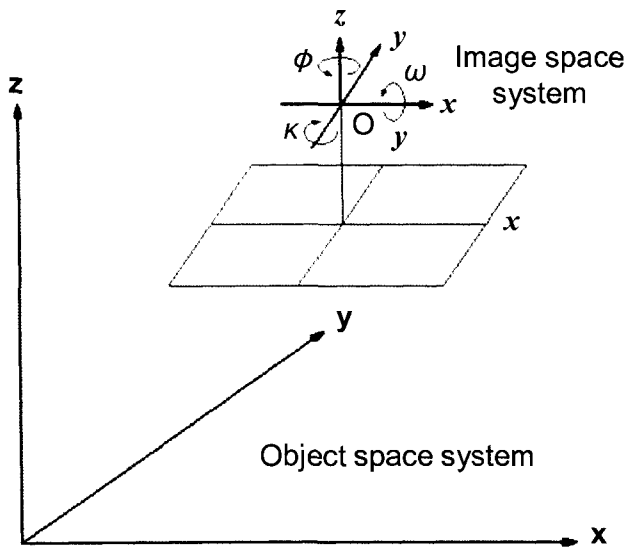

Figure 69 Exterior orientation elements

Geometry of two cameras

In the single camera case, it is not possible to determine the three-dimensional location of object point *A* from its projection point *a*. This is because a light ray that hits a given pixel could come from any point along the ray (Figure 70).

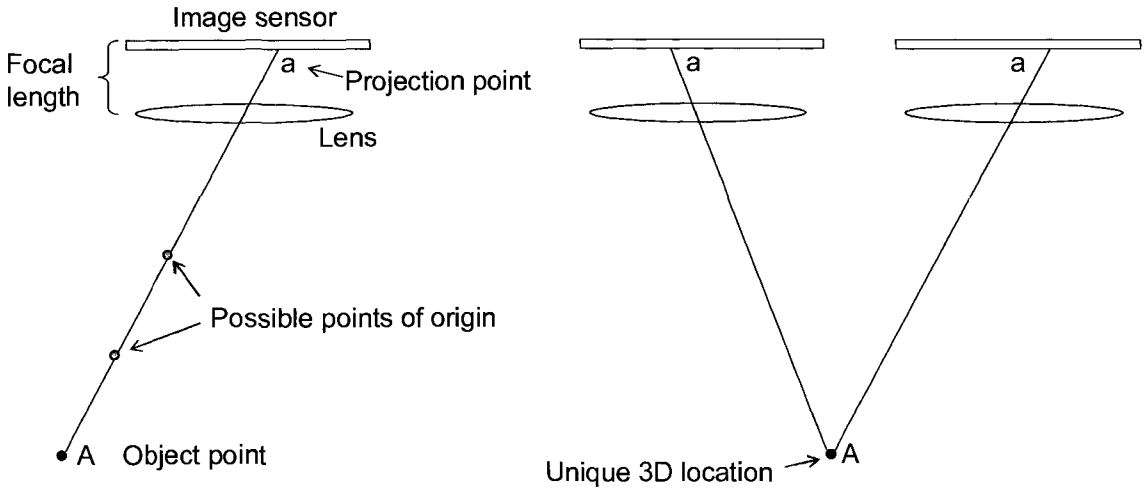

Figure 70 Object point captured from single and from two camera locations

If the same object point is imaged from two camera locations (Figure 70) then a unique 3D location of point *A* can be determined using intersection of the light rays. The

problem can be solved using coplanarity equations of an object position vectors, and least square estimation method (Cooper & Robson, 2001).

Camera calibration

A theoretical model to describe the image formation inside a camera given as seen in Figure 67 is a mathematical model known as *perspective projection.* In a real life, the image acquired on a digital camera sensor will be different than the mathematical model due to lens distortions and aberrations. The procedure for identifying how much the geometry of the real image differs from the mathematical model is known as a camera calibration. According to Moffitt & Mikhail (1980) the purpose of camera calibration is to reconstruct the geometry of bundle of rays coming from the three-dimensional object, and entering the camera during exposure, from the two-dimensional measurement of points captured on the resulting image.

Metrical characteristics that are determined during the camera calibration process are:

- Real focal length of the camera lens (c).
- Position of the principal point (x_o, y_o).
- Radial and tangential distortion of the lens (coefficients k_1, k_2, k_3, k_4, P_1, P_2).
- Flatness of the focal plane (B_1, B_2).

Focal length: Principal distance c varies with the focal setting of the lens. Moreover, for a given focal setting the principal distance is not constant for all incident rays, and depends upon the angle of incidence. This is due to imperfections in construction of camera lenses. Even though the lenses for photogrammetric cameras are designed to produce more precise images that are very close to the perspective projection model, imperfections in assembled lenses during manufacture are inevitable. Therefore, the variation of principal distance with focus setting must be determined through camera calibration.

Principal point: In the central perspective projection (Figure 67), the optical axis Op is orthogonal to the image and intersects the image plane at the principal point p. Point p is also an intersection point of *fiducial axes.* These axes are orthogonal, lie in the image

plane and represent a datum for point coordinate definition in the image. Due to faulty lens construction the principal point is usually offset from the intersection point of the fiducial axes x and y (Figure 68). The coordinates (x_o, y_o) of the principal point with respect to the axes x and y should be determined through the camera calibration. Once the coordinates (x_o, y_o) are known the fiducial coordinates (x_a, y_a) of image point a can be reduced to the principal point to give photo-coordinates:

$$x = x_a - x_o$$
$$y = y_a - y_o \qquad \text{Equation 14}$$

Radial and tangential distortion: Another phenomenon known as *lens aberration* also contributes the fact that the image point formed at the projection plane does not take the theoretically correct position. The ray of light (Figure 71) directed from object point A to the front nodal point N emerges from the rear nodal point N' with changed direction. The ray should leave the rear nodal point N' undeviated along the dashed line $N'a'$. Instead, lens distortion causes the emergent ray to travel along the line $N'a$. Therefore, the image point is displayed at the distance Δr from its theoretically correct position. The displacement Δr is known as a *radial distortion.*

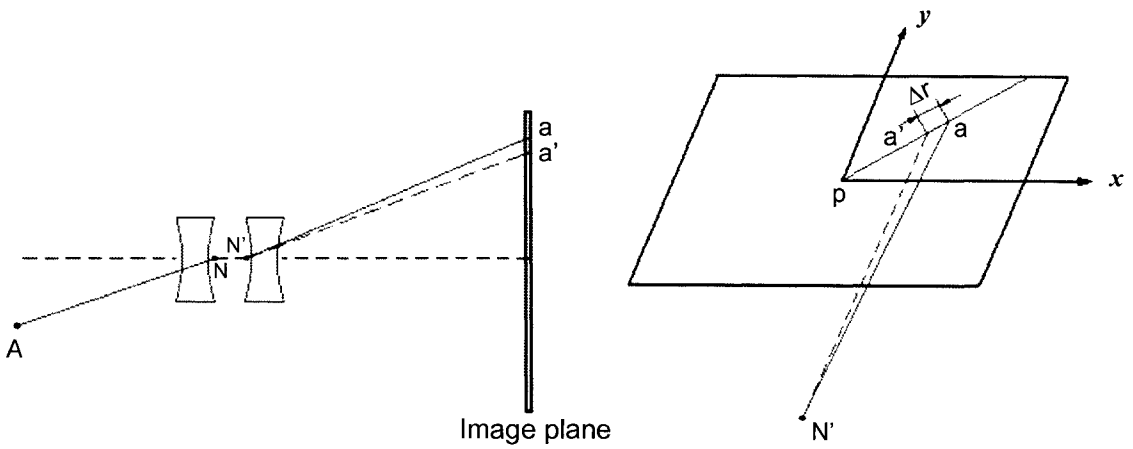

Figure 71 Radial and tangential distortion

Radial distortion is expressed as a polynomial function of the radial distance from the principal point (Cooper & Robson, 2001):

$$\Delta r = k_1 r^3 + k_2 r^5 + k_3 r^7 + k_4 r^9 \qquad \text{Equation 15}$$

$$r = \sqrt{\left[(x - x_0)^2 + (y - y_0)^2\right]} \qquad \text{Equation 16}$$

Resolved into two components:

$$\Delta r_x = \frac{\Delta r}{r}(x - x_0)$$
$$\Delta r_y = \frac{\Delta r}{r}(y - y_0) \qquad \text{Equation 17}$$

Where,

x, y are the fiducial coordinates of the image point

x_o, y_o are the fiducial coordinates of the principal point

$\kappa_1, \kappa_2, \kappa_3, \kappa_4$ are coefficients whose values depend upon the camera focal setting.

The component of the displacement of the image point that is normal to a radial line through the principal point is termed *tangential distortion*, and is consequence of the imperfect assembly of the lens.

The displacement described by two polynomials for each photo-coordinate axis:

$$\Delta t_x = P_1\left[r^2 + 2(x - x_0)^2\right] + 2P_2(x - x_0)(y - y_0)$$
$$\Delta t_y = P_2\left[r^2 + 2(y - y_0)^2\right] + 2P_1(x - x_0)(y - y_0) \qquad \text{Equation 18}$$

Where P_1 and P_2 are coefficients whose values depends upon camera focal setting.

Flatness of the focal plane: Image plane surfaces in traditional cameras or image sensors in digital cameras are never perfectly flat. In digital cameras, the rectangular array of columns and rows of pixels is usually used as an image sensor coordinate system (Figure 72). The system is made of an integer number of rows and columns that covers the whole surface area of the sensor. The camera calibration process provides some analytical methods for correcting the geometry of the image due to lack of flatness and non-orthogonallity to the principal axis. Correction of photo coordinates for this effect is known as *image refinement.*

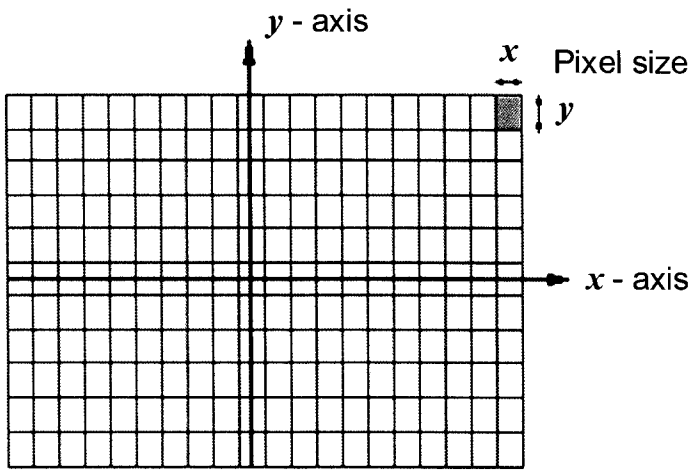

Figure 72 Photo coordinates of digital image plane

The camera and lens used for this research had previously been calibrated using 3DM CalibCam. The interior orientation parameters determined during the calibration of the Canon EF 35 mm f/1.4L USM lens for three different object-distance to camera-distance ratios are given in Table 11. The calibrations were obtained with manual focus set to infinity and f8 aperture.

Table 11 Camera calibration files

		Camera type	*Canon EOS 1Ds Mark II*									
		Image size	*4992x3328*									
		Pixel size	*0.00721x0.00721*									
		Lens type	*Canon EF 35 mm f/1.4L USM*									
Calibration file	B/D ratio	Interior orientation coefficients										
		C (mm)	x_o (mm)	y_o (mm)	P_1	P_2	B_1	B_2	k_1	k_2	k_3	k_4
BO 0.5 f8	0.5	34.2899192	0.10774916	-0.1860171	-8.7428495	3.39039743	-0.0002725	-0.0001621	8.95681321	-1.3711283	2.54028473	-6.1588494
BO 0.33 f8	0.33	34.2884685	0.09456201	-0.1645154	-3.2614426	8.99285775	-0.0002676	-0.0001341	8.65391623	-6.3491140	-2.6770155	5.89547319
BO 0.14 f8	0.14	34.2886669	0.09211900	-0.1850106	-4.1487998	1.01091554	-0.0001870	-0.0001219	9.13833406	-1.4737253	3.03813014	-7.3647902

Appendix B: Image Processing

Introduction

ADAM Technology's photogrammetric software package was used for measurements and generation of digital terrain models. The package consists of 3DM CalibCam and 3DM Analyst. The first one is used to determine the special relationship between the images and known locations (camera stations and control targets) in the scene and completed bundle adjustments. The second software accepts processed digital images and extracts 3D data from these by automatically generating a 3D surface model of the scene. Also, 3DM Analyst is used to measure the dimensions and coordinates of objects (bench, overburden piles), generate cross sections and compute the volumes.

The software 3DM CalibCam can use two or more images and can process them simultaneously. The general procedure applied during the image processing is:

1. *Import files.* Images acquired from the field, using strip, convergent or fan modes, are imported together with a corresponding text file containing coordinates of the camera locations and the control target locations. An external camera calibration file containing interior orientation parameters is also loaded into a project.
2. *Digitize control targets.* The special relationship between a series of images and the local mine coordinate system is established by digitizing all control targets visible on each image (Figure 73). A target centroiding tool is used to locate the centre of each target.
3. *Digitize natural targets.* Natural targets are image points whose coordinates are not known. The same points have to appear on at least two images. If the same points appear on more than one image pair (in strip or fan mode) digitizing them will improve the strength of absolute orientation. In addition to helping solve the orientation of the model, it is recommended to manually digitize many natural points and spread them evenly over the image. An automatic image matching feature in 3DM CalibCam speeds-up this process and locates natural points by performing least square matching (Figure 73).

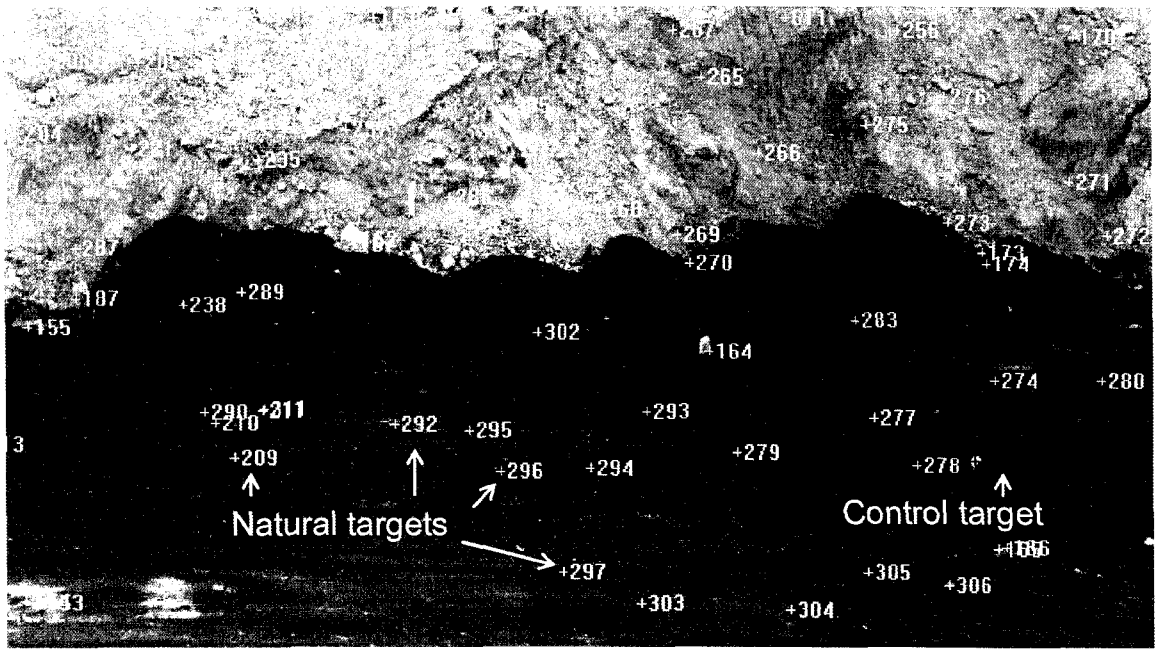

Figure 73 Digitized control and natural targets

4. *Perform bundle adjustment.* According to Cooper & Robinson (2001) the least square estimation method in photogrammetry provides a systematic method for computing unique values of exterior orientation parameters (position and orientation), based on a large number of redundant measurements. The system of equations can be solved only if a reasonable first approximation is provided for the solution. Resection is a process that foregoes bundle adjustment, to initially evaluate values of unknown orientation parameters. This method, however, does not provide accurate and reliable estimate. They need to be refined by a full bundle adjustment procedure, which gives results of higher quality than resection. The unknown elements of exterior orientation are the position of the camera's perspective center (x_o, y_o, z_o) and camera's orientation (ω, ϕ, κ) (Figure 67 and Figure 69). The bundle adjustment utilises all images and control points to compute each camera's position and orientation.

Bundle adjustment reports

Bundle adjustment reports are generated upon the completion of the bundle adjustment procedure within 3DM CalibCam. The reports contain information about absolute orientation errors and image residuals for group of captured images:

- *Image point residuals* represent an error summary in pixels for all image active points. These values are used for digital model accuracy estimation. When a digital terrain model is created from a specific number of subsequent strip images, or from several single digital models merged into one, the accuracy estimation of the final model is based on image point accuracy A_p determined as an average value of image points error (in pixels) for a set of images.
- *Control point residuals* represent the accuracy of control points.
- *Exterior orientation* gives the camera position and rotation summary.

The following tables give a summary of these parameters for each cast blast.

Blast #1

Pre-blast spoil side

Control Point File:	Apr28-before-bench.txt
Active Image Files:	VV2R0759 (1)1.TIF; VV2R0760 (1)2.TIF; VV2R0761 (1)3.TIF; VV2R0762 (1)4.TIF; VV2R0763 (1)5.TIF; VV2R0764 (1)6.TIF; VV2R0765 (1)7.TIF; VV2R0766 (1)8.TIF;
Number of Active Image Files:	8
Number of Camera Stations:	8

Image Residuals

Image Names	RMS Error (Pixel)	Active Points
VV2R0759 (1)1.TIF	0.097	59
VV2R0760 (1)2.TIF	0.117	98
VV2R0761 (1)3.TIF	0.123	125
VV2R0762 (1)4.TIF	0.127	142
VV2R0763 (1)5.TIF	0.115	155
VV2R0764 (1)6.TIF	0.104	135
VV2R0765 (1)7.TIF	0.123	108
VV2R0766 (1)8.TIF	0.108	46

Control Point Residuals

Control Point Names	Raw Data			Residuals		
	X	Y	Z	X	Y	Z
101	289.492	-1377.099	750.602	-0.034	-0.153	0.011
102	358.315	-1393.746	750.332	-0.081	-0.041	0.005
103	426.722	-1415.105	750.374	0.007	-0.099	0.018
104	493.656	-1437.854	748.735	-0.027	-0.165	0.002
105	594.543	-1485.274	747.450	0.192	0.063	-0.042
Control Point RMS				0.107	0.129	0.024
Total					0.169	

Exterior Orientation

Image Names	Camera Location						Camera Rotation - Omega(ω), phi(φ) and kappa(κ)					
	X	Y	Z	δ_X	δ_Y	δ_Z	ω (°)	φ (°)	κ (°)	δ_ω (')	δ_φ (')	δ_κ (')
VV2R0759 (1)1.TIF	259.025	-1538.018	747.183	0.054	0.051	0.046	74.985	19.799	-4.775	3.645	1.796	2.020
VV2R0760 (1)2.TIF	298.126	-1547.067	744.000	0.042	0.042	0.038	74.646	18.383	-4.287	3.587	1.664	1.796
VV2R0761 (1)3.TIF	345.413	-1565.651	743.797	0.035	0.034	0.032	74.497	22.051	-5.371	3.714	1.555	1.828
VV2R0762 (1)4.TIF	385.370	-1585.432	743.586	0.034	0.033	0.031	75.792	20.935	-5.152	3.745	1.503	1.658
VV2R0763 (1)5.TIF	419.063	-1596.215	742.516	0.033	0.031	0.031	74.490	25.246	-6.975	3.815	1.513	1.826
VV2R0764 (1)6.TIF	454.560	-1617.878	741.555	0.036	0.035	0.034	74.278	31.705	-7.558	4.088	1.608	2.333
VV2R0765 (1)7.TIF	490.201	-1641.256	743.026	0.044	0.042	0.040	73.350	30.678	-7.383	4.018	1.746	2.267
VV2R0766 (1)8.TIF	514.436	-1653.944	742.783	0.054	0.049	0.046	73.583	31.446	-7.136	4.090	1.894	2.387

Pre-blast highwall side

Control Point File:	Apr28-before-stockpile.txt
Active Image Files:	VV2R0775 (1)17.TIF; VV2R0774 (1)16.TIF; VV2R0773 (1)15.TIF; VV2R0772 (1)14.TIF; VV2R0771 (1)13.TIF; VV2R0770 (1)12.TIF; VV2R0769 (1)11.TIF; VV2R0768 (1)10.TIF; VV2R0767 (1)9.TIF;
Number of Active Image Files:	9
Number of Camera Stations:	9

Image Residuals

Image Names	RMS Error (Pixel)	Active Points
VV2R0775 (1)17.TIF	0.170	71
VV2R0774 (1)16.TIF	0.166	120
VV2R0773 (1)15.TIF	0.156	144
VV2R0772 (1)14.TIF	0.141	170
VV2R0771 (1)13.TIF	0.181	161
VV2R0770 (1)12.TIF	0.178	152
VV2R0769 (1)11.TIF	0.243	151
VV2R0768 (1)10.TIF	0.261	113
VV2R0767 (1)9.TIF	0.152	78

Control Point Residuals

Control Point Names	Raw Data			Residuals		
	X	Y	Z	X	Y	Z
106	517.769	-1656.802	741.949	-0.034	0.133	0.049
107	485.915	-1636.917	741.465	-0.044	0.038	0.002
108	415.134	-1594.929	741.302	0.007	0.087	-0.046
109	341.257	-1567.199	743.623	0.068	0.006	-0.047
110	260.941	-1539.124	746.339	0.059	0.007	0.020
Control Point RMS				0.053	0.082	0.042
Total					0.106	

Exterior Orientation

Image Names	Camera Location						Camera Rotation - Omega(ω), phi(φ) and kappa(κ)					
	X	Y	Z	δ_X	δ_Y	δ_Z	ω (°)	φ (°)	κ (°)	δ_ω (')	δ_φ (')	δ_κ (')
VV2R0775 (1)17.TIF	561.538	-1552.873	742.287	0.060	0.061	0.068	-69.398	-28.112	169.769	2.577	1.405	1.696
VV2R0774 (1)16.TIF	533.816	-1536.029	742.322	0.052	0.052	0.061	-68.821	-29.818	169.021	2.606	1.241	1.712
VV2R0773 (1)15.TIF	500.746	-1510.627	742.766	0.046	0.045	0.056	-68.350	-29.718	169.585	2.585	1.178	1.704
VV2R0772 (1)14.TIF	467.757	-1489.706	742.870	0.042	0.041	0.052	-70.334	-27.506	171.615	2.534	1.140	1.678
VV2R0771 (1)13.TIF	428.918	-1473.343	743.997	0.041	0.040	0.049	-70.434	-24.331	171.692	2.464	1.136	1.636
VV2R0770 (1)12.TIF	389.430	-1459.137	744.621	0.044	0.042	0.050	-71.291	-22.189	173.300	2.429	1.143	1.619
VV2R0769 (1)11.TIF	348.767	-1446.189	744.931	0.049	0.048	0.054	-72.072	-19.295	175.360	2.378	1.186	1.597
VV2R0768 (1)10.TIF	308.782	-1433.492	745.563	0.057	0.056	0.062	-72.293	-17.617	174.828	2.369	1.264	1.593
VV2R0767 (1)9.TIF	264.171	-1418.599	746.452	0.071	0.068	0.074	-74.890	-13.329	177.588	2.301	1.479	1.574

Post-blast spoil side

Control Point File:	Control Point Data
Active Image Files:	VV2R0781 (1)23.TIF; VV2R0782 (1)24.TIF; VV2R0783 (1)25.TIF; VV2R0784 (1)26.TIF; VV2R0786 (1)28.TIF; VV2R0787 (1)29.TIF; VV2R0788 (1)30.TIF; VV2R0789 (1)31.TIF;
Number of Active Image Files:	8
Number of Camera Stations:	8

Image Residuals

Image Names	RMS Error (Pixel)	Active Points
VV2R0781 (1)23.TIF	0.120	61
VV2R0782 (1)24.TIF	0.130	93
VV2R0783 (1)25.TIF	0.130	97
VV2R0784 (1)26.TIF	0.107	69
VV2R0786 (1)28.TIF	0.081	79
VV2R0787 (1)29.TIF	0.082	94
VV2R0788 (1)30.TIF	0.077	134
VV2R0789 (1)31.TIF	0.078	112

Control Point Residuals

Control Point Names	Raw Data			Residuals		
	X	Y	Z	X	Y	Z
101	289.540	-1376.701	750.585	0.014	0.245	-0.006
102	358.441	-1393.959	750.263	0.045	-0.254	-0.064
103	493.556	-1437.606	748.817	-0.127	0.083	0.084
104	594.345	-1485.348	747.469	-0.006	-0.011	-0.023
Control Point RMS				0.078	0.209	0.062
Total					0.232	

Exterior Orientation

Image Names	Camera Location						Camera Rotation - Omega(ω), phi(φ) and kappa(κ)					
	X	Y	Z	δ_X	δ_Y	δ_Z	ω (°)	φ (°)	κ (°)	δ_ω (')	δ_φ (')	δ_κ (')
VV2R0781 (1)23.TIF	265.711	-1539.005	746.653	0.039	0.040	0.041	72.368	17.025	-4.631	1.176	0.997	0.857
VV2R0782 (1)24.TIF	305.307	-1551.558	745.673	0.035	0.034	0.037	73.856	18.198	-4.707	1.174	0.930	0.858
VV2R0783 (1)25.TIF	354.221	-1569.080	744.289	0.034	0.031	0.036	72.899	18.709	-6.623	1.176	0.833	0.855
VV2R0784 (1)26.TIF	391.078	-1590.736	744.186	0.045	0.034	0.041	70.930	21.308	-6.330	1.191	0.910	0.871
VV2R0786 (1)28.TIF	476.512	-1631.822	742.119	0.042	0.034	0.038	70.435	32.234	-11.440	1.611	1.259	1.459
VV2R0787 (1)29.TIF	511.591	-1653.521	742.936	0.037	0.031	0.037	71.527	25.589	-9.487	1.455	1.238	1.368
VV2R0788 (1)30.TIF	553.747	-1673.544	741.145	0.039	0.036	0.038	71.871	28.546	-8.971	1.523	1.250	1.408
VV2R0789 (1)31.TIF	570.428	-1682.939	740.240	0.042	0.040	0.040	72.006	26.958	-8.577	1.488	1.264	1.389

Post-blast highwall side

Control Point File:	Apr28-after-stockpile.txt
Active Image Files:	VV2R0799 (1)41.TIF; VV2R0798 (1)40.TIF; VV2R0797 (1)39.TIF; VV2R0795 (1)37.TIF; VV2R0794 (1)36.TIF; VV2R0793 (1)35.TIF; VV2R0792 (1)34.TIF; VV2R0791 (1)33.TIF; VV2R0790 (1)32.TIF;
Number of Active Image Files:	9
Number of Camera Stations:	9

Image Residuals

Image Names	RMS Error (Pixel)	Active Points
VV2R0799 (1)41.TIF	0.121	46
VV2R0798 (1)40.TIF	0.119	52
VV2R0797 (1)39.TIF	0.149	67
VV2R0795 (1)37.TIF	0.146	82
VV2R0794 (1)36.TIF	0.152	69
VV2R0793 (1)35.TIF	0.180	95
VV2R0792 (1)34.TIF	0.320	70
VV2R0791 (1)33.TIF	0.214	62
VV2R0790 (1)32.TIF	0.169	46

Control Point Residuals

Control Point Names	Raw Data			Residuals		
	X	Y	Z	X	Y	Z
105	548.633	-1671.504	740.566	0.133	0.007	0.047
106	512.532	-1654.469	742.028	0.061	0.025	0.019
107	439.541	-1609.244	741.341	0.003	0.034	-0.051
108	356.434	-1570.334	743.072	0.072	0.063	-0.053
109	263.854	-1539.578	746.146	0.073	-0.205	0.006
Control Point RMS				0.089	0.109	0.045
Total					0.148	

Exterior Orientation

Image Names	Camera Location						Camera Rotation - Omega(ω), phi(φ) and kappa(κ)					
	X	Y	Z	δ_X	δ_Y	δ_Z	ω (°)	φ (°)	κ (°)	δ_ω (')	δ_φ (')	δ_κ (')
VV2R0799 (1)41.TIF	633.955	-1520.632	748.406	0.069	0.071	0.075	-69.903	-29.858	169.856	1.814	1.343	1.366
VV2R0798 (1)40.TIF	595.017	-1486.176	748.392	0.057	0.057	0.063	-69.969	-31.406	169.035	1.741	1.094	1.369
VV2R0797 (1)39.TIF	569.383	-1467.888	747.486	0.053	0.053	0.059	-69.647	-26.868	171.262	1.658	1.027	1.316
VV2R0795 (1)37.TIF	519.916	-1445.640	749.446	0.052	0.047	0.054	-71.373	-24.521	173.759	1.610	0.984	1.318
VV2R0794 (1)36.TIF	475.369	-1426.086	749.975	0.053	0.045	0.052	-71.195	-22.376	171.980	1.583	0.971	1.323
VV2R0793 (1)35.TIF	429.449	-1415.601	751.095	0.051	0.046	0.052	-69.360	-19.249	173.153	1.553	1.002	1.298
VV2R0792 (1)34.TIF	391.189	-1401.940	751.404	0.054	0.049	0.055	-71.601	-15.837	174.864	1.523	1.044	1.292
VV2R0791 (1)33.TIF	357.360	-1393.430	751.289	0.059	0.055	0.061	-70.131	-17.821	174.591	1.576	1.139	1.313
VV2R0790 (1)32.TIF	329.981	-1384.399	751.327	0.069	0.064	0.069	-72.163	-17.583	174.607	1.641	1.284	1.332

Blast #2

Pre-blast spoil side

Control Point File:	May5-before-bench.txt
Active Image Files:	VV2R0815 (1).TIF; VV2R0816 (1).TIF; VV2R0817 (1).TIF; VV2R0818 (1).TIF; VV2R0824 (1).TIF; VV2R0825 (1).TIF; VV2R0826 (1).TIF; VV2R0827 (1).TIF; VV2R0828 (1).TIF;
Number of Active Image Files:	9
Number of Camera Stations:	9

Image Residuals

Image Names	RMS Error (Pixel)	Active Points
VV2R0815 (1).TIF	0.177	61
VV2R0816 (1).TIF	0.152	116
VV2R0817 (1).TIF	0.133	105
VV2R0818 (1).TIF	0.135	107
VV2R0824 (1).TIF	0.147	152
VV2R0825 (1).TIF	0.154	149
VV2R0826 (1).TIF	0.134	173
VV2R0827 (1).TIF	0.124	162
VV2R0828 (1).TIF	0.125	125

Control Point Residuals

Control Point Names	Raw Data			Residuals		
	X	Y	Z	X	Y	Z
101	-695.571	-2142.764	708.239	-0.003	0.071	0.038
102	-672.971	-2114.198	707.798	0.085	0.021	-0.034
103	-641.305	-2071.298	707.578	0.125	0.138	-0.030
104	-611.211	-2033.387	709.122	0.023	-0.017	-0.060
105	-590.237	-2002.122	708.608	0.096	-0.006	-0.062
106	-562.893	-1969.146	708.292	-0.049	0.120	0.007
107	-534.876	-1939.447	706.629	-0.095	0.037	0.094
Control Point RMS				0.086	0.082	0.057
Total					0.132	

Exterior Orientation

Image Names	Camera Location						Camera Rotation - Omega(ω), phi(φ) and kappa(κ)					
	X	Y	Z	δ_X	δ_Y	δ_Z	ω (°)	φ (°)	κ (°)	δ_ω (')	δ_φ (')	δ_κ (')
VV2R0815 (1).TIF	-684.312	-2186.729	728.168	0.081	0.087	0.058	74.178	-49.998	12.911	5.719	1.828	4.477
VV2R0816 (1).TIF	-655.197	-2152.676	729.906	0.058	0.055	0.048	73.525	-45.895	13.728	5.241	1.632	4.100
VV2R0817 (1).TIF	-622.994	-2111.487	729.754	0.046	0.053	0.038	73.165	-49.544	13.173	5.587	1.437	4.342
VV2R0818 (1).TIF	-595.812	-2078.568	729.722	0.037	0.041	0.034	72.704	-51.570	13.923	5.814	1.408	4.511
VV2R0824 (1).TIF	-564.331	-2046.944	730.860	0.032	0.034	0.036	72.899	-49.992	14.030	5.626	1.410	4.349
VV2R0825 (1).TIF	-538.680	-2015.275	730.607	0.033	0.033	0.039	75.087	-49.184	12.138	5.570	1.370	4.320
VV2R0826 (1).TIF	-525.013	-1996.052	730.983	0.037	0.036	0.041	74.894	-49.479	11.403	5.600	1.385	4.342
VV2R0827 (1).TIF	-514.798	-1983.655	731.221	0.041	0.040	0.044	73.266	-49.415	12.614	5.569	1.435	4.306
VV2R0828 (1).TIF	-504.231	-1968.772	731.375	0.047	0.044	0.047	72.722	-46.730	12.900	5.278	1.460	4.078

Pre-blast highwall side

Control Point File:	May5-before-stockpile.txt
Active Image Files:	VV2R0801 (1).TIF; VV2R0802 (1).TIF; VV2R0803 (1).TIF; VV2R0804 (1).TIF; VV2R0805 (1).TIF; VV2R0812 (1).TIF; VV2R0813 (1).TIF; VV2R0814 (1).TIF;
Number of Active Image Files:	8
Number of Camera Stations:	8

Image Residuals

Image Names	RMS Error (Pixel)	Active Points
VV2R0801 (1).TIF	0.063	97
VV2R0802 (1).TIF	0.073	201
VV2R0803 (1).TIF	0.073	184
VV2R0804 (1).TIF	0.075	173
VV2R0805 (1).TIF	0.076	133
VV2R0812 (1).TIF	0.072	155
VV2R0813 (1).TIF	0.089	94
VV2R0814 (1).TIF	0.101	45

Control Point Residuals

Control Point Names	Raw Data			Residuals		
	X	Y	Z	X	Y	Z
101	-514.009	-1915.056	706.181	0.029	0.151	-0.046
102	-534.723	-1939.443	706.587	0.058	0.041	0.052
103	-562.873	-1969.212	708.268	-0.029	0.054	-0.017
104	-590.314	-2002.202	708.629	0.019	-0.086	-0.041
105	-611.251	-2033.483	709.222	-0.017	-0.113	0.040
106	-641.475	-2071.512	707.605	-0.045	-0.076	-0.003
107	-673.088	-2114.239	707.842	-0.032	-0.020	0.010
108	-695.620	-2142.799	708.228	-0.052	0.036	0.027
Control Point RMS				0.040	0.089	0.037
Total					0.104	

Exterior Orientation

Image Names	Camera Location						Camera Rotation - Omega(ω), phi(φ) and kappa(κ)					
	X	Y	Z	δ_X	δ_Y	δ_Z	ω (°)	φ (°)	κ (°)	δ_ω (')	δ_φ (')	δ_κ (')
VV2R0801 (1).TIF	-574.558	-1891.529	746.432	0.027	0.025	0.028	-64.336	51.317	-161.287	1.998	0.758	1.553
VV2R0802 (1).TIF	-600.627	-1922.470	746.512	0.022	0.020	0.024	-64.856	51.033	-160.945	1.985	0.704	1.543
VV2R0803 (1).TIF	-624.695	-1954.051	746.041	0.019	0.017	0.020	-64.101	49.340	-159.209	1.911	0.691	1.480
VV2R0804 (1).TIF	-654.327	-1985.356	746.969	0.017	0.017	0.020	-65.361	47.204	-160.751	1.845	0.677	1.430
VV2R0805 (1).TIF	-681.776	-2022.534	745.506	0.017	0.017	0.020	-64.682	48.293	-159.960	1.896	0.689	1.456
VV2R0812 (1).TIF	-703.490	-2049.814	746.420	0.019	0.019	0.021	-64.029	48.264	-160.311	1.891	0.709	1.448
VV2R0813 (1).TIF	-726.288	-2079.402	745.446	0.022	0.022	0.024	-64.476	48.872	-160.482	1.932	0.729	1.475
VV2R0814 (1).TIF	-741.518	-2096.699	745.503	0.025	0.025	0.027	-62.558	49.051	-157.976	1.950	0.772	1.481

Post-blast spoil side

Control Point File:	May5-after-right.txt
Active Image Files:	VV2R0840 (1).TIF; VV2R0841 (1).TIF; VV2R0836 (1).TIF; VV2R0837 (1).TIF; VV2R0835 (1).TIF;
Number of Active Image Files:	5
Number of Camera Stations:	4

Image Residuals

Image Names	RMS Error (Pixel)	Active Points
VV2R0841 (1).TIF	0.197	25
VV2R0836 (1).TIF	0.178	52
VV2R0835 (1).TIF	0.239	30

Control Point Residuals

Control Point Names	Raw Data			Residuals		
	X	Y	Z	X	Y	Z
101	-737.021	-2089.632	744.342	0.139	-0.130	-0.087
102	-746.927	-2052.222	744.295	0.056	-0.012	0.100
Control Point RMS				0.150	0.131	0.132
Total					0.239	

Exterior Orientation

Image Names	Camera Location						Camera Rotation - Omega(ω), phi(φ) and kappa(κ)					
	X	Y	Z	δ_X	δ_Y	δ_Z	ω (°)	φ (°)	κ (°)	δ_ω (')	δ_φ (')	δ_κ (')
VV2R0841 (1).TIF	-529.563	-1999.843	731.086	0.104	0.126	0.120	-48.749	-69.869	139.005	7.723	2.848	8.053
VV2R0836 (1).TIF	-585.032	-1894.509	746.944	0.089	0.079	0.083	-68.861	-37.414	167.965	2.350	2.794	7.205
VV2R0835 (1).TIF	-608.579	-1896.125	746.251	0.108	0.081	0.083	-69.334	-25.581	171.067	2.785	2.944	6.371

Blast #3

Pre-blast spoil side

Number of Control Points:	10
Active Image Files:	b1.TIF; b2.TIF; b3.TIF; b4.TIF; b5.TIF; b6.TIF; b7.TIF; b8.TIF; b9.TIF;
Number of Active Image Files:	9
Number of Camera Stations:	9

Image Residuals

Image Names	RMS Error (Pixel)	Active Points
b1.TIF	0.137	139
b2.TIF	0.389	192
b3.TIF	0.534	187
b4.TIF	0.285	168
b5.TIF	0.157	171
b6.TIF	0.159	178
b7.TIF	0.139	209
b8.TIF	0.147	206
b9.TIF	0.144	149

Control Point Residuals

Control Point Names	Raw Data			Residuals		
	X	Y	Z	X	Y	Z
101	-520.683	-1911.624	705.960	-0.151	-0.202	-0.005
102	-502.612	-1877.489	705.693	-0.108	-0.123	-0.062
103	-488.558	-1847.183	708.286	-0.109	-0.057	-0.021
104	-466.267	-1819.165	708.821	0.007	-0.037	0.056
105	-434.558	-1782.491	707.690	0.223	-0.040	0.037
Control Point RMS				0.155	0.125	0.047
Total					0.205	

Exterior Orientation

Image Names	Camera Location						Camera Rotation - Omega(ω), phi(φ) and kappa(κ)					
	X	Y	Z	δ_X	δ_Y	δ_Z	ω (°)	φ (°)	κ (°)	δ_ω (')	δ_φ (')	δ_κ (')
b1.TIF	-495.067	-1961.019	731.602	0.092	0.090	0.097	74.740	-46.452	10.173	7.609	2.765	6.535
b2.TIF	-483.470	-1950.173	731.764	0.083	0.081	0.089	77.279	-41.408	7.597	6.954	2.683	6.049
b3.TIF	-471.617	-1935.492	732.134	0.074	0.072	0.079	74.766	-46.017	10.956	7.534	2.730	6.474
b4.TIF	-454.115	-1921.401	731.061	0.066	0.065	0.074	78.655	-48.603	6.989	7.996	2.634	6.868
b5.TIF	-423.450	-1906.043	717.156	0.062	0.063	0.084	85.612	-43.400	1.690	7.281	2.528	6.318
b6.TIF	-409.305	-1855.165	733.262	0.063	0.064	0.070	77.796	-48.679	8.842	7.997	2.655	6.848
b7.TIF	-404.619	-1836.344	734.372	0.069	0.070	0.073	78.294	-47.509	8.393	7.820	2.649	6.703
b8.TIF	-382.269	-1815.745	734.876	0.084	0.085	0.092	76.037	-51.418	11.097	8.456	2.713	7.214
b9.TIF	-359.223	-1799.747	735.339	0.101	0.101	0.113	71.735	-59.568	14.439	10.227	2.833	8.749

Pre-blast highwall side

Number of Control Points:	10
Active Image Files:	s1.TIF; s2.TIF; s3.TIF; s4.TIF; s5.TIF; s6.TIF; s7.TIF; s8.TIF;
Number of Active Image Files:	8
Number of Camera Stations:	8

Image Residuals

Image Names	RMS Error (Pixel)	Active Points
S1.TIF	0.078	87
S2.TIF	0.079	138
S3.TIF	0.134	160
S4.TIF	0.174	194
S5.TIF	0.181	199
S6.TIF	0.147	172
S7.TIF	0.121	171
S8.TIF	0.114	129

Control Point Residuals

Control Point Names	Raw Data			Residuals		
	X	Y	Z	X	Y	Z
106	-413.124	-1801.390	708.984	0.111	0.015	-0.064
107	-440.549	-1846.217	709.766	0.160	0.025	-0.078
108	-455.294	-1880.627	714.566	0.064	0.061	0.049
109	-478.276	-1900.841	709.021	0.113	0.110	0.002
110	-510.824	-1939.737	710.643	0.048	0.057	-0.019
Control Point RMS				0.120	0.071	0.057
Total					0.150	

Exterior Orientation

Image Names	Camera Location						Camera Rotation - Omega(ω), phi(φ) and kappa(κ)					
	X	Y	Z	δ_X	δ_Y	δ_Z	ω (°)	φ (°)	κ (°)	δ_ω (')	δ_φ (')	δ_κ (')
S1.TIF	-459.771	-1729.596	755.833	0.054	0.054	0.060	-58.776	51.260	-157.632	3.269	1.497	3.016
S2.TIF	-479.134	-1760.942	755.510	0.043	0.043	0.048	-56.279	51.416	-155.467	3.235	1.474	2.983
S3.TIF	-503.812	-1794.671	751.973	0.034	0.034	0.038	-59.430	47.325	-157.985	2.998	1.418	2.777
S4.TIF	-524.668	-1821.985	750.781	0.032	0.032	0.035	-58.559	46.620	-156.100	2.948	1.427	2.730
S5.TIF	-539.354	-1843.081	748.395	0.032	0.032	0.036	-54.198	48.309	-152.864	3.000	1.474	2.765
S6.TIF	-550.632	-1858.776	747.933	0.035	0.035	0.039	-56.177	47.009	-155.631	2.947	1.455	2.722
S7.TIF	-566.619	-1881.829	747.105	0.041	0.041	0.046	-52.668	51.931	-151.428	3.224	1.499	2.962
S8.TIF	-578.151	-1893.463	746.723	0.045	0.045	0.052	-55.818	51.146	-153.134	3.211	1.472	2.956

Post-blast spoil side

Number of Control Points:	5
Active Image Files:	ab1.TIF; ab2.TIF; ab3.TIF; ab4.TIF; ab5.TIF; ab6.TIF; ab7.TIF;
Number of Active Image Files:	7
Number of Camera Stations:	7

Image Residuals

Image Names	RMS Error (Pixel)	Active Points
ab1.TIF	0.112	43
ab2.TIF	0.097	65
ab3.TIF	0.176	51
ab4.TIF	0.319	26
ab5.TIF	0.198	47
ab6.TIF	0.070	63
ab7.TIF	0.078	53

Control Point Residuals

Control Point Names	Raw Data			Residuals		
	X	Y	Z	X	Y	Z
101	-611.292	-1865.213	746.496	0.032	-0.079	-0.045
102	-588.199	-1841.524	747.340	0.028	-0.029	0.068
103	-571.094	-1821.246	747.429	0.044	0.061	-0.032
104	-566.187	-1811.364	750.390	-0.019	0.111	0.026
105	-534.015	-1771.583	752.343	0.016	0.139	0.015
Control Point RMS				0.033	0.103	0.046
Total					0.118	

Exterior Orientation

Image Names	Camera Location						Camera Rotation - Omega(ω), phi(φ) and kappa(κ)					
	X	Y	Z	δ_X	δ_Y	δ_Z	ω (°)	φ (°)	κ (°)	δ_ω (')	δ_φ (')	δ_κ (')
ab1.TIF	-487.405	-1953.923	731.545	0.053	0.050	0.064	73.954	-47.032	11.746	2.310	1.422	2.042
ab2.TIF	-473.356	-1940.295	732.378	0.048	0.046	0.056	71.776	-49.887	14.105	2.384	1.334	2.140
ab3.TIF	-453.029	-1925.508	732.841	0.046	0.042	0.050	73.980	-45.396	11.828	2.259	1.236	1.974
ab4.TIF	-405.727	-1894.323	721.114	0.049	0.050	0.049	78.521	-49.475	9.513	2.368	1.236	2.147
ab5.TIF	-407.203	-1846.114	734.486	0.043	0.045	0.048	72.027	-51.702	13.779	2.496	1.248	2.197
ab6.TIF	-394.596	-1829.350	735.652	0.049	0.049	0.055	75.641	-39.594	8.423	2.223	1.311	1.800
ab7.TIF	-379.713	-1812.189	734.820	0.057	0.059	0.065	75.620	-42.996	9.342	2.288	1.488	1.912

Post-blast highwall side

Number of Control Points:	5
Active Image Files:	as1.TIF; as2.TIF; as3.TIF; as4.TIF; as5.TIF; as6.TIF; as7.TIF; as8.TIF;
Number of Active Image Files:	8
Number of Camera Stations:	8

Image Residuals

Image Names	RMS Error (Pixel)	Active Points
as1.TIF	0.161	80
as2.TIF	0.157	94
as3.TIF	0.160	99
as4.TIF	0.165	88
as5.TIF	0.169	75
as6.TIF	0.154	72
as7.TIF	0.180	49
as8.TIF	0.180	19

Control Point Residuals

Control Point Names	Raw Data			Residuals		
	X	Y	Z	X	Y	Z
106	-386.179	-1820.222	734.229	-0.010	0.071	0.053
107	-399.915	-1837.724	734.686	-0.036	0.036	-0.011
108	-410.667	-1889.586	719.444	0.017	-0.203	-0.167
109	-458.163	-1928.161	732.091	-0.083	-0.137	-0.045
110	-476.856	-1944.880	731.555	-0.045	-0.246	0.139
Control Point RMS				0.051	0.178	0.114
Total					0.218	

Exterior Orientation

Image Names	Camera Location						Camera Rotation - Omega(ω), phi(φ) and kappa(κ)					
	X	Y	Z	δ_X	δ_Y	δ_Z	ω (°)	φ (°)	κ (°)	δ_ω (')	δ_φ (')	δ_κ (')
as1.TIF	-464.388	-1681.573	757.604	0.057	0.058	0.067	-68.362	42.184	-165.191	1.961	1.205	2.246
as2.TIF	-482.848	-1702.553	756.604	0.050	0.051	0.058	-68.977	41.650	-166.082	1.942	1.172	2.229
as3.TIF	-500.354	-1724.045	756.203	0.045	0.045	0.050	-68.657	40.310	-165.623	1.895	1.154	2.182
as4.TIF	-523.128	-1750.412	755.773	0.042	0.041	0.044	-68.800	41.869	-166.028	1.948	1.145	2.233
as5.TIF	-542.042	-1779.101	752.881	0.040	0.041	0.043	-68.230	38.882	-166.923	1.848	1.156	2.132
as6.TIF	-565.094	-1808.215	751.379	0.042	0.044	0.049	-64.949	46.247	-161.934	2.110	1.191	2.378
as7.TIF	-582.807	-1834.515	748.216	0.047	0.047	0.057	-63.600	43.431	-161.586	2.001	1.234	2.259
as8.TIF	-613.969	-1868.135	747.446	0.064	0.065	0.074	-64.689	52.586	-159.618	2.552	1.508	2.759

Blast #4

Pre-blast spoil side

Number of Control Points:	5
Active Image Files:	c1-1.TIF; c1-2.TIF; c2-1.TIF; c2-2.TIF; c3-1.TIF; c3-2.TIF; c4-1.TIF; c4-2.TIF; c5-1.TIF; c5-2.TIF; c6-1.TIF; c6-2.TIF;
Number of Active Image Files:	12
Number of Camera Stations:	6

Image Residuals

Image Names	RMS Error (Pixel)	Active Points
c1-1.TIF	0.104	72
c1-2.TIF	0.099	88
c2-1.TIF	0.102	50
c2-2.TIF	0.095	64
c3-1.TIF	0.094	107
c3-2.TIF	0.094	142
c4-1.TIF	0.088	172
c4-2.TIF	0.100	143
c5-1.TIF	0.106	156
c5-2.TIF	0.106	130
c6-1.TIF	0.100	109
c6-2.TIF	0.077	98

Control Point Residuals

Control Point Names	Raw Data			Residuals		
	X	Y	Z	X	Y	Z
101	424.106	-1399.560	750.818	0.026	-0.042	-0.001
102	456.431	-1412.131	749.340	-0.014	-0.102	-0.010
103	508.005	-1440.584	748.325	0.023	-0.068	0.024
104	548.959	-1457.636	747.076	-0.035	-0.079	-0.053
105	577.270	-1473.992	747.873	0.005	-0.063	0.011
Control Point RMS				0.025	0.082	0.030
Total					0.091	

Exterior Orientation

Image Names	Camera Location						Camera Rotation - Omega(ω), phi(φ) and kappa(κ)					
	X	Y	Z	δ_X	δ_Y	δ_Z	ω (°)	φ (°)	κ (°)	δ_ω (')	δ_φ (')	δ_κ (')
c1-1.TIF	285.525	-1499.080	740.836	0.040	0.035	0.035	75.233	-7.507	2.802	0.961	0.979	0.709
c1-2.TIF	285.525	-1499.080	740.836	0.040	0.035	0.035	76.495	10.888	-2.894	0.987	0.980	0.713
c2-1.TIF	339.087	-1513.311	739.439	0.027	0.025	0.026	76.796	15.371	-4.164	0.962	0.608	0.681
c2-2.TIF	339.087	-1513.311	739.439	0.027	0.025	0.026	75.068	35.638	-10.658	1.097	0.610	0.805
c3-1.TIF	396.655	-1535.882	739.056	0.021	0.019	0.021	79.134	16.248	-4.361	0.965	0.565	0.690
c3-2.TIF	396.655	-1535.882	739.056	0.021	0.019	0.021	78.802	25.998	-6.666	1.020	0.565	0.736
c4-1.TIF	444.401	-1559.826	738.124	0.019	0.019	0.020	77.453	22.358	-6.586	0.995	0.575	0.714
c4-2.TIF	444.401	-1559.826	738.124	0.019	0.019	0.020	75.168	38.470	-9.552	1.126	0.579	0.839
c5-1.TIF	496.941	-1591.539	736.506	0.023	0.022	0.026	78.182	23.422	-5.336	1.003	0.588	0.728
c5-2.TIF	496.941	-1591.539	736.506	0.023	0.022	0.026	75.062	40.501	-11.021	1.155	0.593	0.873
c6-1.TIF	549.980	-1618.816	735.704	0.029	0.029	0.035	81.228	18.286	-4.716	0.979	0.590	0.713
c6-2.TIF	549.980	-1618.816	735.704	0.029	0.029	0.035	79.261	32.171	-7.076	1.076	0.593	0.798

Pre-blast highwalll side (I)

Control Point File:	Before-Stockpile(28July).txt
Active Image Files:	MergeImgC7-123.tif; MergeImgC8-123.tif;
Number of Active Image Files:	2
Number of Camera Stations:	2

Image Residuals

Image Names	RMS Error (Pixel)	Active Points
MergeImgC7-123.tif	0.213	410
MergeImgC8-123.tif	0.203	409

Control Point Residuals

Control Point Names	Raw Data			Residuals		
	X	Y	Z	X	Y	Z
106	503.092	-1532.233	704.713	0.201	0.026	0.059
107	456.877	-1511.418	707.561	-0.147	0.029	0.014
108	418.355	-1494.313	709.465	-0.007	0.059	-0.006
Control Point RMS				0.176	0.050	0.043
Total					0.188	

Exterior Orientation

Image Names	Camera Location						Camera Rotation - Omega(ω), phi(φ) and kappa(κ)					
	X	Y	Z	δ_X	δ_Y	δ_Z	ω (°)	φ (°)	κ (°)	δ_ω (')	δ_φ (')	δ_κ (')
MergeImgC7-123.tif	542.762	-1477.143	741.907	0.101	0.104	0.107	-71.065	-29.444	172.687	7.556	4.494	6.275
MergeImgC8-123.tif	514.608	-1459.661	742.324	0.092	0.099	0.108	-73.615	-12.046	177.274	7.880	4.542	5.547

Pre-blast highwalll side (II)

Control Point File:	Before-Stockpile(28July).txt
Active Image Files:	MergeImgC7-345.tif; MergeImgC8-345.tif;
Number of Active Image Files:	2
Number of Camera Stations:	2

Image Residuals

Image Names	RMS Error (Pixel)	Active Points
MergeImgC7-345.tif	0.150	297
MergeImgC8-345.tif	0.178	296

Control Point Residuals

Control Point Names	Raw Data			Residuals		
	X	Y	Z	X	Y	Z
101	502.967	-1532.334	704.684	0.076	-0.075	0.030
102	456.959	-1511.347	707.588	-0.065	0.100	0.041
103	418.310	-1494.332	709.331	-0.052	0.040	-0.140
104	381.596	-1478.258	713.227	0.081	-0.038	0.088
Control Point RMS				0.080	0.079	0.100
Total					0.150	

Exterior Orientation

Image Names	Camera Location						Camera Rotation - Omega(ω), phi(φ) and kappa(κ)					
	X	Y	Z	δ_X	δ_Y	δ_Z	ω (°)	φ (°)	κ (°)	δ_ω (')	δ_φ (')	δ_κ (')
MergeImgC7-345.tif	542.848	-1477.161	741.945	0.075	0.084	0.082	-43.120	-66.040	138.935	7.654	2.807	7.264
MergeImgC8-345.tif	514.530	-1459.555	742.333	0.066	0.074	0.083	-54.558	-58.489	149.767	6.712	2.834	5.598

Post-blast spoil side (I)

Number of Control Points:	4
Active Image Files:	MergeImgC13-123.tif; MergeImgC14-123.tif;
Number of Active Image Files:	2
Number of Camera Stations:	2

Image Residuals

Image Names	RMS Error (Pixel)	Active Points
MergeImgC13-123.tif	0.268	177
MergeImgC14-123.tif	0.230	177

Control Point Residuals

Control Point Names	Raw Data			Residuals		
	X	Y	Z	X	Y	Z
102	457.313	-1371.229	749.633	-0.008	-0.104	0.020
103	497.402	-1387.820	749.327	0.024	0.104	-0.019
Control Point RMS				0.025	0.148	0.028
Total					0.152	

Exterior Orientation

Image Names	Camera Location						Camera Rotation - Omega(ω), phi(φ) and kappa(κ)					
	X	Y	Z	δ_X	δ_Y	δ_Z	ω (°)	φ (°)	κ (°)	δ_ω (')	δ_φ (')	δ_κ (')
MergeImgC13-123.tif	361.249	-1519.845	740.267	0.127	0.127	0.151	77.902	-6.686	2.506	9.554	4.588	11.634
MergeImgC14-123.tif	401.191	-1535.727	738.327	0.121	0.121	0.151	77.359	-4.630	1.546	9.174	4.661	11.564

Post-blast spoil side (II)

Control Point File:	After-Bench(28July).txt
Active Image Files:	MergeImgC13-345.tif; MergeImgC14-2345.tif;
Number of Active Image Files:	2
Number of Camera Stations:	2

Image Residuals

Image Names	RMS Error (Pixel)	Active Points
MergeImgC13-345.tif	0.137	292
MergeImgC14-2345.tif	0.173	292

Control Point Residuals

Control Point Names	Raw Data			Residuals		
	X	Y	Z	X	Y	Z
102	457.353	-1371.153	749.604	0.032	-0.028	-0.009
103	497.390	-1387.922	749.368	0.012	0.002	0.022
104	537.794	-1412.549	748.972	-0.039	0.016	-0.015
Control Point RMS				0.036	0.023	0.020
Total					0.047	

Exterior Orientation

Image Names	Camera Location						Camera Rotation - Omega(ω), phi(φ) and kappa(κ)					
	X	Y	Z	δ_X	δ_Y	δ_Z	ω (°)	φ (°)	κ (°)	δ_ω (')	δ_φ (')	δ_κ (')
MergeImgC13-345.tif	361.116	-1519.878	740.284	0.077	0.077	0.083	70.759	50.028	-14.991	2.971	2.320	6.077
MergeImgC14-2345.tif	401.335	-1535.684	738.313	0.071	0.072	0.082	73.584	40.601	-10.383	2.476	2.211	5.225

Post-blast highwalll side (I)

Control Point File:	After-Stockpile(28July).txt
Active Image Files:	MergeImgC11-123.tif; MergeImgC12-123.tif;
Number of Active Image Files:	2
Number of Camera Stations:	2

Image Residuals

Image Names	RMS Error (Pixel)	Active Points
MergeImgC11-123.tif	0.358	70
MergeImgC12-123.tif	0.323	72

Control Point Residuals

Control Point Names	Raw Data			Residuals		
	X	Y	Z	X	Y	Z
105	455.901	-1565.924	736.914	0.231	0.355	0.031
106	400.661	-1537.463	737.992	-0.266	-0.224	-0.056
107	349.286	-1514.813	738.484	-0.013	0.016	-0.027
108	299.693	-1503.666	739.532	-0.029	0.038	0.058
Control Point RMS				0.204	0.244	0.052
Total					0.322	

Exterior Orientation

Image Names	Camera Location						Camera Rotation - Omega(ω), phi(φ) and kappa(κ)					
	X	Y	Z	δ_X	δ_Y	δ_Z	ω (°)	φ (°)	κ (°)	δ_ω (')	δ_φ (')	δ_κ (')
MergeImgC11-123.tif	527.944	-1405.225	750.053	0.167	0.172	0.178	-71.716	-6.817	178.796	5.727	3.698	5.257
MergeImgC12-123.tif	483.759	-1379.251	750.639	0.169	0.165	0.184	-69.841	-3.322	179.000	5.883	3.701	5.206

Post-blast highwalll side (II)

Control Point File:	Control Point Data
Active Image Files:	MergeImgC11-345.tif; MergeImgC12-345.tif;
Number of Active Image Files:	2
Number of Camera Stations:	2

Image Residuals

Image Names	RMS Error (Pixel)	Active Points
MergeImgC11-345.tif	0.200	74
MergeImgC12-345.tif	0.220	73

Control Point Residuals

Control Point Names	Raw Data			Residuals		
	X	Y	Z	X	Y	Z
105	455.573	-1566.236	736.895	-0.097	0.043	0.012
106	400.788	-1537.370	738.064	-0.139	-0.131	0.016
107	349.456	-1514.717	738.514	0.157	0.112	0.003
108	299.717	-1503.785	739.442	-0.005	-0.081	-0.032
Control Point RMS				0.134	0.113	0.022
Total					0.176	

Exterior Orientation

Image Names	Camera Location						Camera Rotation - Omega(ω), phi(φ) and kappa(κ)					
	X	Y	Z	δ_X	δ_Y	δ_Z	ω (°)	φ (°)	κ (°)	δ_ω (')	δ_φ (')	δ_κ (')
MergeImgC11-345.tif	527.706	-1404.965	749.909	0.104	0.108	0.109	-60.308	-53.660	152.442	3.848	2.387	5.218
MergeImgC12-345.tif	484.004	-1379.268	750.791	0.102	0.103	0.113	-59.884	-47.784	155.155	3.461	2.456	4.606

Blast #5

Post-blast spoil side

Control Point File:	Control Point Data
Active Image Files:	MergeImgC10.tif;MergeImgC11.tif;
Number of Active Image Files:	2
Number of Camera Stations:	2

Image Residuals

Image Names	RMS Error (Pixel)	Active Points
MergeImgC10.tif	0.699	335
MergeImgC11.tif	0.695	335

Control Point Residuals

Control Point Names	Raw Data			Residuals		
	X	Y	Z	X	Y	Z
101	961.809	-1729.717	745.964	-0.021	0.011	-0.001
Control Point RMS				0.021	0.011	0.001
Total					0.023	

Exterior Orientation

Image Names	Camera Location						Camera Rotation - Omega(ω), phi(φ) and kappa(κ)					
	X	Y	Z	δ_X	δ_Y	δ_Z	ω (°)	φ (°)	κ (°)	δ_ω (')	δ_φ (')	δ_κ (')
MergeImgC10.tif	840.537	-1800.059	731.447	0.361	0.360	0.492	71.661	30.447	-9.650	79.515	41.151	81.699
MergeImgC11.tif	856.350	-1809.753	732.113	0.341	0.341	0.491	75.026	25.141	-7.896	86.335	37.366	80.102

Post-blast highwall side

Control Point File:	Control Point Data
Active Image Files:	MergeImgC1.tif; MergeImgC2.tif; MergeImgC3.tif;
Number of Active Image Files:	3
Number of Camera Stations:	3

Image Residuals

Image Names	RMS Error (Pixel)	Active Points
MergeImgC1.tif	0.212	289
MergeImgC2.tif	0.238	355
MergeImgC3.tif	0.217	317

Control Point Residuals

Control Point Names	Raw Data			Residuals		
	X	Y	Z	X	Y	Z
105	871.037	-1817.990	731.279	0.308	0.016	-0.036
104	833.849	-1797.009	731.242	0.110	-0.055	0.055
103	791.447	-1766.467	729.971	-0.595	-0.026	0.123
102	761.265	-1750.003	730.143	0.074	0.176	-0.144
Control Point RMS				0.395	0.108	0.116
Total					0.425	

Exterior Orientation

Image Names	Camera Location						Camera Rotation - Omega(ω), phi(φ) and kappa(κ)					
	X	Y	Z	δ_X	δ_Y	δ_Z	ω (°)	φ (°)	κ (°)	δ_ω (')	δ_φ (')	δ_κ (')
MergeImgC1.tif	724.390	-1567.237	747.676	0.089	0.090	0.098	-68.649	41.542	-164.334	3.756	3.106	11.615
MergeImgC2.tif	716.791	-1569.429	748.113	0.089	0.090	0.091	-67.764	43.992	-163.320	4.329	3.215	12.027
MergeImgC3.tif	708.642	-1571.690	748.184	0.090	0.091	0.090	-67.889	42.541	-164.229	3.968	3.199	11.751

Blast #6

Pre-blast spoil side (camera stations C7&C8)

Control Point File:	Before-Bench(Sep1).txt
Active Image Files:	MergeImgC7.tif; MergeImgC8.tif;
Number of Active Image Files:	2
Number of Camera Stations:	2

Image Residuals

Image Names	RMS Error (Pixel)	Active Points
MergeImgC7.tif	0.161	195
MergeImgC8.tif	0.165	195

Control Point Residuals

Control Point Names	Raw Data			Residuals		
	X	Y	Z	X	Y	Z
101	1312.090	-1998.334	712.652	-0.084	-0.191	0.052
102	1337.040	-2024.527	714.812	0.078	-0.024	0.030
103	1347.240	-2043.899	716.175	0.043	0.149	-0.076
Control Point RMS				0.087	0.172	0.068
Total					0.205	

Exterior Orientation

Image Names	Camera Location						Camera Rotation - Omega(ω), phi(φ) and kappa(κ)					
	X	Y	Z	δ_X	δ_Y	δ_Z	ω (°)	φ (°)	κ (°)	δ_ω (')	δ_φ (')	δ_κ (')
MergeImgC7.tif	1191.066	-2019.384	742.174	0.084	0.084	0.086	61.021	55.827	-22.367	10.691	3.218	4.937
MergeImgC8.tif	1204.525	-2032.562	741.984	0.077	0.077	0.084	62.978	52.709	-20.624	10.765	3.238	4.543

Pre-blast spoil side (camera stations C9&C10)

Control Point File:	Before-Bench(Sep1).txt
Active Image Files:	MergeImgC9.tif; MergeImgC10.tif;
Number of Active Image Files:	2
Number of Camera Stations:	2

Image Residuals

Image Names	RMS Error (Pixel)	Active Points
MergeImgC9.tif	0.276	406
MergeImgC10.tif	0.290	406

Control Point Residuals

Control Point Names	Raw Data			Residuals		
	X	Y	Z	X	Y	Z
102	1337.222	-2024.542	714.585	0.260	-0.039	-0.197
103	1346.968	-2043.978	716.407	-0.229	0.070	0.156
Control Point RMS				0.346	0.080	0.252
Total					0.435	

Exterior Orientation

Image Names	Camera Location						Camera Rotation - Omega(ω), phi(φ) and kappa(κ)					
	X	Y	Z	δ_X	δ_Y	δ_Z	ω (°)	φ (°)	κ (°)	δ_ω (')	δ_φ (')	δ_κ (')
MergeImgC9.tif	1254.120	-2068.968	742.167	0.144	0.144	0.155	-16.476	73.908	-111.284	31.010	18.479	28.763
MergeImgC10.tif	1256.727	-2081.147	735.386	0.145	0.145	0.156	1.837	76.276	-89.652	29.478	16.535	48.358

Pre-blast highwall side (camera stations C1&C2)

Control Point File: Before-Spoileside(Sep1).txt
Active Image Files: MergeImgc1.tif; MergeImgc2.tif;
Number of Active Image Files: 2
Number of Camera Stations: 2

Image Residuals

Image Names	RMS Error (Pixel)	Active Points
MergeImgc1.tif	0.192	216
MergeImgc2.tif	0.171	216

Control Point Residuals

Control Point Names	Raw Data			Residuals		
	X	Y	Z	X	Y	Z
104	1294.979	-2055.816	714.685	-0.022	0.170	0.007
105	1294.574	-2026.597	713.029	-0.052	0.048	0.009
106	1271.572	-1993.987	712.017	0.030	-0.135	-0.024
Control Point RMS				0.045	0.157	0.019
Total					0.165	

Exterior Orientation

Image Names	Camera Location						Camera Rotation - Omega(ω), phi(φ) and kappa(κ)					
	X	Y	Z	δ_X	δ_Y	δ_Z	ω (°)	φ (°)	κ (°)	δ_ω (')	δ_φ (')	δ_κ (')
MergeImgc1.tif	1365.035	-2116.839	739.055	0.088	0.088	0.093	54.157	-65.897	32.671	18.547	5.731	32.677
MergeImgc2.tif	1376.079	-2103.791	740.611	0.089	0.087	0.106	39.344	-71.903	48.975	24.643	8.559	37.771

Pre-blast highwall side (camera stations C5&C6)

Control Point File:	Before-Spoileside(Sep1).txt
Active Image Files:	MergeImgC5.tif; MergeImgC6.tif;
Number of Active Image Files:	2
Number of Camera Stations:	2

Image Residuals

Image Names	RMS Error (Pixel)	Active Points
MergeImgC5.tif	0.166	276
MergeImgC6.tif	0.186	276

Control Point Residuals

Control Point Names	Raw Data			Residuals		
	X	Y	Z	X	Y	Z
104	1294.997	-2055.964	714.677	-0.004	0.022	-0.001
105	1294.650	-2026.626	713.031	0.024	0.019	0.011
106	1271.505	-1993.876	712.031	-0.037	-0.024	-0.010
Control Point RMS				0.031	0.027	0.011
Total					0.043	

Exterior Orientation

Image Names	Camera Location						Camera Rotation - Omega(ω), phi(φ) and kappa(κ)					
	X	Y	Z	δ_X	δ_Y	δ_Z	ω (°)	φ (°)	κ (°)	δ_ω (')	δ_φ (')	δ_κ (')
MergeImgC5.tif	1367.618	-1994.693	743.895	0.088	0.088	0.095	-59.435	-57.932	153.613	8.309	4.210	11.383
MergeImgC6.tif	1348.393	-1984.530	743.982	0.078	0.078	0.083	-64.384	-54.032	155.538	7.578	4.250	10.240

Post-blast spoil side (camera stations C15&C16)

Control Point File:	After-Bench(Sep1).txt
Active Image Files:	MergeImgC15.tif;MergeImgC16.tif;
Number of Active Image Files:	2
Number of Camera Stations:	2

Image Residuals

Image Names	RMS Error (Pixel)	Active Points
MergeImgC15.tif	0.215	305
MergeImgC16.tif	0.227	305

Control Point Residuals

Control Point Names	Raw Data			Residuals		
	X	Y	Z	X	Y	Z
101	1307.948	-1898.965	742.711	-0.219	-0.217	-0.001
102	1365.635	-1933.983	743.653	0.217	0.122	0.002
Control Point RMS				0.308	0.249	0.002
Total					0.396	

Exterior Orientation

Image Names	Camera Location						Camera Rotation - Omega(ω), phi(φ) and kappa(κ)					
	X	Y	Z	δ_X	δ_Y	δ_Z	ω (°)	φ (°)	κ (°)	δ_ω (')	δ_φ (')	δ_κ (')
MergeImgC15.tif	1149.409	-1982.105	740.541	0.111	0.112	0.112	57.308	59.232	-31.697	8.951	3.755	8.990
MergeImgC16.tif	1156.793	-1987.140	740.498	0.108	0.109	0.112	58.769	59.460	-29.926	8.838	3.689	9.156

Post-blast spoil side (camera stations C17&C18)

Control Point File: After-Bench(Sep1).txt
Active Image Files: MergeImgC17.tif; MergeImgC18.tif;
Number of Active Image Files: 2
Number of Camera Stations: 2

Image Residuals

Image Names	RMS Error (Pixel)	Active Points
MergeImgC17.tif	0.138	111
MergeImgC18.tif	0.144	111

Control Point Residuals

Control Point Names	Raw Data			Residuals		
	X	Y	Z	X	Y	Z
102	1365.419	-1934.107	743.651	0.001	-0.002	0.000
Control Point RMS				0.001	0.002	0.000
Total					0.002	

Exterior Orientation

Image Names	Camera Location						Camera Rotation - Omega(ω), phi(φ) and kappa(κ)					
	X	Y	Z	δ_X	δ_Y	δ_Z	ω (°)	φ (°)	κ (°)	δ_ω (')	δ_φ (')	δ_κ (')
MergeImgC17.tif	1211.479	-2035.284	741.339	0.072	0.072	0.100	50.101	72.212	-37.138	26.615	18.340	69.119
MergeImgC18.tif	1218.825	-2042.333	742.249	0.071	0.071	0.100	60.210	66.897	-24.766	17.072	14.415	61.085

Post-blast spoil side (camera stations C19&C20)

Control Point File:	After-Bench(Sep1).txt
Active Image Files:	MergeImgC19.tif; MergeImgC20.tif;
Number of Active Image Files:	2
Number of Camera Stations:	2

Image Residuals

Image Names	RMS Error (Pixel)	Active Points
MergeImgC19.tif	0.231	323
MergeImgC20.tif	0.228	324

Control Point Residuals

Control Point Names	Raw Data			Residuals		
	X	Y	Z	X	Y	Z
101	1308.139	-1898.740	742.839	-0.028	0.008	0.127
102	1365.180	-1934.358	743.508	-0.238	-0.253	-0.143
103	1372.390	-2103.453	738.273	0.439	-0.199	0.058
Control Point RMS				0.353	0.228	0.141
Total					0.444	

Exterior Orientation

Image Names	Camera Location						Camera Rotation - Omega(ω), phi(φ) and kappa(κ)					
	X	Y	Z	δ_X	δ_Y	δ_Z	ω (°)	φ (°)	κ (°)	δ_ω (')	δ_φ (')	δ_κ (')
MergeImgC19.tif	1247.446	-2061.628	741.409	0.099	0.102	0.115	46.455	69.807	-37.465	10.611	3.922	11.454
MergeImgC20.tif	1253.578	-2068.397	741.821	0.099	0.100	0.112	59.380	59.244	-24.065	7.392	3.442	8.562

Post-blast highwall side (camera stations C11&C12)

Control Point File:	After-Spoileside(Sep1).txt
Active Image Files:	MergeImgC11.tif; MergeImgC12.tif;
Number of Active Image Files:	2
Number of Camera Stations:	2

Image Residuals

Image Names	RMS Error (Pixel)	Active Points
MergeImgC11.tif	0.114	285
MergeImgC12.tif	0.124	285

Control Point Residuals

Control Point Names	Raw Data			Residuals		
	X	Y	Z	X	Y	Z
104	1290.687	-2051.028	715.689	-0.122	0.072	0.017
105	1212.119	-2034.660	740.040	0.077	-0.024	-0.029
Control Point RMS				0.144	0.076	0.034
Total					0.166	

Exterior Orientation

Image Names	Camera Location						Camera Rotation - Omega(ω), phi(φ) and kappa(κ)					
	X	Y	Z	δ_X	δ_Y	δ_Z	ω (°)	φ (°)	κ (°)	δ_ω (')	δ_φ (')	δ_κ (')
MergeImgC11.tif	1364.086	-2117.191	738.967	0.057	0.058	0.065	76.995	-19.941	3.853	7.568	2.114	5.383
MergeImgC12.tif	1372.342	-2105.582	739.807	0.058	0.059	0.059	75.063	-20.656	7.588	7.517	2.174	5.380

Post-blast highwall side (camera stations C13&C14)

Control Point File:	Control Point Data
Active Image Files:	MergeImgC14.tif; MergeImgC13.tif;
Number of Active Image Files:	2
Number of Camera Stations:	2

Image Residuals

Image Names	RMS Error (Pixel)	Active Points
MergeImgC14.tif	0.789	80
MergeImgC13.tif	0.824	80

Control Point Residuals

Control Point Names	Raw Data			Residuals		
	X	Y	Z	X	Y	Z
103	1371.930	-2103.265	737.691	-0.030	0.035	-0.001
Control Point RMS				0.030	0.035	0.001
Total					0.046	

Exterior Orientation

Image Names	Camera Location						Camera Rotation - Omega(ω), phi(φ) and kappa(κ)					
	X	Y	Z	δ_X	δ_Y	δ_Z	ω (°)	φ (°)	κ (°)	δ_ω (')	δ_φ (')	δ_κ (')
MergeImgC14.tif	1135.184	-1885.372	730.822	0.448	0.432	0.591	-80.248	50.305	-174.158	26.116	36.082	270.562
MergeImgC13.tif	1146.214	-1880.350	730.941	0.444	0.425	0.591	-79.638	50.881	-174.698	29.619	37.892	273.281

Appendix C: Point-Cloud Models

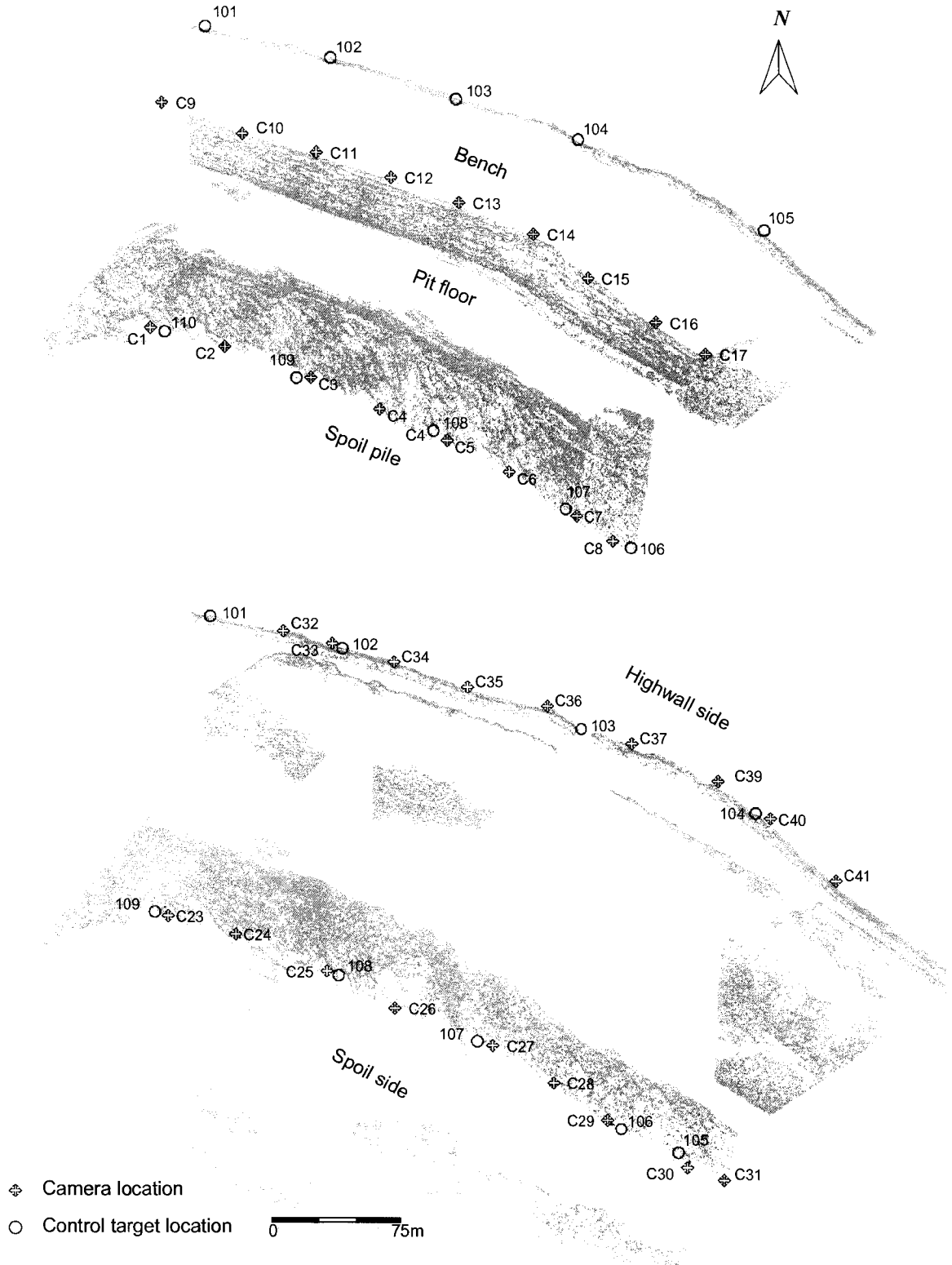

Figure 74 Blast #1: Pre-blast and post-blast point-cloud models - plan view

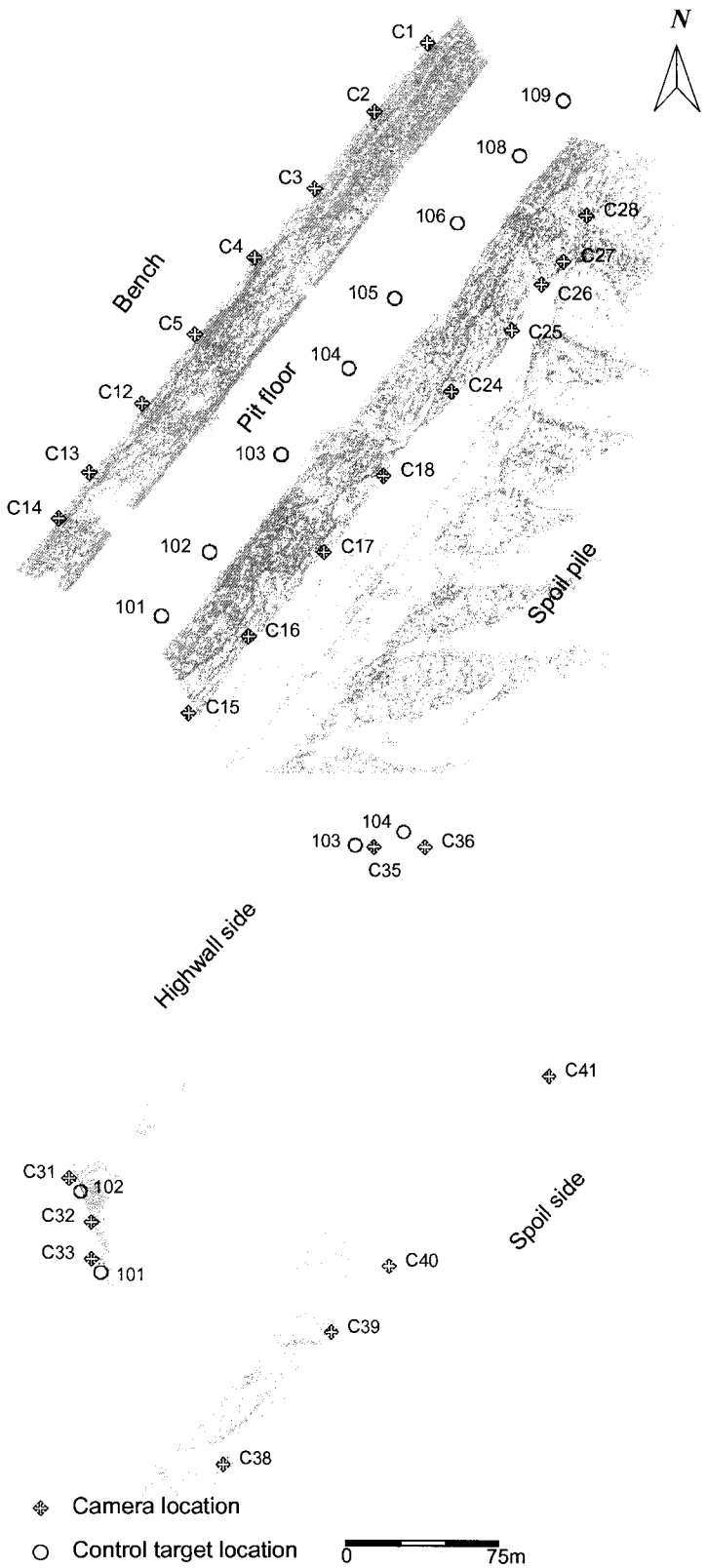

Figure 75 Blast #2: Pre-blast and post-blast point-cloud models - plan view

Figure 76 Blast #3: Pre-blast and post-blast point-cloud models - plan view

Figure 77 Blast #4: Pre-blast and post-blast point-cloud models - plan view

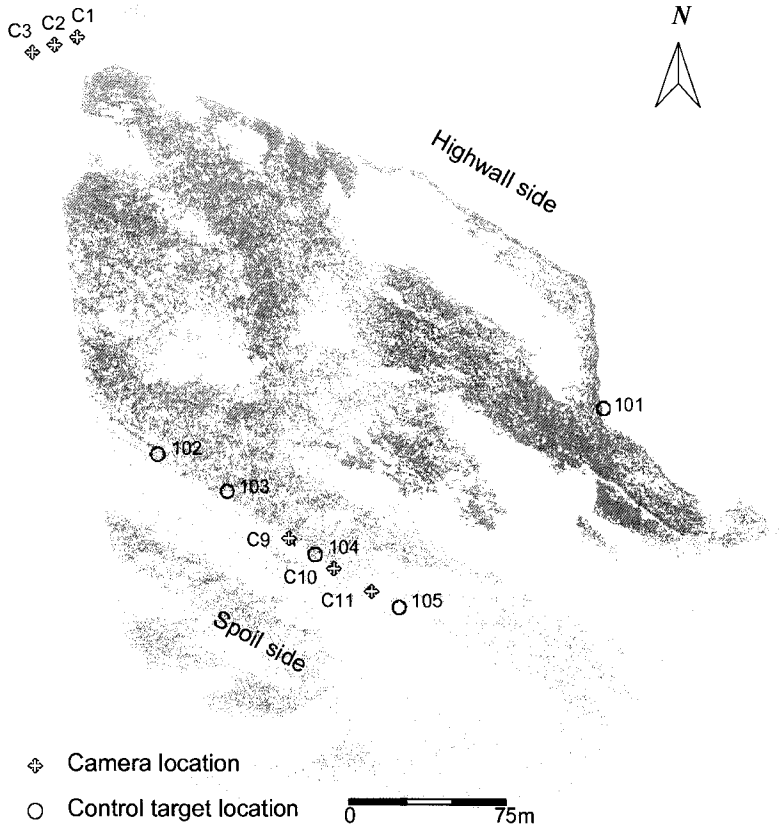

Figure 78 Blast #5: Post-blast point-cloud models - plan view

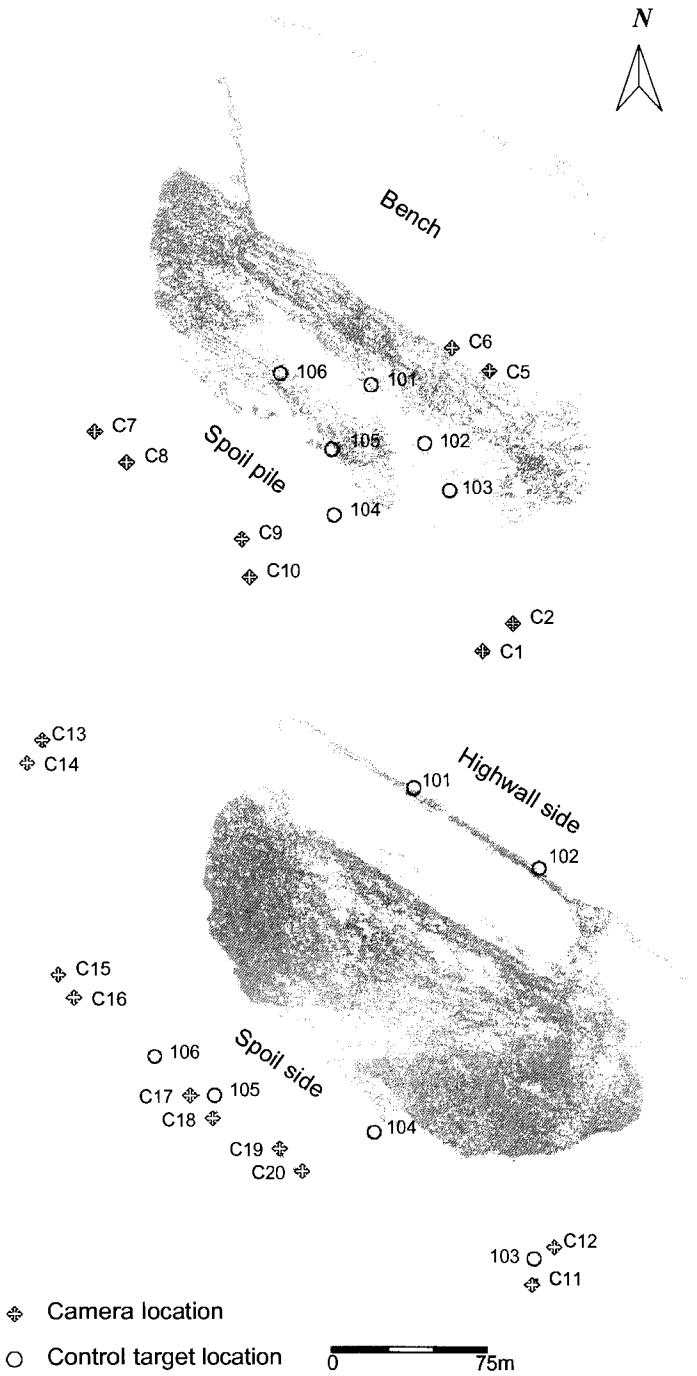

Figure 79 Blast #6: Pre-blast and post-blast point-cloud models - plan view

Appendix D: Pre- and Post-Blast DTMs

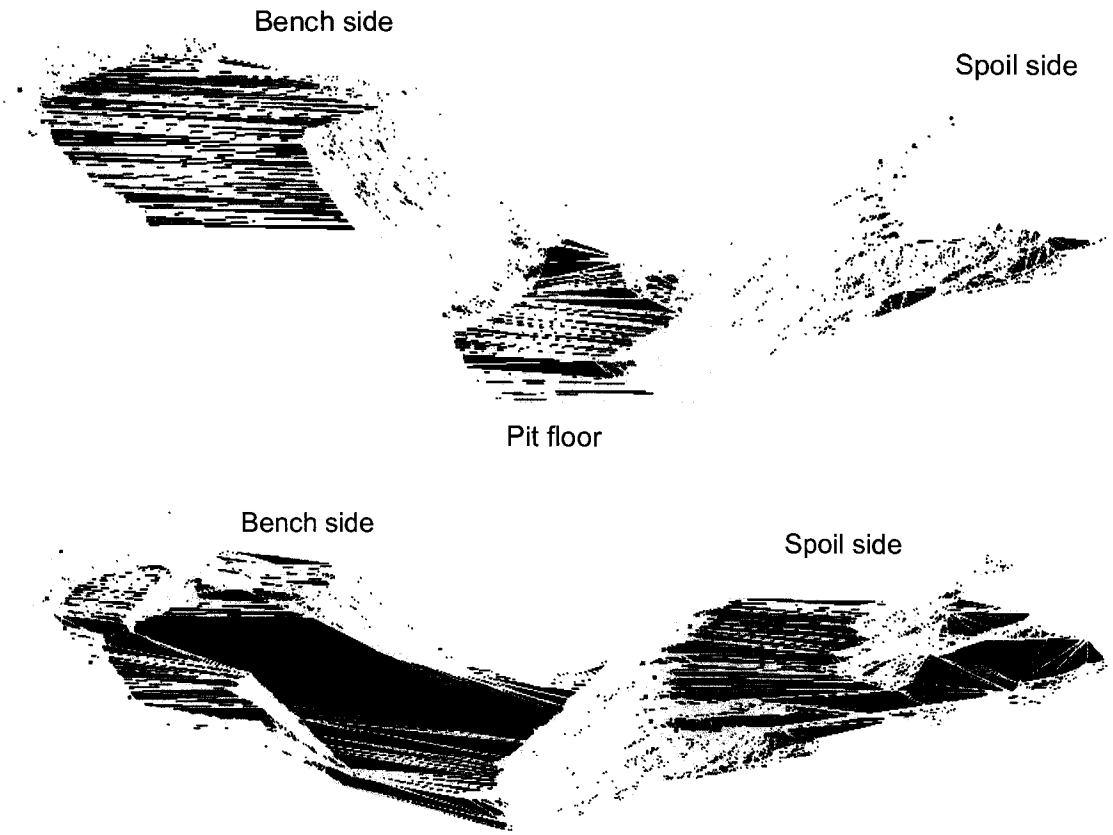

Figure 80 Cast blast #1 (April 28, 2005)

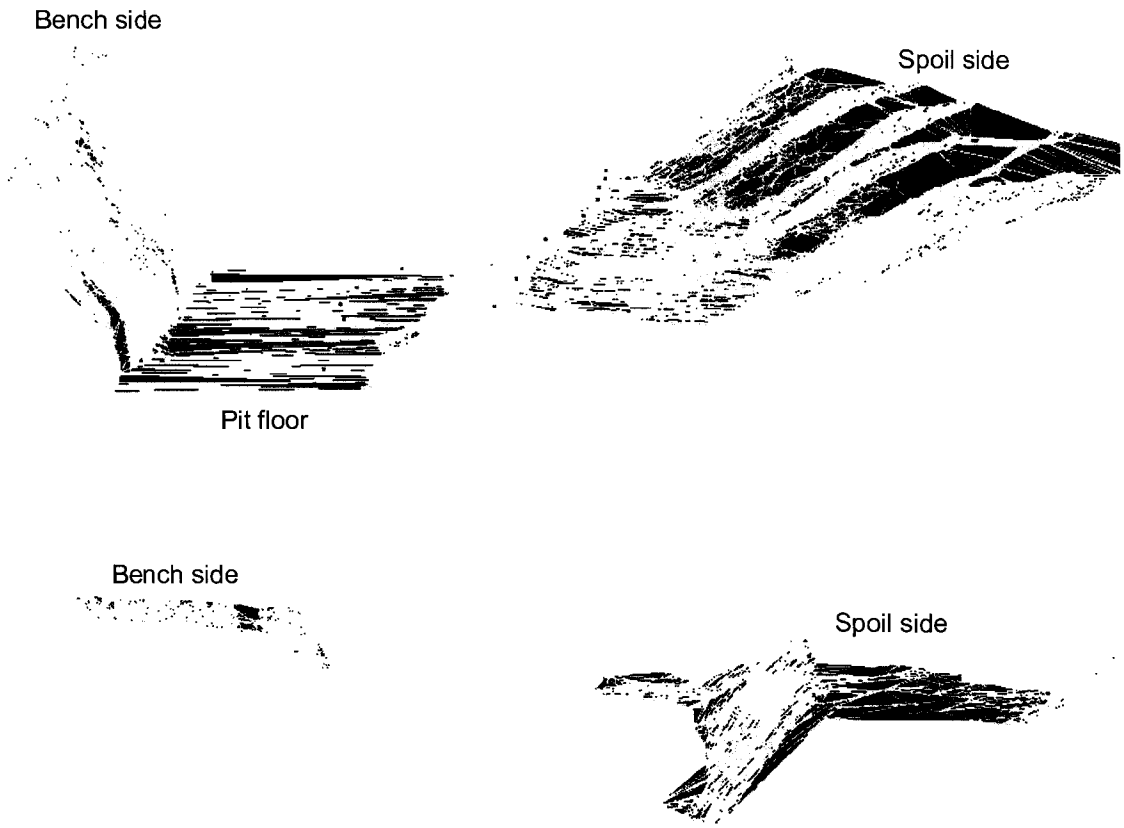

Figure 81 Cast blast #2 (May 5, 2005)

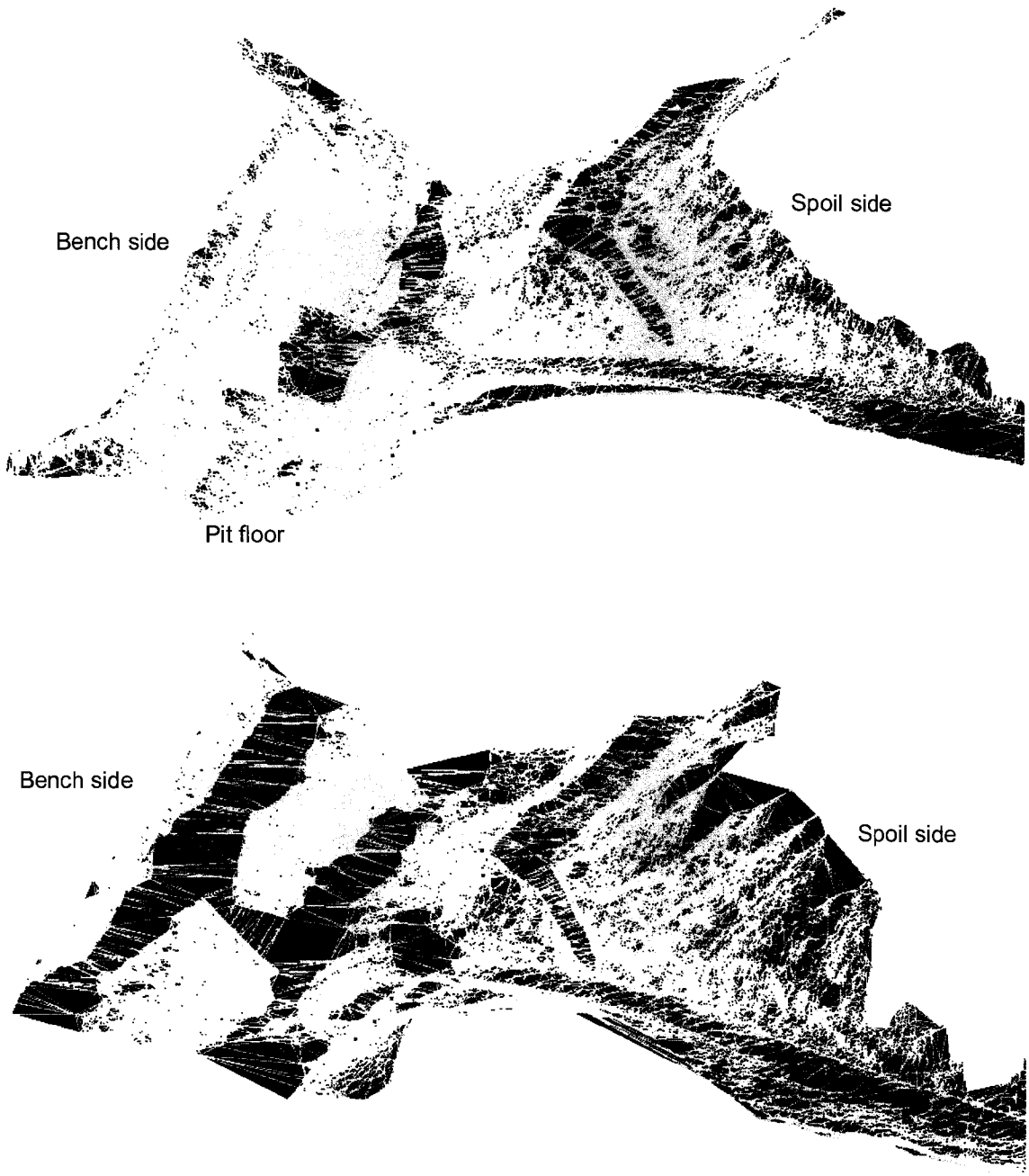

Figure 82 Cast blast #3 (May 26, 2005)

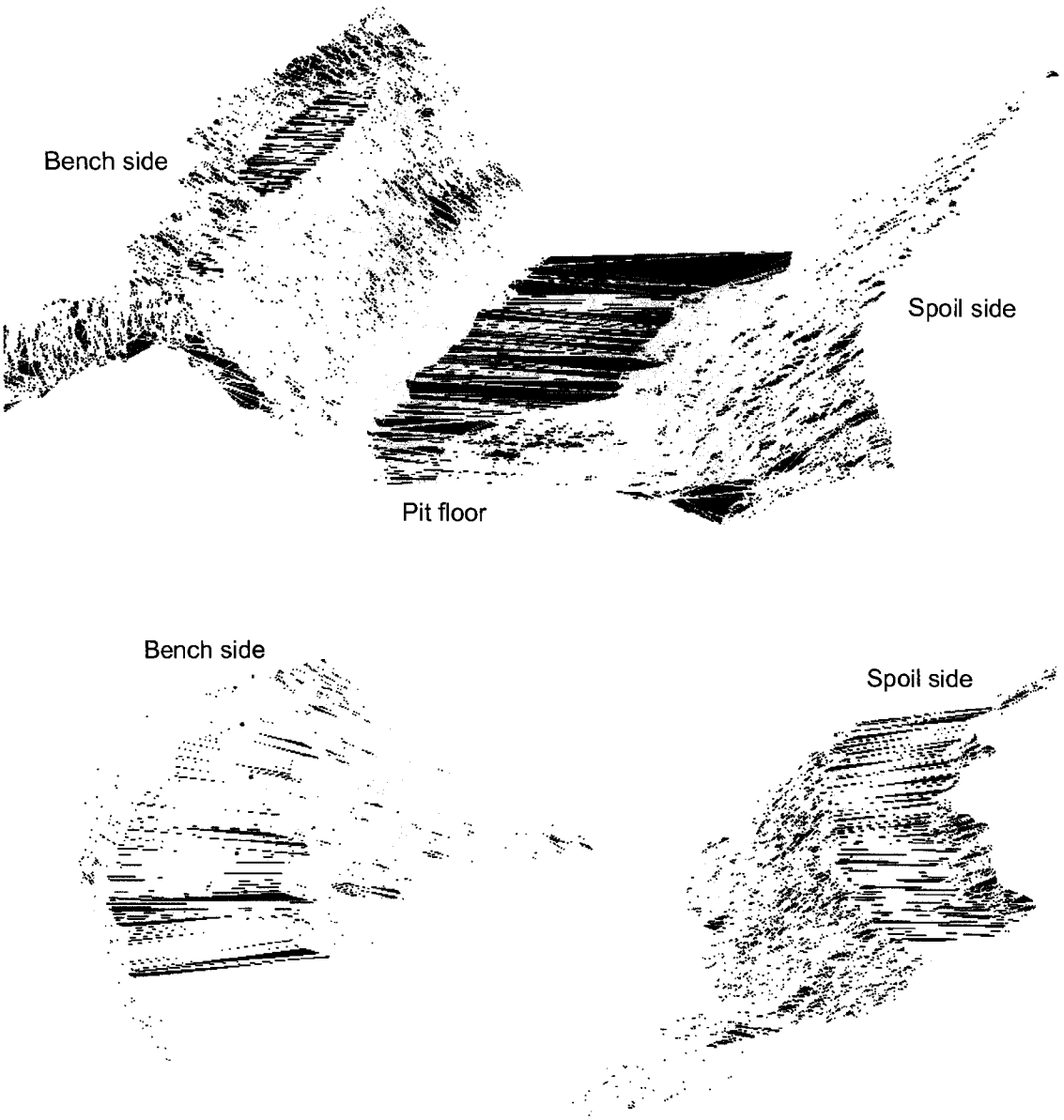

Figure 83 Cast blast #4 (July 28, 2005)

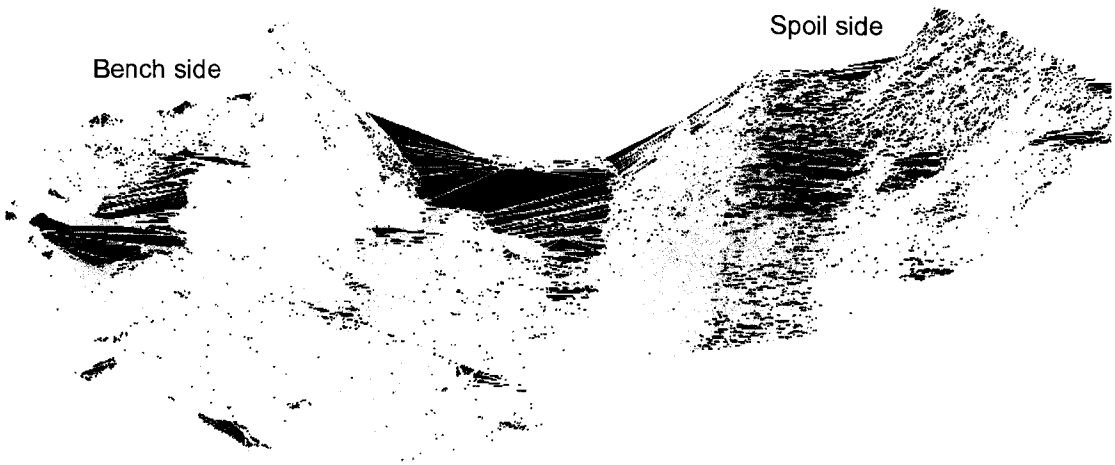

Figure 84 Cast blast #5 (August 11, 2005)

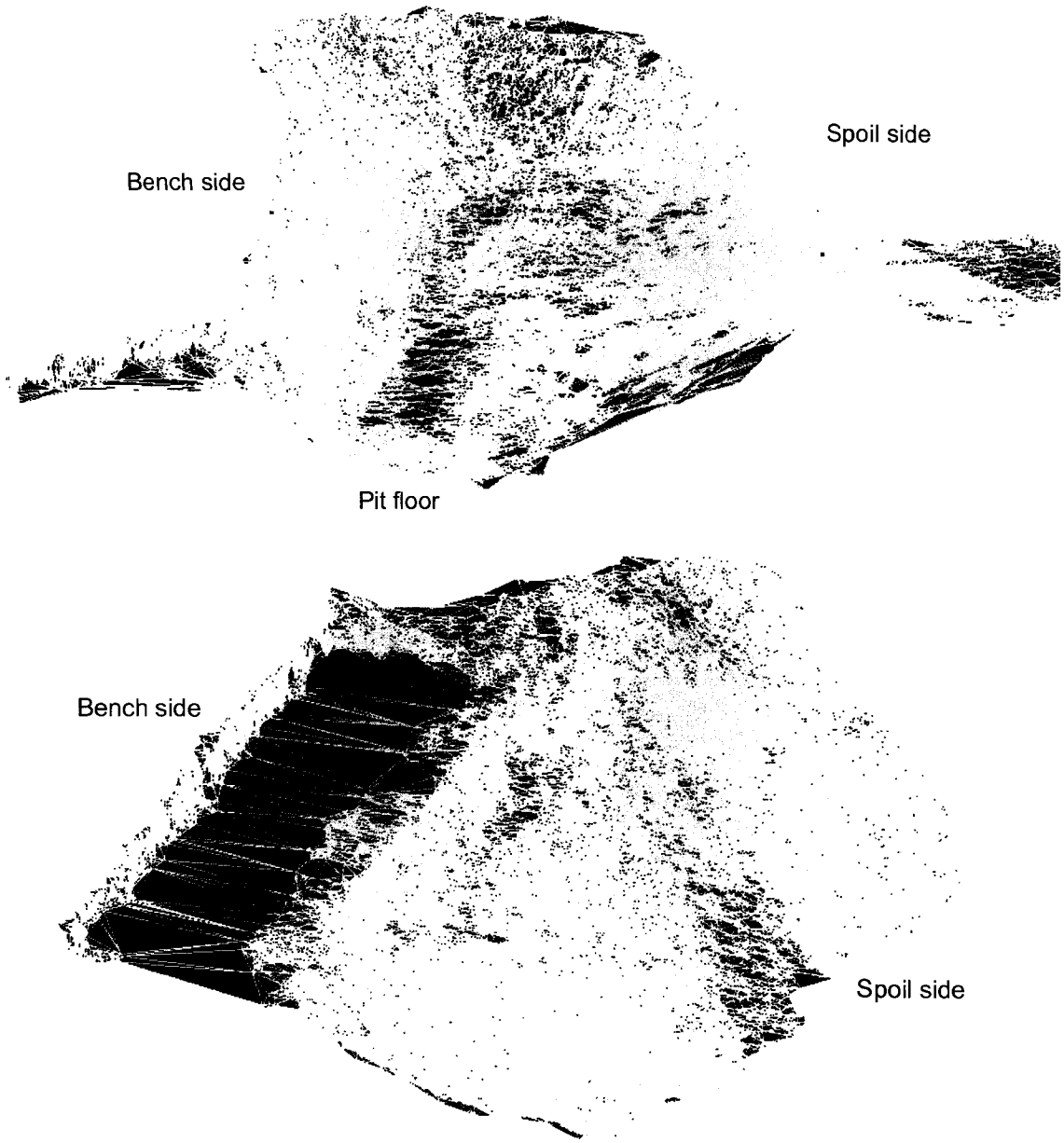

Figure 85 Cast blast #6 (September 1, 2005)

Appendix E: Camera and Lens Specifications

Canon EOS-1Ds Mark II Specification Sheet (Canon, 2005).

Manufacturer	Canon
Product Name	EOS-1Ds Mark II
Type	SLR
Weight	42.9 oz
Pixels	17.2
Effective Pixels	16.7
Sensor Type	Single-plate CMOS sensor
Image Size	4992 x 3328, 3600 x 2400, 3072 x 2048, 2946 x 1664
Aspect Ratio	3:02
Color Filter System	RGB
Image Format	JPEG (Exif 2.2)
File Size	14.6 MB - 1.9 MB
Compression	JPEG (Exif 2.2), RAW, SuperFine, Fine, Normal
Lens Mount	Canon EF Mount
Compatible Lenses	Canon EF Lenses
Viewfinder	Fixed eye-level pentaprism
Diopter Adjustment	-3.0 - +1.0 diopter
LCD	2" TFT
Auto Focus Type	TTL-AREA-SIR with AF-dedicated CMOS Sensor
Focusing Modes	One-Shot AF, AI Servo AF, Manual Focusing
Focusing Points	45 Points
Detecting Range	EV 0-18
AF Assist Illuminator	Emitted by the dedicated Speedlite
Metering Modes	Evaluative metering, Partial metering, Center spot metering, AF point-linked spot metering, Multi-spot metering, Centerweighted averaged metering
Shutter Type	Electronically-controlled focal-plane shutter, 180 Specifications Shutter speeds
Shutter Speed	30-1/8000 sec

Canon EF Lens and Specifications & Accessories (Canon, 2006)

Lens		EF 35 mm f/1.4L USM
Angle of view	Horizontal	54°
	Vertical	38°
	Diagonal	63°
Lens construction (Groups, Elements)		9,11
Number of diaphragm blades		8
Minimum aperture (f)		22
Closest focusing distance (m)		0.3
Maximum magnification (x)		0.18
AF Actuator		Ring USM
Filter diameter (mm)		72
Maximum diameter x Length		79x103
Weight (g)		580